MIXED FINITE ELEMENT METHODS WITH PIECE-WISE CONSTANT FLUXES

A Dissertation

Presented to

the Faculty of the Department of Mathematics

University of Houston

In Partial Fulfillment

of the Requirements for the Degree

Doctor of Philosophy

By

Zhuo Liu

May 2015

MIXED FINITE ELEMENT METHODS WITH PIECE-WISE CONSTANT FLUXES

Zhuo Liu

APPROVED:

Dr. Yuri Kuznetsov, Chairman

Dr. Maxim Olshanskii

Dr. Annalisa Quaini

Dr. Serguei Maliassov,
ExxonMobil Upstream Research Company

Dean, College of Natural Sciences and Mathematics

Acknowledgements

I would never have been able to finish my dissertation without the guidance of my committee members, help from friends, and support from my family.

I would like to express my deepest gratitude to my advisor, Dr. Yuri Kuznetsov, for his excellent guidance, caring, patience, and providing me with an excellent atmosphere for doing research. His rigorous attitude to work and research influenced me deeply, and made me improved all the time. I also would like to express my thanks to my committee members, Dr. Maxim Olshanskii, Dr. Annalisa Quaini and Dr. Serguei Maliassov, for their valuable feedback and helpful suggestions to improve this work.

I am thankful to my fellow group members, Dr. Evgeny Kikinzon and Dr. Jielin Xu for many insightful discussions and helpful advices. I would like to thank all my friends here who gave me this unforgettable and wonderful five years' graduate studying experience.

Finally, I would like to thank my parents, who were consistently encouraging and supporting me during all these years.

MIXED FINITE ELEMENT METHODS WITH PIECE-WISE CONSTANT FLUXES

An Abstract of a Dissertation
Presented to
the Faculty of the Department of Mathematics
University of Houston

In Partial Fulfillment
of the Requirements for the Degree
Doctor of Philosophy

By
Zhuo Liu
May 2015

Abstract

In this dissertation, we consider a new mixed finite element discretization, its error estimation, monotonicity and the approaches to implement local refinement. We also do some numerical experiments to verify error estimates and to see the effect of distorted faces.

In the first part, we introduce a discontinuous Galerkin method based on piecewise constant fluxes, we elaborate its construction and discretization on triangular meshes. We then consider the monotonicity of this method, compare it with classical RT_0 method and extend to KR methods. Finally, error estimation is investigated.

In the second part, we start from reviewing traditional approaches to implement local refinement for the new mixed finite element method. Because of disappearance of monotonicity, we then try to find an alternative way to do local refinement to keep monotonicity.

In the third part, we implement this method on a specially constructed prismatic grid. Numerical results are provided. We then verify the error estimates from the numerical results.

Contents

List of Figures

List of Tables

CHAPTER 1

Introduction

The diffusion equation is one type of partial differential equations describing density dynamics in a material undergoing diffusion. The diffusion type problems are governed by the second-order elliptic differential equation:

$$-\nabla \cdot (K\nabla p) + cp = f \qquad \text{in} \quad \Omega, \tag{1.1}$$

where $K = K(x)$ is a diffusion tension, $f = f(x)$ is a source function, $c = c(x)$ is a non-negative function (dissipation coefficient) and Ω is a bounded domain in $\mathbb{R}^2$ or $\mathbb{R}^3$ with boundary $\partial\Omega$.

Equation (1.1) usually has the boundary conditions:

$$\begin{aligned} p &= g_D \qquad \text{on} \quad \Gamma_D, \\ (K\nabla p)\cdot \mathbf{n} &= g_N \qquad \text{on} \quad \Gamma_N, \end{aligned} \tag{1.2}$$

where $\mathbf{n}$ is the outward unit normal vector to $\partial\Omega$, $\Gamma_D \cap \Gamma_N = \emptyset$ and $\partial\Omega = \overline{\Gamma_D} \cap \overline{\Gamma_N}$, g_D, g_N are given functions defined on Γ_D and Γ_N, respectively.

1.1 Review of approximation methods for diffusion equations

There are many discretization methods deveploed for diffusion equations. The most famous ones are Finite Difference (FD), Finite Element (FE), Finite Volume (FV), Mixed Finite Element (MFE) and Mixed Hybrid Finite Element (MHFE) methods.

The finite difference methods are one of the oldest and simplest methods to solve differential equations. It was first introduced by L. Euler in one-dimensional space in 1768 and then was extended to dimension two probably by C. Runge in 1908. FD is widely used for uniform rectangular grids because of its simplicity for implementing. However, there are also some disadvantages and restrictions for FD. For instace, because of restriction to rectangular grids, there are potential bottlenecks of FD when handling complex geometries in multiple dimensions. Please refer to G. Forsythe, W. Wasow [24] for complete information about FD method.

The finite element methods are the most popular and powerful methods for modern applications. Its development started from the work by A. Hrennikoff [29] and

R. Courant [18]. Later in China, to do the computations of dam constructions, a systematic numerical method for solving partial differential equations was proposed by K. Feng, which was called the finite difference method based on variational principle [22], and actually was another independent invention of finite element method. The term “finite element method” was proposed by R.W. Clough in [17].

A FE method is often composed by a variational formulation, a discretization method, solution algorithms and post-processing procedures. The solution from variational formulation is called “weak solution”. The weak solution belongs to a certain explicitly constructed Hilbert space Q. Existence and uniqueness of the solution can be proved by using certain properties of Hilbert space. Then, by following three steps of discretization method: (1) construction of finite element mesh, (2) definition of basis function on reference elements and (3) mapping of reference elements onto the elements of the mesh, we can contructe the corresponding algebraic system. At last, by direct or iterative solvers, a finite element approximation $p_h \in Q_h$ of the solution p of corresponding diffusion problems is obtained.

The main advantage of FE method over FD method is that FE method is more flexible in terms of dealing with complex geometry and complicated boundary conditions. The application of FE method on domain with curved boundaries can be found at [3, 7, 42, 55].

Different from FD method, which is based on a discretization of the differential form of the conservation equations, the finite volume (FV) method [21] is based on discretization of the integral forms of the conservation equations. “Finite volume” refers to the small volume surrounding each node point on a mesh. In the FV methods, by using the divergence theorem, volume integrals involving divergence terms are converted to surface integrals. These terms on surfaces are called fluxes. Since the flux entering a given volume is identical to that leaving the adjacent volume, FV methods are conservative. The fluxes on the surfaces are then approximated by the discrete unknowns for the solution function. Although conservative, compared to FE methods, FV methods are limited to certain types of meshes, for instance, Voronoi mesh [44].

Very often instead of the second-order diffusion equation, researchers and engineers consider the first order system:

$$\begin{aligned} K^{-1}\mathbf{u} \;&+\; \nabla p \;=\; 0 \quad \text{in} \quad \Omega, \\ \nabla\cdot\mathbf{u} \;&+\; cp \;=\; f \quad \text{in} \quad \Omega, \end{aligned} \tag{1.3}$$

where the unknown vector function $\mathbf{u}$ is called the flux. The corresponding mixed variational formulation is: find $(\mathbf{u}, p) \in \mathbf{V} \times Q$ such that

$$\begin{cases} \int_\Omega (K^{-1}\mathbf{u})\cdot\mathbf{v}dx \;-\; \int_\Omega p(\nabla\cdot\mathbf{v})dx \;=\; -\int_{\partial\Omega} \nabla\cdot(g_D\mathbf{v})ds \\ \int_\Omega (\nabla\cdot\mathbf{u})qdx \;+\; \int_\Omega cpqdx \;=\; \int_\Omega fqdx \end{cases} \tag{1.4}$$

for all $(\mathbf{v}, q) \in \mathbf{V} \times Q$, where $\mathbf{V} = H_{div}(\Omega)$ and $Q = L_2(\Omega)$. For this mixed formulation, both flux $\mathbf{u}$ and solution p are computed simultaneously. Mixed finite element (MFE) methods are then introduced based on this mixed formulation and certain discretization strategies $\mathbf{V}_h \subset \mathbf{V}$ and $Q_h \subset Q$. Subspaces $\mathbf{V}_h$ and Q_h are required to satisfy so-called discrete LBB (Ladyzhenskaya-Babushka-Brezzi) condition:

$$\beta||q_h||_Q \leq \sup_{\mathbf{v}_h \in \mathbf{V}_h} \frac{(\nabla \cdot \mathbf{v}_h, q)}{||\mathbf{v}_h||_{H(div,\Omega)}}, \tag{1.5}$$

for all $q_h \in Q_h$ and certain constant $\beta > 0$. This condition is essential for the stability and error estimation of the numerical solutions.

For MFE method, the spaces $\mathbf{V}_h$ for fluxes are first constructed on simple mesh cells, such as triangles and rectangles in 2D, and tetrahedra, triangular prisms, rectangular parallelepipeds in 3D. The examples of such spaces include the Raviart-Thomas spaces RT_m, Brezzi-Douglas-Fortin-Marini spaces $BDFM_m$, and Brezzi-Douglas-Marini spaces BDM_m, etc, which are introduced and investigated in [8, 9, 13, 46, 48].

By the strategy of change of variables, "simple" FE spaces can be extended to general convex quadrilaterals in 2D, and hexahedral or distorted prismatic cells in 3D. MFE spaces based on Piola transformation are investigated in [25, 51]. Error estimates are strongly dependent on the properties of the Jacobian of transformation. Convergence and superconvergence estimates for MFE method can be found in [48, 20, 45, 54, 26], for instace.

Lots of effort are also involved in how to solve the linear system efficiently from MFE method, which is a saddle-point problem, for example, [28, 19, 27, 2]. The earliest successful technique was the mixed hybrid finite element method (MHFE) [25]. This strategy turns the saddle-point problem into a semi-definite problem, but pays the price of significantly inceasing the degree of freedoms.

The relationship between MFE method and cell-centered FV method has been researched, under the assumption that K in (1.1) is a scalar or diagonal matrix. For rectangular meshes, RT_0 can be reduced to a standard cell-centered FV method, by applying appropriate quadrature rules [49, 12]. Based on this observation, Weiser and Wheeler [54] were able to analyze and prove superconvergence for the approximation solution generated by this method. This result was also extendeded to triangular meshes [1].

In [41, 36], Yu. Kuznetsov and S. Repin introduced one new approach to define a space of fluxes $\mathbf{V}_h$ on general polygonal and polyhedral meshes. The idea of this discretization is to partition a complicated polygonal or polyhedral cell into simple cells, the finite element space of fluxes $\mathbf{V}_h$ is then defined as a subset of corresponding RT_0 space on this cell. They imposed the condition $\nabla \cdot \mathbf{u} = const$ on the cell to eliminate the degrees of freedom on auxiliary interfaces between partitioned cells.

In [38], Yu. Kuznetsov proposed another new discretization method for 2D diffusion equation on polygonal meshes with mixed cells. In [39], the method was further extended to 3D diffusion problems. In [40], the error estimates on fluxes for this new approach was proved:

$$||\mathbf{u}^* - \mathbf{u}_h||_{K^{-1}} \leq 2||\mathbf{u}^* - \mathbf{u}^*_{h,int}||_{K^{-1}}, \tag{1.6}$$

for triangular and quadrilateral mesh in 2D, and tetrahedral and pyramidal mesh in 3D.

In this dissertation, we will take further investigation on the new discretization method proposed by Yu. Kuznetsov. We will verify the error estimate (1.6) by numerical experiments, explore the error estimate on solution p, investigate the case when local refinement appears, and check if discrete maximum principle holds for this method.

1.2 Review of discrete maximum principle and monotonicity

The maximum principle is one of the most important and useful properties for some partial differential equations. A natural question in numerical analysis is whether the approximate solution keeps the property of the maximum principle as well. This problem is referred to the discrete maximum principle (DMP) or monotonicity of the numerical method.

In mathematical modeling, the maximum principle indicates natural nonnegativity of some quantities like temperature, density, concentration, etc. Therefore, the reliability of numerical models often highly depends on validity of the discrete maximum principle. Numerical results with negative concentrations, or heat fluxes from colder to warmer places are not accepted and considered as unreliable.

Mathematicians have studied and analyzed the DMP for a long time. The ealiest results on the FD discretization appeared in 1960s [6, 5, 15, 52], etc. The DMP for FE approximations was first derived in [16] for linear elliptic equations. Other techniques are basd on elliptic estimates [50] or matrix properties [30]. It is well known that the DMP are strongly related to monotone matrices, especially the theory of M-matrices. The monograph [53] is fundamental and pioneering in this field. It is also well known that the validity of DMP is closely related to geometric properties of the finite-element meshes, see, [14, 33, 34]. DMP for convection-diffusion equations have been derived in [11]. It has also been studied for finite volume [4], finite difference schemes [35], RT_0 in 2D [43].

1.3 Dissertation outline

The dissertation is organized as follows. Chapter 2 focus on the MFE formulation. In Section 2.1, we introduce the differential diffusion problem and corresponding integration, mixed and macro-hybrid mixed forms. In Section 2.2, we introduce how to construct FV scheme and a general way to obtain discretization of mixed form. In Section 2.3, a well-known mesh, Voronoi mesh is described. This section introduces the algorithms to generate such meshes and investigates when Voronoi mesh is not good for finite volume scheme.

The topic for Chapter 3 is the new discretization method, PWCF method, without refinement. In Section 3.1, we show how to construct such PWCF scheme based on Discontinuous Galerkin method. Although it is similar to but still different from classical MFE methods. In Section 3.2, we investigate the monotonicity of this method on triangular and tetrahedral meshes, and do a comparison with RT_0 methods. For rectangular mesh, monotonicity is obvious. In Section 3.3, the error estimation on solution p is derived for triangular mesh. In Section 3.4, we compare PWCF method with classical finite volume method on rectangular and triangular meshes, to see if they are equivalent under certain assumptions.

In Chapter 4, PWCF method on the meshes with local refinement is investigated. In Section 4.1, we first introduce a straight-forward way to construct refinement for rectangular mesh. In Section 4.2, we compare different refinement approaches for triangular meshes.

Chapter 5 gives some numerical results for PWCF methods. We start from introducing a 3D prismatic grid, where diffusion problem is defined. The prismatic grid cells may have distorted faces. Then, the algebraic system from PWCF method is built. At last, by checking numerical results, the theoretical error estimations are verified.

The main results obtained in this thesis are:

1. Under the condition of regular and quasi-uniform for meshes, the error estimate holds for numerical solutions from PWCF methods on triangular meshes:

$$||p_h - p^*||_2 \leq c(||\mathbf{u}^*_{h,int} - \mathbf{u}^*||_2 + ||p^*_{h,int} - p^*||_2). \tag{1.7}$$

2. The condensed matrices S_λ for RT_0 and PWCF methods coincide.

3. PWCF methods are monotone on triangular and tetrahedral meshes for certain geometric conditions, i.e., the angle between any two sides or faces for triangular or tetrahedral cells is less than or equal to 90 degree.

4. The usual approach to implement local refinement on triangular mesh destroys monotonicity for PWCF methods.

CHAPTER 2

Classical Numerical Methods and Voronoi Mesh

2.1 Problem formulation

2.1.1 Differential formulation

Consider the diffusion equation:

$$-\nabla \cdot (K \nabla p) = f \qquad \text{in} \quad \Omega, \tag{2.1}$$

where $K = K(x)$ is a diffusion tension, $f = f(x)$ is a source function, Ω is a simply-connect bounded polygonal domain in $\mathbb{R}^2$ or polyhedral domain in $\mathbb{R}^3$ with boundary $\partial\Omega$. We assume f and K are piecewise smooth and bounded. We also assume $K(x)$

is a symmetric positive definite matrix for any point $x \in \Omega$.

We consider the case with Dirichlet boundary only, i.e., $\partial\Omega = \Gamma_D$. Then, we complete equation (2.1) with the boundary condition:

$$p = g_D \qquad \text{on} \quad \Gamma_D, \tag{2.2}$$

where g_D is a given function defined on Γ_D.

Let $\mathbf{u} = -K\nabla p$, which is called flux. Then, (2.1), (2.2) have equivalent mixed form:

$$\begin{cases} K^{-1}\mathbf{u} \;+\; \nabla p \;=\; 0 \quad \text{in} \quad \Omega, \\ \nabla \cdot \mathbf{u} \;=\; f \quad \text{in} \quad \Omega, \\ p \;=\; g_D \quad \text{on} \quad \partial\Omega. \end{cases} \tag{2.3}$$

2.1.2 Balance formulation

The balance equation for (2.1) is:

$$-\int_{\partial E} (K\nabla p) \cdot \mathbf{n} ds = \int_E f dx, \qquad \forall E \subset \Omega, \tag{2.4}$$

where $\mathbf{n}$ denotes the unit outwards normal vector of ∂E.

2.1.3 Mixed variational formulation

The weak form for (2.3) is as follows: find $(\mathbf{u}, p) \in \mathbf{V} \times \mathbf{P}$ such that

$$\left\{\begin{array}{lclcl} \int_\Omega (K^{-1}\mathbf{u}) \cdot \mathbf{v} dx & - & \int_\Omega p(\nabla \cdot \mathbf{v}) dx & = & -\int_{\partial\Omega} \nabla \cdot (g_D \mathbf{v}) ds \\ \int_\Omega (\nabla \cdot \mathbf{u}) q dx & & & = & \int_\Omega f q dx \end{array}\right. \tag{2.5}$$

for all $(\mathbf{v}, q) \in \mathbf{V} \times \mathbf{P}$. Here, $\mathbf{V} = H_{div}(\Omega)$ and $\mathbf{P} = L_2(\Omega)$.

2.1.4 Macro-hybrid mixed formulation

If Ω is partitioned into non-overlapping polygonal or polyhedral cells E_k, $k = 1, \cdots, m$, and f is sufficiently smooth and bounded in each E_k, then (2.3) is equivalent to the problem:

$$\left\{\begin{array}{lclcccc} K^{-1}\mathbf{u}_k & + & \nabla p_k & = & 0 & \text{in} & E_k, \\ \nabla \cdot \mathbf{u}_k & & & = & f_k & \text{in} & E_k, \\ & & p_k & = & p_l & \text{on} & \Gamma_{kl}, \\ \mathbf{u}_k \cdot \mathbf{n}_k & + & \mathbf{u}_l \cdot \mathbf{n}_l & = & 0 & \text{on} & \Gamma_{kl}, \\ & & p_k & = & g_D & \text{on} & \partial\Omega. \end{array}\right. \tag{2.6}$$

The weak formulation of (2.6), or the maco-hybrid mixed formulation of (2.1), (2.2) is as follows: find $(\bar{u}, \bar{p}, \bar{\lambda}) \in \mathbf{V} \times \mathbf{P} \times \mathbf{\Lambda}$ such that

$$\begin{cases} a(\bar{u}, \bar{v}) \;+\; b(\bar{p}, \bar{v}) \;+\; c(\bar{\lambda}, \bar{v}) = l_D(\bar{v}) \\ b(\bar{q}, \bar{u}) = l(\bar{q}) \\ c(\bar{u}, \bar{\mu}) = 0 \end{cases} \tag{2.7}$$

for all $(\bar{v}, \bar{q}, \bar{\mu}) \in \mathbf{V} \times \mathbf{P} \times \mathbf{\Lambda}$, where

$$\mathbf{V} = V_1 \times \cdots \times V_m, \tag{2.8}$$

$$\mathbf{P} = P_1 \times \cdots \times P_m, \tag{2.9}$$

$$\mathbf{\Lambda} = \prod_{1 \leq k < l \leq m}^{m} \Lambda_{kl}, \tag{2.10}$$

with $V_k = H_{div}(E_k)$, $P_k = L_2(E_k)$, and $\Lambda_{kl} = L_2(\Gamma_{kl})$, $k < l$, $|\Gamma_{kl}| \neq 0$. And

$$a(\bar{u}, \bar{v}) = \sum_k \int_{E_k} (K^{-1}\mathbf{u}_k) \cdot \mathbf{v}_k dx, \tag{2.11}$$

$$b(\bar{p}, \bar{v}) = \sum_k \int_{E_k} p_k (\nabla \cdot \mathbf{v}_k) dx, \tag{2.12}$$

$$c(\bar{\lambda}, \bar{v}) = \sum_{k<l} \int_{\Gamma_{kl}} \boldsymbol{\lambda}(\mathbf{v}_k \cdot \mathbf{n}_{kl}) ds, \tag{2.13}$$

$$l_D(\bar{v}) = -\sum_{\Gamma_{ki} \subset \partial\Omega} \int_{\Gamma_{ki}} g_D(\mathbf{v}_k \cdot \mathbf{n}_{ki}) ds, \tag{2.14}$$

$$l(\bar{q}) = \sum_k \int_{E_k} f q_k dx. \tag{2.15}$$

Here, $\mathbf{n}_{kl}$ is the unit outward normal vector on Γ_{kl} from E_k to E_l and $\Gamma_{ki} = \partial E_k \cap \partial\Omega_i$.

2.2 Classical discretization methods

2.2.1 Finite volume methods

Finite volume methods are based on the discretization on balance equation (2.4). The discretization consists by following steps:

1. Approximate domain Ω by a finite non-overlapping subset $\mathfrak{E} = \{E_k, k = 1, \cdots, n\}$.

2. Approximate the function p by p_h in a N-dimensional space V.

3. Approximate boundary flux $(K\nabla p) \cdot \mathbf{n}$ on ∂E_k by a discrete one $(K\nabla_h p_h) \cdot \mathbf{n}$.

As a result, finite volume methods can be written as:

$$-\int_{\partial E_k} (K\nabla_h p_h) \cdot \mathbf{n} ds = \int_{E_k} f dx, \qquad \forall E_k \subset \Omega, \quad k = 1, \cdots, n. \tag{2.16}$$

Because boundary fluxes need to be approximated by corresponding function values p_h, the meshes for finite volume methods are usually specially constructed. One of the most famous meshes for finite volume methods is Voronoi mesh, for example, Figure 2.1. On such Voronoi meshes, the term $\int_{\partial E_k} (\nabla_h p_h).\mathbf{n} ds$ can be written as:

$$\int_{\partial E_k} (\nabla_h p_h) \cdot \mathbf{n} ds = \sum_{j=1}^{m} \frac{(p_j - p_k)|\Gamma_{kj}|}{d(c_j, c_k)}, \tag{2.17}$$

where m is the number of sides for E_k, $\Gamma_{kj} = E_k \cap E_j$, c_j is the node in E_j, $d(c_j, c_k)$ is the distance between two nodes in two cells, and p_j is the solution on c_j.

Further discussion on Voronoi meshes continues in Section 2.3.

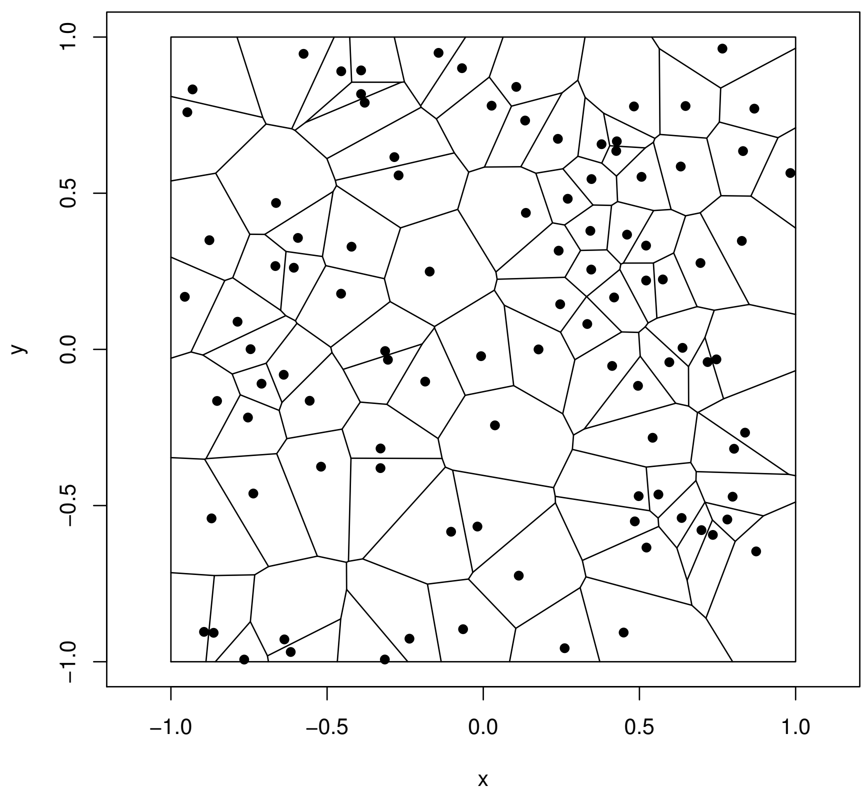

Figure 2.1: Voronoi mesh generated from 100 uniform distributed random points

2.2.2 Mixed hybrid finite element methods

In order to obtain a proper algebraic system from (2.7), the approximation spaces for $\mathbf{V}$, $\mathbf{P}$, $\mathbf{\Lambda}$ need to be introduced. In this thesis, we define subspaces $P_h \equiv P_h(E) \subset P = L_2(E)$ and $\Lambda_{i,h} \equiv \Lambda_{i,h}(\Gamma_i) \subset L_2(\Gamma_i)$ by

$$P_h = \{q : q \equiv \text{const} \quad \text{in } E\}, \tag{2.18}$$

$$\Lambda_{i,h} = \{\lambda : \lambda \equiv \text{const} \quad \text{on } \Gamma_i\}, \tag{2.19}$$

and space Λ_h by

$$\Lambda_h = \Lambda_h(\partial E) = \prod_{i=1}^{t_N} \Lambda_{i,h}. \tag{2.20}$$

We assume that any vector function $\mathbf{v}_h \in V_h \equiv V_h(E) \subseteq H_{div}(E)$ satisfies the following conditions:

$$\begin{aligned} &(a) \qquad \nabla \cdot \mathbf{v}_h = \text{const}_E \qquad \text{in } E, \\ &(b) \qquad \mathbf{v}_h \cdot \mathbf{n}_i = v_i = \text{const} \qquad \text{on each } \Gamma_i, \end{aligned} \tag{2.21}$$

where $\mathbf{n}_i$ are outward unit normals to ∂E on Γ_i.

One of the most widely used subspace $V_h(E) \subseteq H_{div}(E)$ is called lowest order Raviart-Thomas space (RT_0) on triangular cells in 2D or tetrahedral cells in 3D. In addition to conditions (a), (b) in (2.21), if we further assume that in cell E, for every basis vector function $\mathbf{w}_i$, there exists a function ψ_i, s.t.

$$\mathbf{w}_i = -\nabla \psi_i, \tag{2.22}$$

then, the basis vector functions obtained from discretization method discribed above are exactly the basis functions of RT_0 method. For example, if E is a triangle, the lowest order Raviart-Thomas basis vector function $\mathbf{w}_i$ ($i = 1, 2, 3$) can be represented as:

$$\mathbf{w}_i = \frac{1}{h_i}(\mathbf{x} - \mathbf{x}_i), \tag{2.23}$$

where $\mathbf{x}_i$ are three vertices of triangle E, and h_i is the height from $\mathbf{x}_i$ to the opposite side Γ_i.

Another way to choose the basis functions on quadrilateral cells is also based on the condition:

$$\mathbf{w}_i = -K\nabla\psi_i. \tag{2.24}$$

This method is known as Kuznetsov-Repin (KR) method. For more information about this method, please refer to [41, 36].

We define local finite element spaces by using the above definitions of the spaces V_h, P_h, Λ_h:

$$V_{k,h} = V_h(E_k), \quad P_{k,h} = P_h(E_k), \quad k = 1, \cdots, m, \tag{2.25}$$

and the global finite element spaces

$$\begin{aligned} \mathbf{V}_h &= \prod_{k=1}^{m} V_{k,h}, \quad \mathbf{P}_h = \prod_{k=1}^{m} P_{k,h}, \\ \mathbf{\Lambda}_h &= \prod_{1\le k<l\le m} \Lambda_h(\Gamma_{kl}). \end{aligned} \tag{2.26}$$

Therefore, the mixed hybrid finite element discretization of (2.1), (2.2) is: find

$(\bar{u}_h, \bar{p}_h, \bar{\lambda}_h) \in \mathbf{V}_h \times \mathbf{P}_h \times \mathbf{\Lambda}_h$ such that

$$\begin{cases} a(\bar{u}_h, \bar{v}_h) & + & b(\bar{p}_h, \bar{v}_h) & + & c(\bar{\lambda}_h, \bar{v}_h) & = & l_D(\bar{v}_h) \\ b(\bar{q}_h, \bar{u}_h) & & & & & = & l(\bar{q}_h) \\ c(\bar{u}_h, \bar{\mu}_h) & & & & & = & 0 \end{cases} \tag{2.27}$$

for all $(\bar{v}_h, \bar{q}_h, \bar{\mu}_h) \in \mathbf{V}_h \times \mathbf{P}_h \times \mathbf{\Lambda}_h$.

Problem (2.27) is equivalent to the algebraic system

$$\mathcal{A} \begin{pmatrix} \bar{u} \\ \bar{p} \\ \bar{\lambda} \end{pmatrix} = \begin{pmatrix} \bar{G}_D \\ \bar{F} \\ 0 \end{pmatrix}, \tag{2.28}$$

with the 3×3 block symmetric matrix

$$\mathcal{A} = \begin{pmatrix} M & B^T & C^T \\ B & 0 & 0 \\ C & 0 & 0 \end{pmatrix} = \sum_{k=1}^{m} \mathcal{N}_k \mathcal{A}_k \mathcal{N}_k^T, \tag{2.29}$$

where

$$\mathcal{A}_k = \begin{pmatrix} M_k & B_k^T & C_k^T \\ B_k & 0 & 0 \\ C_k & 0 & 0 \end{pmatrix} \tag{2.30}$$

is local matrix defined on E_k, and $\mathcal{N}_k$ is an appropriate subassembling matrix, $k =$

$1, \cdots, m$. In fact,

$$M = \mathrm{diag}\{M_1, \cdots, M_m\}, \tag{2.31}$$

$$B = \mathrm{diag}\{B_1, \cdots, B_m\}, \tag{2.32}$$

$$C = (\widetilde{C}_1, \cdots, \widetilde{C}_m), \tag{2.33}$$

where $\widetilde{C}_k = \mathcal{N}_{k,\lambda} C_k$, $k = 1, \cdots, m$.

In Chapter 3, a new mixed finite element method based on so-called "weak formulation" is introduced, which is one type of discontinuous galerkin (DG) methods.

2.3 Voronoi mesh

Let P be a set of n distinct points (nodes or sites) in a region Ω. The Voronoi mesh (or Voronoi diagram) of P is the subdivison of the region Ω into n cells, one for each node. A point q lies in the cell corresponding to a node $p_i \in P$ if and only if

$$d(q, p_i) < d(q, p_j), \tag{2.34}$$

for each $p_j \in P, j \neq i$, where $d(\cdot, \cdot)$ reprensents the Euclidean distance. There are some important properties for Voronoi mesh:

1. The line segment connecting two nodes whose cells are adjacent to each other is perpendicular to the edge shared by these two cells.

2. Each point on an edge is the center of a circle passing through two nodes.

3. Each vertex (not on the boundary) is the center of a circle passing through three nodes (see Figure 2.2).

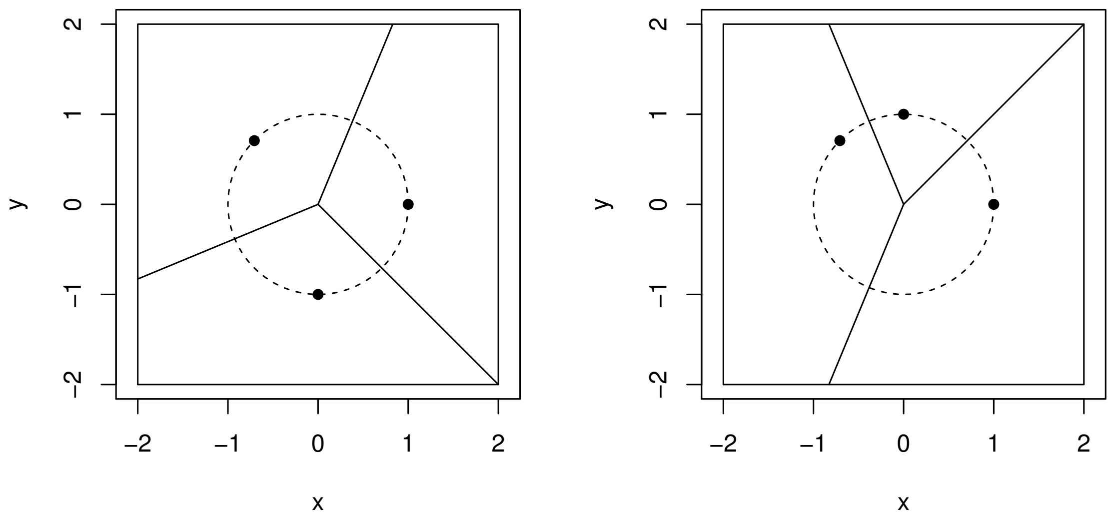

Figure 2.2: Circle centering at a vertex and crossing three nodes

There are several famous algorithms to generate Voronoi mesh:

- Compute the intersection of $n-1$ half-planes for each node, and "merge" the cells into the mesh $\left[O(n^2log(n))\right]$
- Divide-and-conquer (1975, Shamos & Hoey) $\left[O(nlog(n))\right]$
- Plane-sweep (1987, Fortune) $\left[O(nlog(n))\right]$
- Randomized incremental construction (1992, Guibas, Knuth & Sharir) $\left[O(nlog(n))\right]$

2.3.1 Plane-sweep algorithm

In this subsection, we use plane-sweep algorithm to generate Voronoi mesh. The main idea of this algorithm is as follows: (See Figure 2.3 to Figure 2.5, graphs are from [47].)

1. Voronoi mesh is constructed as horizontal line sweeps the set of nodes from top to bottom.

2. The bisector between a node and the horizontal line is a parabola. The beach line is the lower envelope of all the parabolas already seen.

3. When sweeping the horizontal line from above, the Voronoi diagram is correct up to the beach line.

4. The breakpoints of the beach line lie on the Voronoi edges of the final diagram.

5. There are two possible events, node(site) event and vertex event. The former one is the sweep line meets a node, so a possible parabola appears.The latter one is an existing arc of the beach line shrinks to a point and disappears, so a Voronoi vertex is created.

Animation of this process can be found at: `http://en.wikipedia.org/wiki/Sweep_line_algorithm`.

2.3.2 "Bad" edges

In Figure 2.2, both Voronoi meshes are composed by three cells, who share one vertex at origin. However, the left-hand side mesh is better than the right-hand side one,

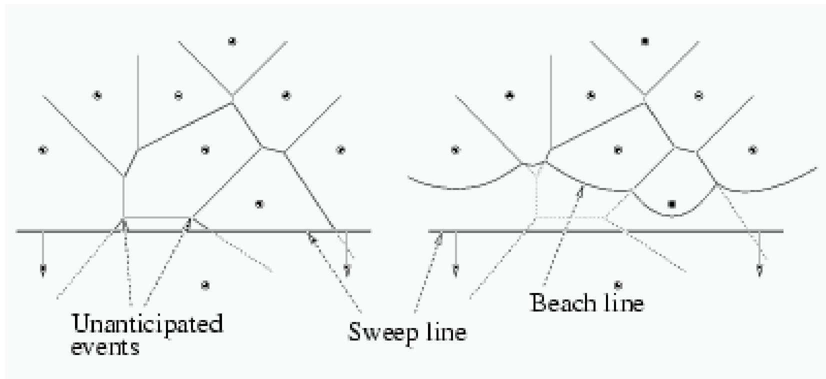

Figure 2.3: Sweep line and beach line, from [47]

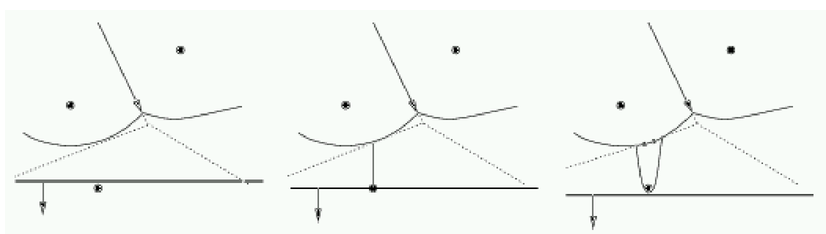

Figure 2.4: Node(site) event, from [47]

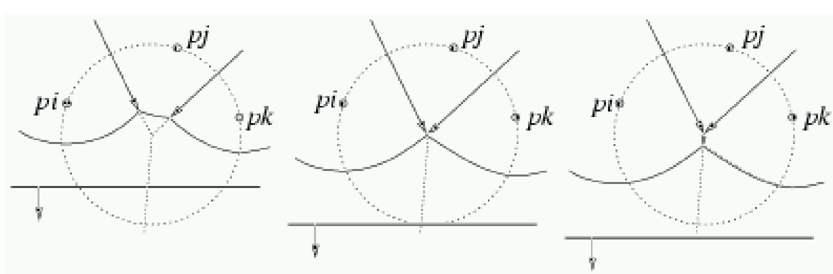

Figure 2.5: Vertex event, from [47]

because the line segment connecting any two nodes intersects with the edge shared by these two cells. This is important, because normal fluxes on such edges can be reasonablely approximated by the values from corresponding two nodes, and finite volume method can be properly applied. However, it is not true for the bottom inner edge from the right-hand side Voronoi mesh.

From Figure 2.2, we can easily find that a “bad” edge appears when all the three line segments between three nodes are at one side of the circle, or equivalently, there exists one diameter that all the three nodes are on one side of the diameter (see Figure 2.6). As a consequence, the triangle formed by these three nodes is an obtuse triangle, and the following statement holds:

A “bad” edge appears only when there are three neighbour nodes who form an obtuse triangle.

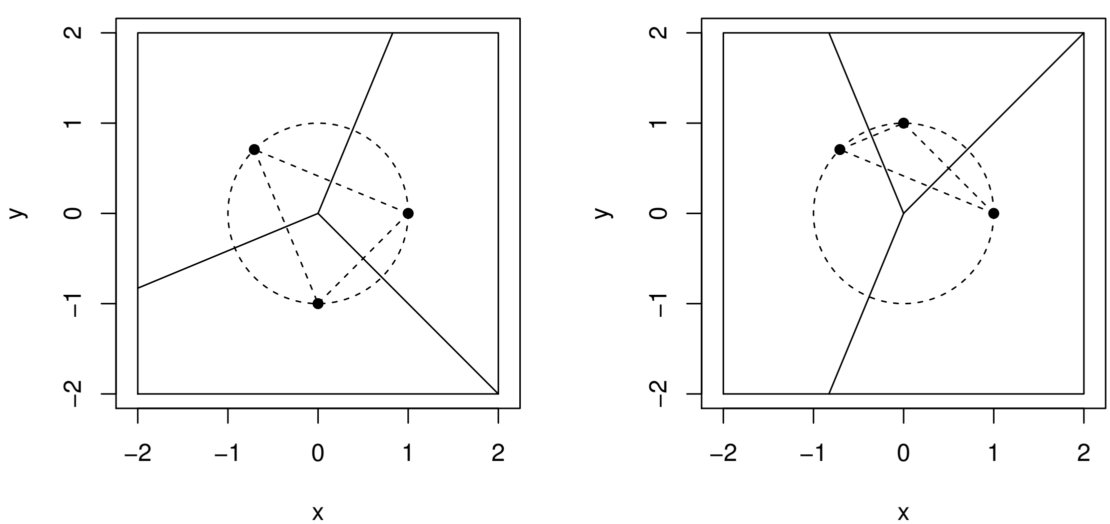

Figure 2.6: Reason why “bad” edge appears

CHAPTER 3

Piece-Wise Constant-Flux (PWCF) Method

Let us consider meshes composed by polygonal cells in 2D and polyhedral cells in 3D. Suppose each mesh cell can be partitioned into two or more triangles or tetrahedrons, with interfaces being line segments in 2D or triangles in 3D. Next, we will show how to construct PWCF scheme on triangular meshes. Implementations of this method on other types of meshes are similar.

3.1 Discretization on triangular mesh

Let Ω_h be a conformal triangular mesh in Ω, i.e., $\Omega_h = \cup E_k$, with interface Γ_{kl} between mesh cells E_k and E_l. This disretization first requires to split each triangular cell into two subtriangles. If we consider the union of two cells, the splitting will have three different cases, see Figure 3.1 to 3.3.

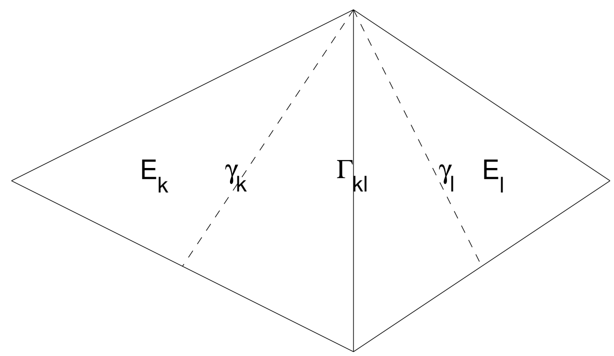

Figure 3.1: Split two adjacent triangular cells into four subtriangles, case 1

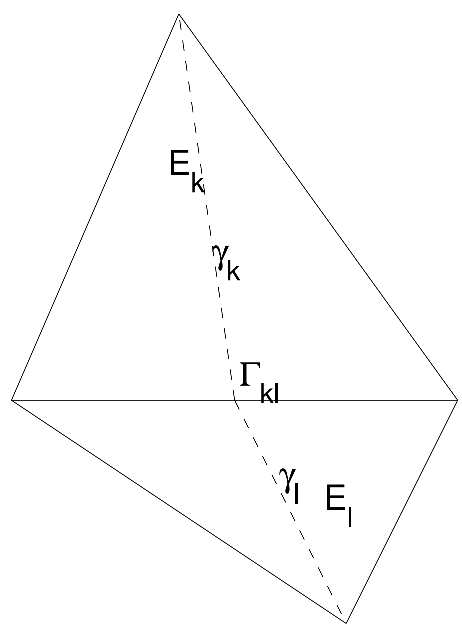

Figure 3.2: Split two adjacent triangular cells into four subtriangles, case 2

Suppose $(\mathbf{u}^*, p^*)$ be the exact solution of (2.3), then for any piecewise constant vector field $\mathbf{w}_{kl}$ satisfying:

1. $\mathbf{w}_{kl}$ is constant in each subtriangles $\omega_{kl} \cap e_i$ correspondingly,

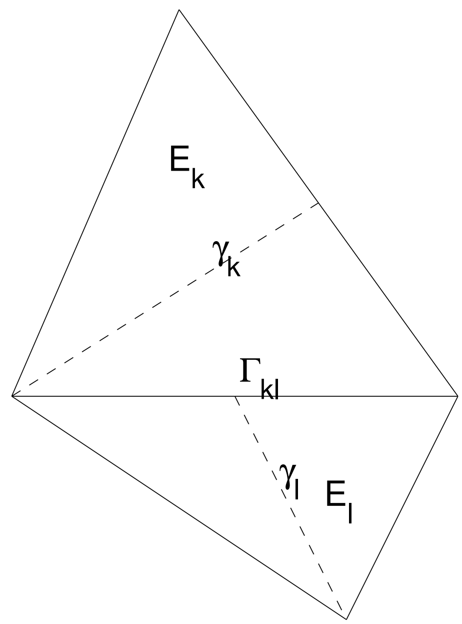

Figure 3.3: Split two adjacent triangular cells into four subtriangles, case 3

2. $\mathbf{w}_{kl} \cdot \mathbf{n}_{kl} = 1$ on Γ_{kl},

3. $\mathbf{w}_{kl} \cdot \mathbf{n} = 0$ on all other edges of $\omega_{kl} \cap E_k$ and $\omega_{kl} \cap E_l$,

4. $\mathbf{w}_{kl} = \mathbf{0}$ in $\Omega \backslash \omega_{kl}$,

we have:

$$\begin{aligned} &\int_\Omega (K^{-1}\mathbf{u}^*) \cdot \mathbf{w}_{kl} dx + \int_\Omega (\nabla p^*) \cdot \mathbf{w}_{kl} dx \\ =& \int_\Omega (K^{-1}\mathbf{u}^*) \cdot \mathbf{w}_{kl} dx + \int_{\omega_{kl}} (\nabla p^*) \cdot \mathbf{w}_{kl} dx \\ =& \int_\Omega (K^{-1}\mathbf{u}^*) \cdot \mathbf{w}_{kl} dx + \int_{\partial\omega_{kl}} p^*(\mathbf{n}_{\omega_{kl}} \cdot \mathbf{w}_{kl}) ds = 0, \end{aligned} \tag{3.1}$$

or equivalently,

$$\int_\Omega (K^{-1}\mathbf{u}^*) \cdot \mathbf{w}_{kl} dx + |\Gamma_{kl}|(p_l^* - p_k^*) = 0, \tag{3.2}$$

where $p_l^* = \frac{1}{|\gamma_l|}\int_{\gamma_l} p^* ds$ and $p_k^* = \frac{1}{|\gamma_k|}\int_{\gamma_k} p^* ds$, and ω_{kl} is the union of two or three or four subtriangles with the common interface Γ_{kl}. Illustrations on ω_{kl} and $\mathbf{w}_{kl}$ are in Figure 3.4 to 3.6.

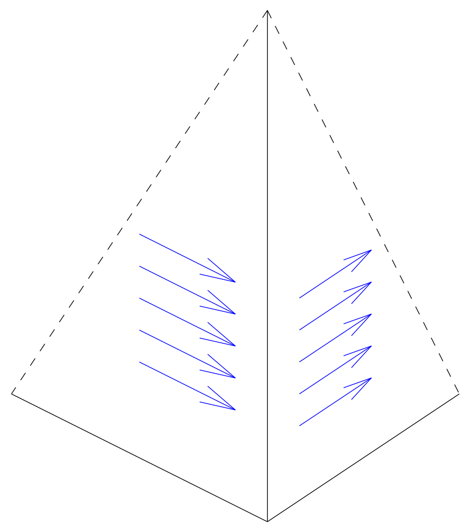

Figure 3.4: ω_{kl} and corresponding piecewise constant vector field $\mathbf{w}_{kl}$ for case 1

Define the finite element spaces as:

$$\mathbf{V}_h = \text{span}\{\mathbf{w}_{kl},\ k < l\}, \tag{3.3}$$

$$\mathbf{P}_h = \text{span}\{\phi_k,\ \phi_k = 1 \text{ in } E_k,\ \phi_k = 0 \text{ in } \Omega\backslash E_k\}, \tag{3.4}$$

then, the discontinuous Galerkin method can be formulated as: find $\mathbf{u}_h = \sum_{kl} u_{kl}\mathbf{w}_{kl} \in \mathbf{V}_h$ and $p_h = \sum_k p_k\phi_k \in \mathbf{P}_h$, such that

$$\begin{cases} \int_\Omega (K^{-1}\mathbf{u}_h)\cdot \mathbf{w}_{kl}dx - |\Gamma_{kl}|(p_k - p_l) & = 0 \qquad \forall\ k < l, \\ \int_{\partial E_k} \mathbf{u}_h \cdot \mathbf{n}_{\partial E_k} ds & = \int_{E_k} f dx \qquad \forall k. \end{cases} \tag{3.5}$$

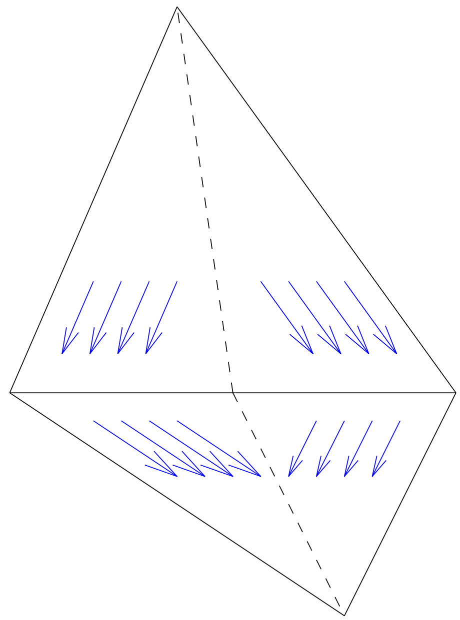

Figure 3.5: ω_{kl} and corresponding piecewise constant vector field $\mathbf{w}_{kl}$ for case 2

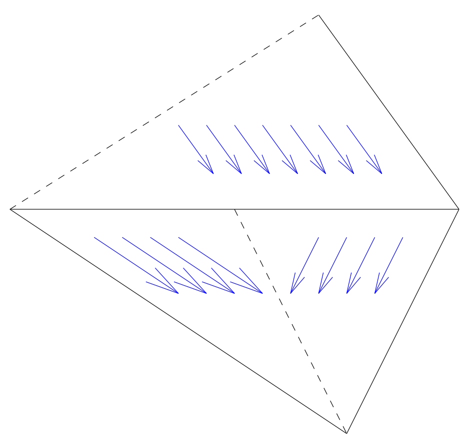

Figure 3.6: ω_{kl} and corresponding piecewise constant vector field $\mathbf{w}_{kl}$ for case 3

If we further define the operators:

$$a(\mathbf{u}, \mathbf{v}) = \int_{\Omega} (K^{-1}\mathbf{u}) \cdot \mathbf{v} dx, \tag{3.6}$$

$$b(p, \mathbf{v}) = \sum_{k<l} |\Gamma_{kl}|(p_l - p_k)v_{kl}, \tag{3.7}$$

$$F(q) = -\int_{\Omega} fq dx, \tag{3.8}$$

$$G_D(\mathbf{v}) = -\sum_{\Gamma_{ki} \subset \partial\Omega} \int_{\Gamma_{ki}} g_D v_{ki} ds, \tag{3.9}$$

then (3.5) is equivalent to: find $(\mathbf{u}_h, p_h) \in \mathbf{V}_h \times \mathbf{P}_h$, such that

$$\begin{cases} a(\mathbf{u}_h, \mathbf{v}_h) + b(p_h, \mathbf{v}_h) & = G_D(\mathbf{v}_h) \\ b(q_h, \mathbf{u}_h) & = F(q_h) \end{cases} \tag{3.10}$$

for any $(\mathbf{v}_h, q_h) \in \mathbf{V}_h \times \mathbf{P}_h$. This finite element problem results in an algebraic system:

$$\begin{pmatrix} M & B^T \\ B & 0 \end{pmatrix} \begin{pmatrix} \bar{u} \\ \bar{p} \end{pmatrix} = \begin{pmatrix} \bar{G}_D \\ \bar{F} \end{pmatrix}. \tag{3.11}$$

If we consider local systems on every macro cells E_k, introduce new variables $\lambda^*_{kl} = \frac{1}{|\Gamma_{kl}|} \int_{\Gamma_{kl}} p^* ds$ for all $\Gamma_{kl} \not\subseteq \partial\Omega$, then integration (3.2) becomes

$$\int_{\omega_{kl} \cap E_k} (K^{-1}\mathbf{u}^*) \cdot \mathbf{w}_{kl} dx + |\Gamma_{kl}|(\lambda^*_{kl} - p^*_k) = 0. \tag{3.12}$$

Assemble all such local systems into universal system, (3.11) will then have a equivalent mixed hybrid form, which results in the following algebraic system:

$$\begin{pmatrix} M & B^T & C^T \\ B & 0 & 0 \\ C & 0 & 0 \end{pmatrix} \begin{pmatrix} \bar{u} \\ \bar{p} \\ \bar{\lambda} \end{pmatrix} = \begin{pmatrix} \bar{G}_D \\ \bar{F} \\ 0 \end{pmatrix}. \tag{3.13}$$

Remark 3.1. *The* 3×3 *block matrix in (3.13) has exactly same blocks* B *and* C *as in classical macro-hybrid mixed finite element methods in (2.29), for instance,* RT_0 *method, the only difference lies on the block diagonal matrix* M.

3.2 Monotonicity

Definition 3.2. An $n \times n$ real matrix A is monotone if $Ax \geq 0$ implies $x \geq 0$, or equivalently if A is nonsingular with $A^{-1} \geq 0$.

Definition 3.3. A real square matrix A is an M-matrix if all its off-diagonal entries are nonpositive and if it is nonsingular and $A^{-1} \geq 0$.

Definition 3.4. A real square matrix A is a Stieltjes matrix if all its off-diagonal entries are nonpositive and if it is symmetric and positive definite.

Definition 3.5. A real square matrix A is a singular M-matrix if it is singular, and for any positive number ϵ, the matrix $A + \epsilon I$ is a M-matrix.

Theorem 3.6. *If* A *is a Stieltjes matrix then it is also an M-matrix, so it is monotone.*

From Section 3.1, we derive that mixed hybrid PWCF method results in a linear system:

$$\begin{pmatrix} M & B^T & C^T \\ B & 0 & 0 \\ C & 0 & 0 \end{pmatrix} \begin{pmatrix} \bar{u} \\ \bar{p} \\ \bar{\lambda} \end{pmatrix} = \begin{pmatrix} \bar{G}_D \\ \bar{F} \\ 0 \end{pmatrix}, \tag{3.14}$$

where

$$\begin{aligned} B &= \operatorname{diag}\{B_1, \cdots, B_m\}, \\ C &= (\widetilde{C}_1, \cdots, \widetilde{C}_m) = (N_1 C_1, \cdots, N_m C_m), \end{aligned} \tag{3.15}$$

with B_k, C_k being local matrices on mesh cell E_k and N_k being assembling matrices.

In this section, the monotonicity of linear system (3.14) is investigated (the results are also published in [32]), i.e., if $f \geq 0$ in Ω (or say, $\bar{F} \leq 0$), can we get $\bar{p} \geq g_D$ and $\bar{\lambda} \geq g_D$? To simplify the problem, we assume that the diffusion problem has homogenous Dirichlet boundary condition, i.e., $\bar{G}_D \equiv 0$. In order to get the monotonicity property, we do the following condensation procedure:

1. First eliminating variable $\bar{u}$, we get the system:

$$\begin{pmatrix} BM^{-1}B^T & BM^{-1}C^T \\ CM^{-1}B^T & CM^{-1}C^T \end{pmatrix} \begin{pmatrix} \bar{p} \\ \bar{\lambda} \end{pmatrix} = \begin{pmatrix} -\bar{F} \\ 0 \end{pmatrix}. \tag{3.16}$$

2. Then, eliminating variable $\bar{p}$, we come to the Schur complement system:

$$S\bar{\lambda} = \bar{\phi}, \tag{3.17}$$

with Schur complement matrix

$$S = CM^{-1}[M - B^T(BM^{-1}B^T)^{-1}B]M^{-1}C^T, \tag{3.18}$$

and right-hand side

$$\begin{aligned}\bar{\phi} &= C[M^{-1} - M^{-1}B^T(BM^{-1}B^T)^{-1}BM^{-1}]\bar{G}_D + C[M^{-1}B^T(BM^{-1}B^T)^{-1}]\bar{F} \\ &= C[M^{-1}B^T(BM^{-1}B^T)^{-1}]\bar{F}.\end{aligned} \tag{3.19}$$

By the representations of matrices B and C in (3.15), matrix S and right-hand side $\bar{\phi}$ can be written in the forms:

$$\begin{aligned}S &= \sum_{k=1}^{m} \widetilde{C}_k M_k^{-1}[M_k - B_k^T(B_k M_k^{-1} B_k^T)^{-1} B_k] M_k^{-1} \widetilde{C}_k^T \\ &= \sum_{k=1}^{m} N_k S_k N_k^T,\end{aligned} \tag{3.20}$$

and

$$\bar{\phi} = \sum_{k=1}^{m} N_k C_k M_k^{-1} B_k^T (B_k M_k^{-1} B_k^T)^{-1} F_k, \tag{3.21}$$

where N_k are assembling matrices and

$$S_k = C_k M_k^{-1}[M_k - B_k^T(B_k M_k^{-1} B_k^T)^{-1} B_k] M_k^{-1} C_k^T. \tag{3.22}$$

Therefore, the monotonicities for local matrices S_k and global matrix S are equivalent, i.e., if S_k are M-matrices (either singular or nonsingular) and at least one of them is nonsingular, then S is monotone. Next, we will start to focus on local monotonicities for different types of meshes.

3.2.1 Triangular mesh

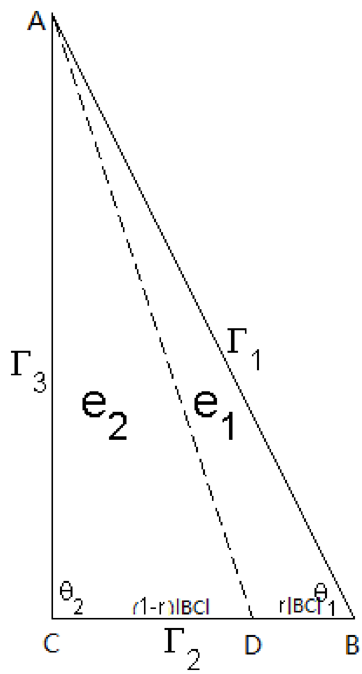

Figure 3.7: Triangular mesh cell with arbitrary shape

Shape of a triangle can be uniquely determined by two angles, so we can fix shape of a triangular cell E_k by fixing two base angles θ_1 and θ_2 ($0 < \theta_1 + \theta_2 < \pi$). If we further fix the height of this triangle to be h, it is uniquely determined. In addition, we suppose $\frac{|BD|}{|BC|} = r$ and $\frac{|CD|}{|BC|} = 1 - r$.

PWCF basis for this cell is:

$$\mathbf{w}_1 = \begin{cases} (\frac{1}{\sin\theta_1}, 0) & \text{in } e_1, \\ (0,0) & \text{in } e_2. \end{cases} \tag{3.23}$$

$$\mathbf{w}_2 = \begin{cases} (\frac{\cos\theta_1}{\sin\theta_1}, -1) & \text{in } e_1, \\ (0,0) & \text{in } e_2. \end{cases} \tag{3.24}$$

$$\mathbf{w}_2' = \begin{cases} (0,0) & \text{in } e_1, \\ (-\frac{\cos\theta_2}{\sin\theta_2}, -1) & \text{in } e_2. \end{cases} \tag{3.25}$$

$$\mathbf{w}_3 = \begin{cases} (0,0) & \text{in } e_1, \\ (-\frac{1}{\sin\theta_2}, 0) & \text{in } e_2. \end{cases} \tag{3.26}$$

and consequently the matrices M_k, B_k and C_k are:

$$M_k = Area_k. \begin{pmatrix} \frac{r}{\sin^2\theta_1} & \frac{r\cos\theta_1}{\sin^2\theta_1} & 0 \\ \frac{r\cos\theta_1}{\sin^2\theta_1} & \frac{r}{\sin^2\theta_1} + \frac{1-r}{\sin^2\theta_2} & \frac{(1-r)\cos\theta_2}{\sin^2\theta_2} \\ 0 & \frac{(1-r)\cos\theta_2}{\sin^2\theta_2} & \frac{1-r}{\sin^2\theta_2} \end{pmatrix}, \tag{3.27}$$

$$B_k = (-\frac{h}{\sin\theta_1}, -\frac{h\cos\theta_1}{\sin\theta_1} - \frac{h\cos\theta_2}{\sin\theta_2}, -\frac{h}{\sin\theta_2}), \tag{3.28}$$

$$C_k = \text{diag}\{\frac{h}{\sin\theta_1}, \frac{h\cos\theta_1}{\sin\theta_1} + \frac{h\cos\theta_2}{\sin\theta_2}, \frac{h}{\sin\theta_2}\}. \tag{3.29}$$

where $Area_k$ is the area of triangle E_k, i.e., $Area_k = \frac{\cot\theta_1 + \cot\theta_2}{2} h^2$. Hence, condensed matrix S_k can be written as:

$$
\begin{aligned}
S_k &= \frac{h^2}{Area_k}\begin{pmatrix} \csc^2\theta_1 & -\cot^2\theta_1-\cot\theta_1\cot\theta_2 & \cot\theta_1\cot\theta_2-1 \\ -\cot^2\theta_1-\cot\theta_1\cot\theta_2 & (\cot\theta_1+\cot\theta_2)^2 & -\cot\theta_1\cot\theta_2-\cot^2\theta_2 \\ \cot\theta_1\cot\theta_2-1 & -\cot\theta_1\cot\theta_2-\cot^2\theta_2 & \csc^2\theta_2 \end{pmatrix} \\
&= \frac{1}{Area_k}\begin{pmatrix} s_1^2||\mathbf{n}_1||^2 & s_1s_2(\mathbf{n}_1\cdot\mathbf{n}_2) & s_1s_3(\mathbf{n}_1\cdot\mathbf{n}_3) \\ s_2s_1(\mathbf{n}_2\cdot\mathbf{n}_1) & s_2^2||\mathbf{n}_2||^2 & s_2s_3(\mathbf{n}_2\cdot\mathbf{n}_3) \\ s_3s_1(\mathbf{n}_3\cdot\mathbf{n}_1) & s_3s_2(\mathbf{n}_3\cdot\mathbf{n}_2) & s_3^2||\mathbf{n}_3||^2 \end{pmatrix},
\end{aligned}
\tag{3.30}
$$

where $\mathbf{n}_i$ are outward unit vectors on Γ_i and s_i are lengths of Γ_i, $i = 1, 2, 3$. Finally, we reach to the monotone condition on condensed matrix for triangular mesh cells:

Theorem 3.7. *S_k is a singular M-matrix if and only if all three angles of E_k are non-obtuse angles.*

3.2.2 Tetrahedral mesh

Let V_i and Γ_i be the vertices and faces of a tetrahedral mesh cell, where V_i is opposite to Γ_i. Let $\mathbf{n}_i$ be the outward normal fluxes on face Γ_i, respectively, $i = 1, \cdots, 4$. By applying PWCF method, the mesh cell is partitioned into two subtetrahedrons e_1 and e_2 by connecting V_1 and mid-point of edge V_2V_3, and connecting V_4 and mid-point of edge V_2V_3, see Figure 3.8. PWCF basis has the properties:

In e_1,

$$
\begin{aligned}
&\mathbf{w}_1\cdot\mathbf{n}_1 = 1, \quad \mathbf{w}_1\cdot\mathbf{n}_3 = 0, \quad \mathbf{w}_1\cdot\mathbf{n}_4 = 0, \\
&\mathbf{w}_2 = \mathbf{0}, \\
&\mathbf{w}_3\cdot\mathbf{n}_1 = 0, \quad \mathbf{w}_3\cdot\mathbf{n}_3 = 1, \quad \mathbf{w}_3\cdot\mathbf{n}_4 = 0, \\
&\mathbf{w}_4\cdot\mathbf{n}_1 = 0, \quad \mathbf{w}_4\cdot\mathbf{n}_3 = 0, \quad \mathbf{w}_4\cdot\mathbf{n}_4 = 1,
\end{aligned}
$$

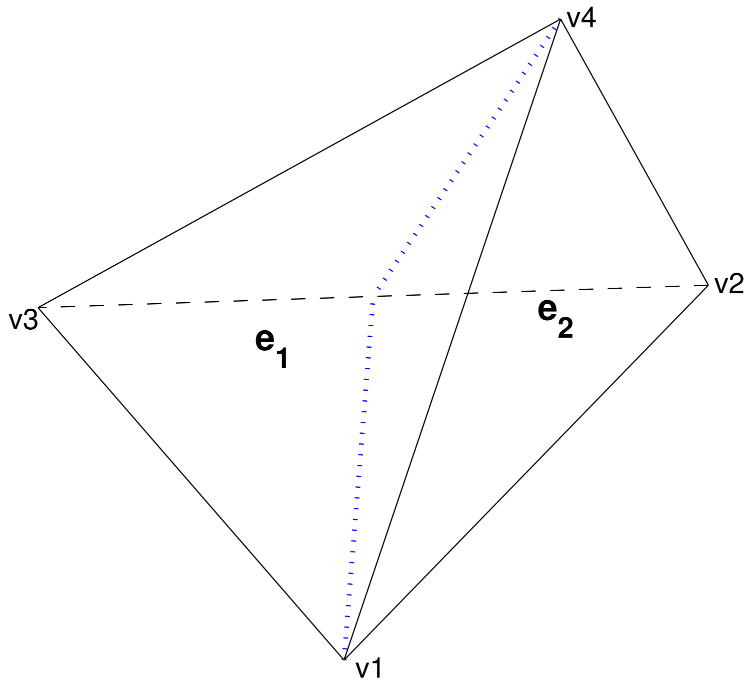

Figure 3.8: Tetrahedral mesh cell

and in e_2,

$$\begin{aligned}
&\mathbf{w}_1 \cdot \mathbf{n}_1 = 1, \quad \mathbf{w}_1 \cdot \mathbf{n}_2 = 0, \quad \mathbf{w}_1 \cdot \mathbf{n}_4 = 0, \\
&\mathbf{w}_2 \cdot \mathbf{n}_1 = 0, \quad \mathbf{w}_2 \cdot \mathbf{n}_2 = 1, \quad \mathbf{w}_2 \cdot \mathbf{n}_4 = 0, \\
&\mathbf{w}_3 = \mathbf{0}, \\
&\mathbf{w}_4 \cdot \mathbf{n}_1 = 0, \quad \mathbf{w}_4 \cdot \mathbf{n}_2 = 0, \quad \mathbf{w}_4 \cdot \mathbf{n}_4 = 1,
\end{aligned}$$

where $\mathbf{n}_i$ are unit outward normal vectors on Γ_i, $i = 1, 2, 3, 4$.

Then, PWCF basis can be represented as:

$$\mathbf{w}_1 = \begin{cases} \frac{\mathbf{n}_3 \times \mathbf{n}_4}{\mathbf{n}_1 \cdot (\mathbf{n}_3 \times \mathbf{n}_4)} & \text{in } e_1, \\ \frac{\mathbf{n}_2 \times \mathbf{n}_4}{\mathbf{n}_1 \cdot (\mathbf{n}_2 \times \mathbf{n}_4)} & \text{in } e_2. \end{cases} \tag{3.31}$$

$$\mathbf{w}_2 = \begin{cases} \mathbf{0} & \text{in } e_1, \\ \frac{\mathbf{n}_1 \times \mathbf{n}_4}{\mathbf{n}_2 \cdot (\mathbf{n}_1 \times \mathbf{n}_4)} & \text{in } e_2. \end{cases} \tag{3.32}$$

$$\mathbf{w}_3 = \begin{cases} \frac{\mathbf{n}_1 \times \mathbf{n}_4}{\mathbf{n}_3 \cdot (\mathbf{n}_1 \times \mathbf{n}_4)} & \text{in } e_1, \\ \mathbf{0} & \text{in } e_2. \end{cases} \tag{3.33}$$

$$\mathbf{w}_4 = \begin{cases} \frac{\mathbf{n}_1 \times \mathbf{n}_3}{\mathbf{n}_4 \cdot (\mathbf{n}_1 \times \mathbf{n}_3)} & \text{in } e_1, \\ \frac{\mathbf{n}_1 \times \mathbf{n}_2}{\mathbf{n}_4 \cdot (\mathbf{n}_1 \times \mathbf{n}_2)} & \text{in } e_2. \end{cases} \tag{3.34}$$

and matrices M_k, B_k and C_k:

$$M_k = \frac{vol}{2}\begin{pmatrix} ||\mathbf{w}_1||^2 & \mathbf{w}_1\cdot\mathbf{w}_2 & \mathbf{w}_1\cdot\mathbf{w}_3 & \mathbf{w}_1\cdot\mathbf{w}_4 \\ \mathbf{w}_2\cdot\mathbf{w}_1 & ||\mathbf{w}_2||^2 & \mathbf{w}_2\cdot\mathbf{w}_3 & \mathbf{w}_2\cdot\mathbf{w}_4 \\ \mathbf{w}_3\cdot\mathbf{w}_1 & \mathbf{w}_3\cdot\mathbf{w}_2 & ||\mathbf{w}_3||^2 & \mathbf{w}_3\cdot\mathbf{w}_4 \\ \mathbf{w}_4\cdot\mathbf{w}_1 & \mathbf{w}_4\cdot\mathbf{w}_2 & \mathbf{w}_4\cdot\mathbf{w}_3 & ||\mathbf{w}_4||^2 \end{pmatrix}, \tag{3.35}$$

$$B_k = (-s_1, -s_2, -s_3, -s_4), \tag{3.36}$$

$$C_k = \mathrm{diag}\{s_1, s_2, s_3, s_4\}, \tag{3.37}$$

where vol denotes the volume of tetrahedral mesh cell E_k, s_i is the area of face Γ_i, $i = 1, \cdots, 4$.

Theorem 3.8. *Let S_k be the condensed matrix defined in (3.22) from PWCF method, then S_k can be represented as:*

$$S_k = \frac{1}{vol}\begin{pmatrix} s_1^2||\mathbf{n}_1||^2 & s_1s_2(\mathbf{n}_1\cdot\mathbf{n}_2) & s_1s_3(\mathbf{n}_1\cdot\mathbf{n}_3) & s_1s_4(\mathbf{n}_1\cdot\mathbf{n}_4) \\ s_2s_1(\mathbf{n}_2\cdot\mathbf{n}_1) & s_2^2||\mathbf{n}_2||^2 & s_2s_3(\mathbf{n}_2\cdot\mathbf{n}_3) & s_2s_4(\mathbf{n}_2\cdot\mathbf{n}_4) \\ s_3s_1(\mathbf{n}_3\cdot\mathbf{n}_1) & s_3s_2(\mathbf{n}_3\cdot\mathbf{n}_2) & s_3^2||\mathbf{n}_3||^2 & s_3s_4(\mathbf{n}_3\cdot\mathbf{n}_4) \\ s_4s_1(\mathbf{n}_4\cdot\mathbf{n}_1) & s_4s_2(\mathbf{n}_4\cdot\mathbf{n}_2) & s_4s_3(\mathbf{n}_4\cdot\mathbf{n}_3) & s_4^2||\mathbf{n}_4||^2 \end{pmatrix}. \tag{3.38}$$

Therefore, S_k is a singular M-matrix if and only if angle between any two faces is less than or equal to 90 degree.

To prove this theorem, we need to introduce some useful lemmas.

Lemma 3.9. *Let* $\mathbf{a}$*,* $\mathbf{b}$*,* $\mathbf{c}$ *be vectors in* $\mathbb{R}^3$*, then*

$$\mathbf{a} \times (\mathbf{b} \times \mathbf{c}) = (\mathbf{a} \cdot \mathbf{c})\mathbf{b} - (\mathbf{a} \cdot \mathbf{b})\mathbf{c}. \tag{3.39}$$

Lemma 3.10. *Let* $\mathbf{a}$*,* $\mathbf{b}$*,* $\mathbf{c}$ *be vectors in* $\mathbb{R}^3$*, then*

$$(\mathbf{a} \times \mathbf{b}) \cdot (\mathbf{c} \times \mathbf{d}) = (\mathbf{a} \cdot \mathbf{c})(\mathbf{b} \cdot \mathbf{d}) - (\mathbf{a} \cdot \mathbf{d})(\mathbf{b} \cdot \mathbf{c}). \tag{3.40}$$

Lemma 3.11. *Let* $\mathbf{a}$*,* $\mathbf{b}$*,* $\mathbf{c}$ *be vectors in* $\mathbb{R}^3$*, then*

$$\Big[\mathbf{a}\cdot(\mathbf{b}\times\mathbf{c})\Big]^2 = ||\mathbf{a}||^2||\mathbf{b}\times\mathbf{c}||^2 - (\mathbf{a}\cdot\mathbf{b})\Big[(\mathbf{b}\times\mathbf{c})\cdot(\mathbf{a}\times\mathbf{c})\Big] + (\mathbf{a}\cdot\mathbf{c})\Big[(\mathbf{b}\times\mathbf{c})\cdot(\mathbf{a}\times\mathbf{b})\Big]. \tag{3.41}$$

Lemma 3.12. *Let* $\mathbf{a}$*,* $\mathbf{b}$*,* $\mathbf{c}$*,* $\mathbf{d}$ *be vectors in* $\mathbb{R}^3$*, then*

$$\begin{aligned} &\Big[\mathbf{a} \cdot (\mathbf{c} \times \mathbf{d})\Big] * \Big[\mathbf{b} \cdot (\mathbf{c} \times \mathbf{d})\Big] \\ =&(\mathbf{a} \cdot \mathbf{b})||\mathbf{c} \times \mathbf{d}||^2 - (\mathbf{a} \cdot \mathbf{c})\Big[(\mathbf{c} \times \mathbf{d}) \cdot (\mathbf{b} \times \mathbf{d})\Big] + (\mathbf{a} \cdot \mathbf{d})\Big[(\mathbf{c} \times \mathbf{d}) \cdot (\mathbf{b} \times \mathbf{c})\Big] \\ =&(\mathbf{a} \cdot \mathbf{b})||\mathbf{c} \times \mathbf{d}||^2 - (\mathbf{b} \cdot \mathbf{c})\Big[(\mathbf{c} \times \mathbf{d}) \cdot (\mathbf{a} \times \mathbf{d})\Big] + (\mathbf{b} \cdot \mathbf{d})\Big[(\mathbf{c} \times \mathbf{d}) \cdot (\mathbf{a} \times \mathbf{c})\Big]. \end{aligned} \tag{3.42}$$

Lemma 3.13. *The inverse of matrix* M_k *defined in (3.35) is:*

$$M_k^{-1} = \frac{1}{vol}\begin{pmatrix} ||\mathbf{n}_1||^2 & \mathbf{n}_1\cdot\mathbf{n}_2 & \mathbf{n}_1\cdot\mathbf{n}_3 & \mathbf{n}_1\cdot\mathbf{n}_4 \\ \mathbf{n}_2\cdot\mathbf{n}_1 & ||\mathbf{n}_2||^2+\frac{(\mathbf{n}_2\cdot(\mathbf{n}_1\times\mathbf{n}_4))^2}{||\mathbf{n}_1\times\mathbf{n}_4||^2} & \mathbf{n}_2\cdot\mathbf{n}_3-\frac{(\mathbf{n}_2\cdot(\mathbf{n}_1\times\mathbf{n}_4))(\mathbf{n}_3\cdot(\mathbf{n}_1\times\mathbf{n}_4))}{||\mathbf{n}_1\times\mathbf{n}_4||^2} & \mathbf{n}_2\cdot\mathbf{n}_4 \\ \mathbf{n}_3\cdot\mathbf{n}_1 & \mathbf{n}_3\cdot\mathbf{n}_2-\frac{(\mathbf{n}_3\cdot(\mathbf{n}_1\times\mathbf{n}_4))(\mathbf{n}_2\cdot(\mathbf{n}_1\times\mathbf{n}_4))}{||\mathbf{n}_1\times\mathbf{n}_4||^2} & ||\mathbf{n}_3||^2+\frac{(\mathbf{n}_3\cdot(\mathbf{n}_1\times\mathbf{n}_4))^2}{||\mathbf{n}_1\times\mathbf{n}_4||^2} & \mathbf{n}_3\cdot\mathbf{n}_4 \\ \mathbf{n}_4\cdot\mathbf{n}_1 & \mathbf{n}_4\cdot\mathbf{n}_2 & \mathbf{n}_4\cdot\mathbf{n}_3 & ||\mathbf{n}_4||^2 \end{pmatrix}. \tag{3.43}$$

Lemma 3.14.

$$s_2\Big[\mathbf{n}_2 \cdot (\mathbf{n}_1 \times \mathbf{n}_4)\Big] = -s_3\Big[\mathbf{n}_3 \cdot (\mathbf{n}_1 \times \mathbf{n}_4)\Big]. \tag{3.44}$$

Proof of Theorm 3.8. Since

$$M^{-1}B^T = \frac{1}{vol}\begin{pmatrix} 0 \\ \left\{\frac{2\Big[\mathbf{n}_2\cdot(\mathbf{n}_1\times\mathbf{n}_4)\Big]\Big[\mathbf{n}_3\cdot(\mathbf{n}_1\times\mathbf{n}_4)\Big]}{||\mathbf{n}_1\times\mathbf{n}_4||^2}\right\}s_3 \\ \left\{\frac{2\Big[\mathbf{n}_2\cdot(\mathbf{n}_1\times\mathbf{n}_4)\Big]\Big[\mathbf{n}_3\cdot(\mathbf{n}_1\times\mathbf{n}_4)\Big]}{||\mathbf{n}_1\times\mathbf{n}_4||^2}\right\}s_2 \\ 0 \end{pmatrix}, \tag{3.45}$$

$$BM^{-1}B^T = -\frac{4}{vol}\left\{\frac{\Big[\mathbf{n}_2\cdot(\mathbf{n}_1\times\mathbf{n}_4)\Big]\Big[\mathbf{n}_3\cdot(\mathbf{n}_1\times\mathbf{n}_4)\Big]}{||\mathbf{n}_1\times\mathbf{n}_4||^2}\right\}s_2s_3, \tag{3.46}$$

$$\begin{aligned} &M^{-1}B^T(BM^{-1}B^T)^{-1}BM^{-1} \\ =&\frac{1}{vol}\begin{pmatrix} 0 & 0 & 0 & 0 \\ 0 & \frac{\Big[\mathbf{n}_2\cdot(\mathbf{n}_1\times\mathbf{n}_4)\Big]^2}{||\mathbf{n}_1\times\mathbf{n}_4||^2} & -\frac{\Big[\mathbf{n}_2\cdot(\mathbf{n}_1\times\mathbf{n}_4)\Big]\Big[\mathbf{n}_3\cdot(\mathbf{n}_1\times\mathbf{n}_4)\Big]}{||\mathbf{n}_1\times\mathbf{n}_4||^2} & 0 \\ 0 & -\frac{\Big[\mathbf{n}_2\cdot(\mathbf{n}_1\times\mathbf{n}_4)\Big]\Big[\mathbf{n}_3\cdot(\mathbf{n}_1\times\mathbf{n}_4)\Big]}{||\mathbf{n}_1\times\mathbf{n}_4||^2} & \frac{\Big[\mathbf{n}_3\cdot(\mathbf{n}_1\times\mathbf{n}_4)\Big]^2}{||\mathbf{n}_1\times\mathbf{n}_4||^2} & 0 \\ 0 & 0 & 0 & 0 \end{pmatrix}, \end{aligned} \tag{3.47}$$

$$M^{-1} - M^{-1}B^T(BM^{-1}B^T)^{-1}BM^{-1}$$
$$= \frac{1}{vol}\begin{pmatrix} ||\mathbf{n}_1||^2 & \mathbf{n}_1\cdot\mathbf{n}_2 & \mathbf{n}_1\cdot\mathbf{n}_3 & \mathbf{n}_1\cdot\mathbf{n}_4 \\ \mathbf{n}_2\cdot\mathbf{n}_1 & ||\mathbf{n}_2||^2 & \mathbf{n}_2\cdot\mathbf{n}_3 & \mathbf{n}_2\cdot\mathbf{n}_4 \\ \mathbf{n}_3\cdot\mathbf{n}_1 & \mathbf{n}_3\cdot\mathbf{n}_2 & ||\mathbf{n}_3||^2 & \mathbf{n}_3\cdot\mathbf{n}_4 \\ \mathbf{n}_4\cdot\mathbf{n}_1 & \mathbf{n}_4\cdot\mathbf{n}_2 & \mathbf{n}_4\cdot\mathbf{n}_3 & ||\mathbf{n}_4||^2 \end{pmatrix}, \tag{3.48}$$

so,

$$S = CM^{-1}\Big[M - B^T(BM^{-1}B^T)^{-1}B\Big]M^{-1}C^T$$
$$= \frac{1}{vol}\begin{pmatrix} s_1^2||\mathbf{n}_1||^2 & s_1s_2(\mathbf{n}_1\cdot\mathbf{n}_2) & s_1s_3(\mathbf{n}_1\cdot\mathbf{n}_3) & s_1s_4(\mathbf{n}_1\cdot\mathbf{n}_4) \\ s_2s_1(\mathbf{n}_2\cdot\mathbf{n}_1) & s_2^2||\mathbf{n}_2||^2 & s_2s_3(\mathbf{n}_2\cdot\mathbf{n}_3) & s_2s_4(\mathbf{n}_2\cdot\mathbf{n}_4) \\ s_3s_1(\mathbf{n}_3\cdot\mathbf{n}_1) & s_3s_2(\mathbf{n}_3\cdot\mathbf{n}_2) & s_3^2||\mathbf{n}_3||^2 & s_3s_4(\mathbf{n}_3\cdot\mathbf{n}_4) \\ s_4s_1(\mathbf{n}_4\cdot\mathbf{n}_1) & s_4s_2(\mathbf{n}_4\cdot\mathbf{n}_2) & s_4s_3(\mathbf{n}_4\cdot\mathbf{n}_3) & s_4^2||\mathbf{n}_4||^2 \end{pmatrix}. \tag{3.49}$$

□

3.2.3 Equivalence of condensed matrices S_λ for PWCF and RT_0 methods

Consider the same diffusion problem (2.3) and same triangular mesh in 2D or tetrahedral mesh in 3D descibed in previous sections. Instead of PWCF method, we apply RT_0 method for this problem. Next, we will show that based on the computation of condensed matrix S_λ for 3D tetrahedral cells (2D triangular cell case was already investigated in [43]), the following theorem holds:

Theorem 3.15. *The condensed matrices S_λ for PWCF and RT_0 methods coincide.*

Remark 3.16. *This theorem is an important observation. In [37], it is proved that the discrete LBB condition for RT_0 method is equivalent to say the minimal eigenvalue α_h for the problem*

$$\begin{cases} M\bar{w} - B^T\bar{p} & = 0 \\ \\ B\bar{w} & = \alpha_h M_p \bar{p} \end{cases} \tag{3.50}$$

has a lower bound. It is also proved that it does have lower bound for RT_0 method. As a result, Theorem 3.15 guarantees that the discrete LBB condition for PWCF method holds as well, and it is essential when investigating error estimation for PWCF method.

Remark 3.17. *The condensed matrix S_λ is independent of basis choice on $\boldsymbol{RT}_0(K)$ space. The reason is that suppose $\{\mathbf{w}_i\}$, $\{\mathbf{e}_i\}$ are two sets of basis for $\boldsymbol{RT}_0(K)$, then there exists a linear transformation P such that*

$$P(\mathbf{w}_1, \mathbf{w}_2, \mathbf{w}_3, \mathbf{w}_4) = (\mathbf{e}_1, \mathbf{e}_2, \mathbf{e}_3, \mathbf{e}_4). \tag{3.51}$$

As a result, for matrices M, B, C for two different basis, we have

$$\begin{aligned} M_e &= P^T M_w P, \\ B_e &= B_w P, \\ C_e &= C_w P. \end{aligned} \tag{3.52}$$

Hence,

$$
\begin{aligned}
S_e &= C_e M_e^{-1}[M_e - B_e^T(B_e M_e^{-1} B_e^T)^{-1} B_e] M_e^{-1} C_e^T \\
&= C_w P P^{-1} M_w^{-1} P^{-T}[P^T M_w P - P^T B_w^T (B_w P P^{-1} M_w^{-1} P^{-T} P^T B_w)^{-1} B_w P] P^{-1} M_w^{-1} P^{-T} P^T C_w^T \\
&= C_w M_w^{-1}[M_w - B_w^T(B_w M_w^{-1} B_w^T)^{-1} B_w] M_w^{-1} C_w^T \\
&= S_k.
\end{aligned}
\tag{3.53}
$$

Proof of Theorm 3.15. Since S_λ is independent of basis choice on $\mathbf{RT}_0(K)$ space, instead of using classical basis $\{\mathbf{w}_i\}$, s.t., $\mathbf{w}_i \cdot \mathbf{n}_j = \delta_{ij}$ on Γ_j, we use the following basis:

$$
\mathbf{e}_1 = \begin{pmatrix} 1 \\ 0 \\ 0 \end{pmatrix}, \quad \mathbf{e}_2 = \begin{pmatrix} 0 \\ 1 \\ 0 \end{pmatrix}, \quad \mathbf{e}_3 = \begin{pmatrix} 0 \\ 0 \\ 1 \end{pmatrix}, \quad \mathbf{e}_4 = \begin{pmatrix} x_1 - x_1^c \\ x_2 - x_2^c \\ x_3 - x_3^c \end{pmatrix}, \tag{3.54}
$$

where $\mathbf{x}^c = (x_1^c, x_2^c, x_3^c)^T$ is the barycenter of E_k, i.e.,

$$x_1^c = \frac{1}{|E_k|}\int_{E_k} x_1 dx, \tag{3.55}$$

$$x_2^c = \frac{1}{|E_k|}\int_{E_k} x_2 dx, \tag{3.56}$$

$$x_3^c = \frac{1}{|E_k|}\int_{E_k} x_3 dx. \tag{3.57}$$

The matrix M_k now becomes a diagonal matrix and can be easily inverted:

$$M_k = vol. \begin{pmatrix} 1 & 0 & 0 & 0 \\ 0 & 1 & 0 & 0 \\ 0 & 0 & 1 & 0 \\ 0 & 0 & 0 & \frac{1}{vol}\int_{E_k}(x_1 - x_1^c)^2 + (x_2 - x_2^c)^2 + (x_3 - x_3^c)^2 dx \end{pmatrix}, \tag{3.58}$$

where $vol = |E_k|$. The corresponding B_k and C_k become:

$$\begin{aligned} B_k &= -\left(\int_{E_k} \nabla \cdot \mathbf{e}_1 dx, \quad \int_{E_k} \nabla \cdot \mathbf{e}_2 dx, \quad \int_{E_k} \nabla \cdot \mathbf{e}_3 dx, \quad \int_{E_k} \nabla \cdot \mathbf{e}_4 dx \right) \\ &= -(0, 0, 0, 3vol), \end{aligned} \tag{3.59}$$

$$\begin{aligned} C_k &= \begin{pmatrix} \int_{\Gamma_1} \mathbf{e}_1 \cdot \mathbf{n}_1 dx & \int_{\Gamma_1} \mathbf{e}_2 \cdot \mathbf{n}_1 dx & \int_{\Gamma_1} \mathbf{e}_3 \cdot \mathbf{n}_1 dx & \int_{\Gamma_1} \mathbf{e}_4 \cdot \mathbf{n}_1 dx \\ \int_{\Gamma_2} \mathbf{e}_1 \cdot \mathbf{n}_2 dx & \int_{\Gamma_2} \mathbf{e}_2 \cdot \mathbf{n}_2 dx & \int_{\Gamma_2} \mathbf{e}_3 \cdot \mathbf{n}_2 dx & \int_{\Gamma_2} \mathbf{e}_4 \cdot \mathbf{n}_2 dx \\ \int_{\Gamma_3} \mathbf{e}_1 \cdot \mathbf{n}_3 dx & \int_{\Gamma_3} \mathbf{e}_2 \cdot \mathbf{n}_3 dx & \int_{\Gamma_3} \mathbf{e}_3 \cdot \mathbf{n}_3 dx & \int_{\Gamma_3} \mathbf{e}_4 \cdot \mathbf{n}_3 dx \\ \int_{\Gamma_4} \mathbf{e}_1 \cdot \mathbf{n}_4 dx & \int_{\Gamma_4} \mathbf{e}_2 \cdot \mathbf{n}_4 dx & \int_{\Gamma_4} \mathbf{e}_3 \cdot \mathbf{n}_4 dx & \int_{\Gamma_4} \mathbf{e}_4 \cdot \mathbf{n}_4 dx \end{pmatrix} \\ &= \begin{pmatrix} |\Gamma_1| n_{1,x_1} & |\Gamma_1| n_{1,x_2} & |\Gamma_1| n_{1,x_3} & \int_{\Gamma_1} n_{1,x_1}(x_1 - x_1^c) + n_{1,x_2}(x_2 - x_2^c) + n_{1,x_3}(x_3 - x_3^c) dx \\ |\Gamma_2| n_{2,x_1} & |\Gamma_2| n_{2,x_2} & |\Gamma_2| n_{2,x_3} & \int_{\Gamma_2} n_{2,x_1}(x_1 - x_1^c) + n_{2,x_2}(x_2 - x_2^c) + n_{2,x_3}(x_3 - x_3^c) dx \\ |\Gamma_3| n_{3,x_1} & |\Gamma_3| n_{3,x_2} & |\Gamma_3| n_{3,x_3} & \int_{\Gamma_3} n_{3,x_1}(x_1 - x_1^c) + n_{3,x_2}(x_2 - x_2^c) + n_{3,x_3}(x_3 - x_3^c) dx \\ |\Gamma_4| n_{4,x_1} & |\Gamma_4| n_{4,x_2} & |\Gamma_4| n_{4,x_3} & \int_{\Gamma_4} n_{4,x_1}(x_1 - x_1^c) + n_{4,x_2}(x_2 - x_2^c) + n_{4,x_3}(x_3 - x_3^c) dx \end{pmatrix}, \end{aligned} \tag{3.60}$$

where $\mathbf{n}_i = (n_{i,x_1}, n_{i,x_2}, n_{i,x_3})^T$, $i = 1, 2, 3, 4$.

Simple calculation leads to:

$$G_k = M_k^{-1} B_k^T = (0, 0, 0, -\frac{3.vol}{\int_{E_k}(x_1 - x_1^c)^2 + (x_2 - x_2^c)^2 + (x_3 - x_3^c)^2 dx})^T, \tag{3.61}$$

$$g_k = B_k M_k^{-1} B_k^T = \frac{9.vol^2}{\int_{E_k}(x_1 - x_1^c)^2 + (x_2 - x_2^c)^2 + (x_3 - x_3^c)^2 dx}, \tag{3.62}$$

$$H_k = M_k^{-1} - \frac{1}{g_k} G_k G_k^T = \frac{1}{vol}.\mathrm{diag}\{1, 1, 1, 0\}, \tag{3.63}$$

and the condensed matrix $S_k = C_k H_k C_k^T$ with entries:

$$(S_k)_{i,j} = \frac{1}{vol}|\Gamma_i||\Gamma_j|\mathbf{n}_i \cdot \mathbf{n}_j, \qquad i, j = 1, 2, 3, 4. \tag{3.64}$$

This matrix is exactly same as the one from PWCF method in (3.38). Similarly, we can reach the same conclusion for 2D triangular cells. □

Hence, the monotone condition on condensed matrix for RT_0 methods is:

Theorem 3.18. *S_{λ,RT_0} is a singular M-matrix if and only if angle between any two sides (for triangles) or faces (for tetrahedrons) is less than or equal to 90 degree.*

Remark 3.19. *Since the condensed matrices for $PWCF$ and RT_0 are the same, why do we find a new method instead of using the classical one? What are the advantages for $PWCF$ method over RT_0 method? There are mainly two reasons:*

1. *The matrix M is much easier to compute for $PWCF$ than RT_0.*

2. *For some meshes, matrix M from RT_0 is much more ill-conditioned than the one from $PWCF$. Consider two types of irregular tetrahedral cells in Figure 3.9 and Figure 3.10. By numerical experiment, for cells of type 1, when $\frac{h_z}{h_{xy}} = 10^2$, $cond(M_{PWCF}) = 6.8546$ and $cond(M_{RT_0}) = 5.33 \times 10^3$; for cells of type 2, when $\frac{h_z}{h_{xy}} = 10^{-2}$, $cond(M_{PWCF}) = 4.5 \times 10^4$ and $cond(M_{RT_0}) = 1.5 \times 10^4$. Same discussion on triangular cells continues in next section when investigating error estimation.*

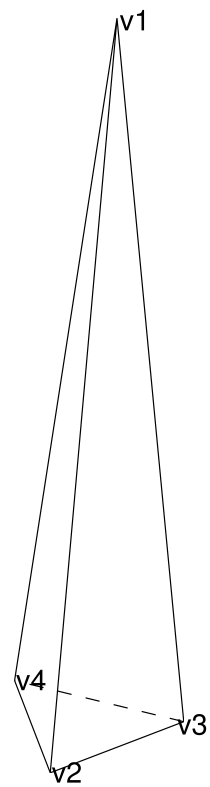

Figure 3.9: Irregular tetrahedral cell of type 1, too tall

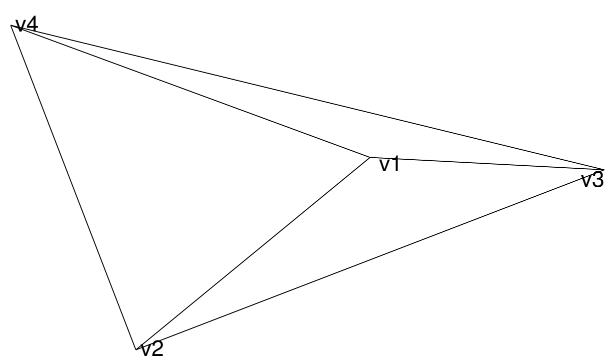

Figure 3.10: Irregular tetrahedral cell of type 2, too flat

3.2.4 Condensed matrix $S_{p,\lambda}$

Let us consider the condensed matrix on p and λ:

$$S_{p,\lambda} = \begin{pmatrix} BM^{-1}B^T & BM^{-1}C^T \\ CM^{-1}B^T & CM^{-1}C^T \end{pmatrix}. \tag{3.65}$$

Next we will derive the formula of this matrix for both PWCF and RT_0 methods.

3.2.4.1 PWCF method

Let

$$\alpha = \frac{\mathbf{n}_2 \cdot (\mathbf{n}_1 \times \mathbf{n}_4)}{||\mathbf{n}_1 \times \mathbf{n}_4||}, \tag{3.66}$$

$$\beta = \frac{\mathbf{n}_3 \cdot (\mathbf{n}_1 \times \mathbf{n}_4)}{||\mathbf{n}_1 \times \mathbf{n}_4||}, \tag{3.67}$$

then from (3.46), (3.45) and (3.43), we have

$$BM^{-1}B^T = -\frac{4\alpha\beta s_2 s_3}{vol}, \tag{3.68}$$

and

$$BM^{-1}C^T = \frac{1}{vol}\begin{pmatrix} 0, & 2\alpha\beta s_2 s_3, & 2\alpha\beta s_2 s_3, & 0 \end{pmatrix}, \tag{3.69}$$

and

$$
\begin{aligned}
&CM^{-1}C^T \\
=&\frac{1}{vol}\begin{pmatrix}
s_1^2||\mathbf{n}_1||^2 & s_1s_2(\mathbf{n}_1\cdot\mathbf{n}_2) & s_1s_3(\mathbf{n}_1\cdot\mathbf{n}_3) & s_1s_4(\mathbf{n}_1\cdot\mathbf{n}_4) \\
s_2s_1(\mathbf{n}_2\cdot\mathbf{n}_1) & s_2^2(||\mathbf{n}_2||^2+\alpha^2) & s_2s_3(\mathbf{n}_2\cdot\mathbf{n}_3-\alpha\beta) & s_2s_4(\mathbf{n}_2\mathbf{n}_4) \\
s_3s_1(\mathbf{n}_3\cdot\mathbf{n}_1) & s_3s_2(\mathbf{n}_3\cdot\mathbf{n}_2-\alpha\beta) & s_3^2(||\mathbf{n}_3||^2+\beta^2) & s_3s_4(\mathbf{n}_3\cdot\mathbf{n}_4) \\
s_4s_1(\mathbf{n}_4\cdot\mathbf{n}_1) & s_4s_2(\mathbf{n}_4\cdot\mathbf{n}_2) & s_4s_3(\mathbf{n}_4\cdot\mathbf{n}_3) & s_4^2||\mathbf{n}_4||^2
\end{pmatrix}.
\end{aligned}
\tag{3.70}
$$

3.2.4.2 RT_0 method

Let

$$\eta = \int_{E_k} (x_1 - x_1^c)^2 + (x_2 - x_2^c)^2 + (x_3 - x_3^c)^2 dx, \tag{3.71}$$

then from (3.61),

$$BM^{-1}B^T = \frac{9vol^2}{\eta}. \tag{3.72}$$

Before exploring the explict representation for other blocks, we need first take a deeper investigation on matrix C_k in (3.60). The last column of C_k is composed by $\int_{\Gamma_i} \mathbf{e}_4.\mathbf{n}_i dx$, where

$$\mathbf{e}_4 = \begin{pmatrix} x_1 - x_1^c \\ x_2 - x_2^c \\ x_3 - x_3^c \end{pmatrix}. \tag{3.73}$$

For any point on face Γ_i, $\mathbf{e}_4.\mathbf{n}_i = \text{dist}(\mathbf{x}^c, \Gamma_i)$, so $\int_{\Gamma_i} \mathbf{e}_4.\mathbf{n}_i dx$ is equal to 3 times the volume of subtetrahedrons whose vertexes are $\mathbf{x}^c$ and three vertexes on Γ_i. One important property for barycenter $\mathbf{x}^c$ is that the the volumes of four subtetrahedrons obtained by connecting $\mathbf{x}^c$ and 4 faces Γ_i are equal, therefore,

$$\int_{\Gamma_1} \mathbf{e}_4 \cdot \mathbf{n}_1 dx = \int_{\Gamma_2} \mathbf{e}_4 \cdot \mathbf{n}_2 dx = \int_{\Gamma_3} \mathbf{e}_4 \cdot \mathbf{n}_3 dx = \int_{\Gamma_4} \mathbf{e}_4 \cdot \mathbf{n}_4 dx. \tag{3.74}$$

Another important equation is:

$$\sum_{i=1}^{4} \int_{\Gamma_i} \mathbf{e}_4 \cdot \mathbf{n}_i dx = \int_E \nabla \cdot \mathbf{e}_4 dx = 3.vol, \tag{3.75}$$

hence,

$$\int_{\Gamma_i} \mathbf{e}_4 \cdot \mathbf{n}_i dx = \frac{3vol}{4}, \qquad i = 1, 2, 3, 4. \tag{3.76}$$

Let us come back to the calculation of $S_{p,\lambda}$. It follows from (3.61) that

$$BM^{-1}C^T = \left(-\tfrac{9.vol^2}{4\eta}, \quad -\tfrac{9.vol^2}{4\eta}, \quad -\tfrac{9.vol^2}{4\eta}, \quad -\tfrac{9.vol^2}{4\eta} \right), \tag{3.77}$$

and

$$\begin{aligned} CM^{-1}C^T =& \frac{1}{vol} \begin{pmatrix} s_1^2||\mathbf{n}_1||^2 & s_1 s_2(\mathbf{n}_1 \cdot \mathbf{n}_2) & s_1 s_3(\mathbf{n}_1 \cdot \mathbf{n}_3) & s_1 s_4(\mathbf{n}_1 \cdot \mathbf{n}_4) \\ s_2 s_1(\mathbf{n}_2 \cdot \mathbf{n}_1) & s_2^2||\mathbf{n}_2||^2 & s_2 s_3(\mathbf{n}_2 \cdot \mathbf{n}_3) & s_2 s_4(\mathbf{n}_2 \mathbf{n}_4) \\ s_3 s_1(\mathbf{n}_3 \cdot \mathbf{n}_1) & s_3 s_2(\mathbf{n}_3 \cdot \mathbf{n}_2) & s_3^2||\mathbf{n}_3||^2 & s_3 s_4(\mathbf{n}_3 \cdot \mathbf{n}_4) \\ s_4 s_1(\mathbf{n}_4 \cdot \mathbf{n}_1) & s_4 s_2(\mathbf{n}_4 \cdot \mathbf{n}_2) & s_4 s_3(\mathbf{n}_4 \cdot \mathbf{n}_3) & s_4^2||\mathbf{n}_4||^2 \end{pmatrix} \\ &+ \frac{1}{vol} \begin{pmatrix} \frac{9.vol^3}{16\eta} & \frac{9.vol^3}{16\eta} & \frac{9.vol^3}{16\eta} & \frac{9.vol^3}{16\eta} \\ \frac{9.vol^3}{16\eta} & \frac{9.vol^3}{16\eta} & \frac{9.vol^3}{16\eta} & \frac{9.vol^3}{16\eta} \\ \frac{9.vol^3}{16\eta} & \frac{9.vol^3}{16\eta} & \frac{9.vol^3}{16\eta} & \frac{9.vol^3}{16\eta} \\ \frac{9.vol^3}{16\eta} & \frac{9.vol^3}{16\eta} & \frac{9.vol^3}{16\eta} & \frac{9.vol^3}{16\eta} \end{pmatrix}. \end{aligned} \tag{3.78}$$

3.2.5 Monotonicity for KR method

Theorem 3.20. *KR methods based on RT_0 or PWCF discretization are monotone if all tetrahedrons from partitions of polyhedral cells satisfy the geometric condition in Theorem 3.8 and Theorem 3.18, i.e., the angle between any two faces is less than or equal to 90 degree.*

Remark 3.21. *With this property, we can apply KR methods based on RT_0 or PWCF methods on many types of polyhedral meshes, with keeping the monotonicity. We show some examples on cube, pyramid and prism from Figure 3.11 to Figure 3.13.*

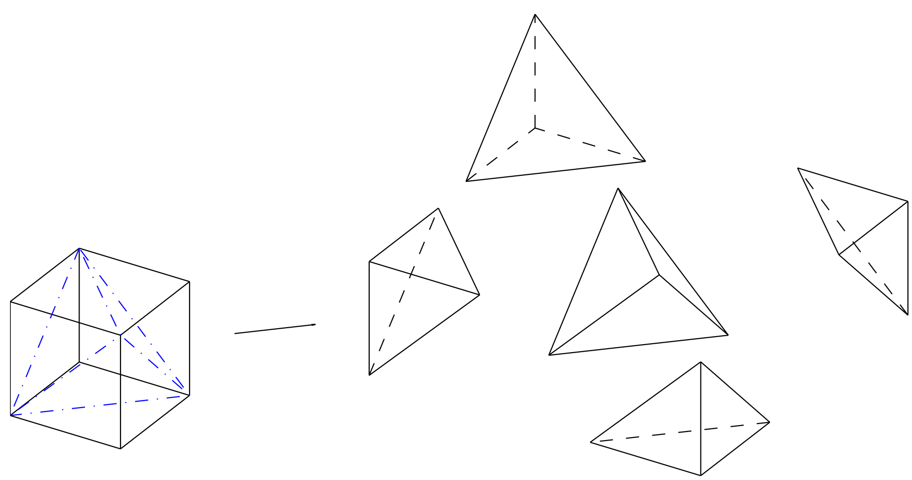

Figure 3.11: Divide a cube into five "good" subtetrahedrons

3.2.6 Monotonicity of condensed system

Now, we already obtained the monotone condition of S_λ from PWCF method for triangular and tetrahedral meshes. By the property of monotone matrix, it follows that $\bar{\phi} \geq 0 \Rightarrow \bar{\lambda} \geq 0$. However, we are more interested in the relationship between

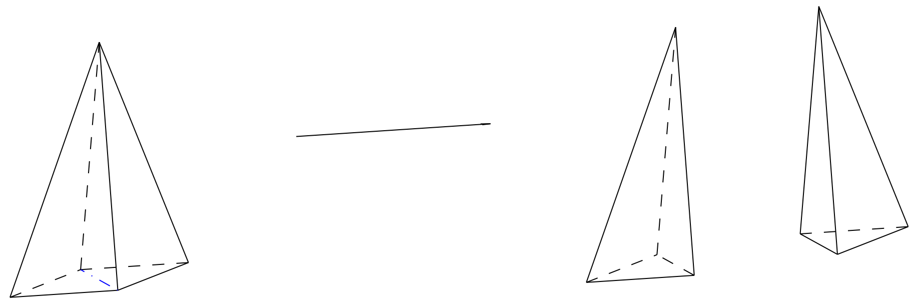

Figure 3.12: Divide a pyramid into two "good" subtetrahedrons

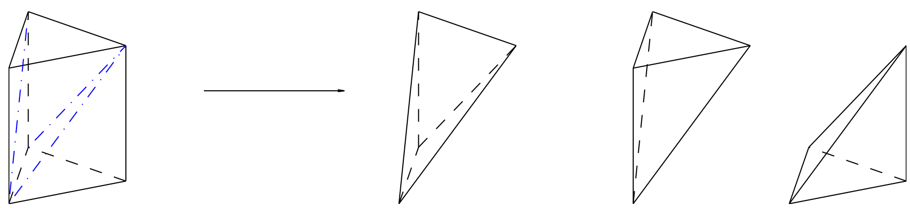

Figure 3.13: Divide a prism into three "good" subtetrahedrons

$\bar{F}$ and $\bar{\lambda}$. Let us investigate the equality (3.21) again:

$$C_k M_k^{-1} B_k^T (B_k M_k^{-1} B_k^T)^{-1} = -(1-r, 0, r)^T \qquad \text{for 2D triangular cells,} \tag{3.79}$$

$$C_k M_k^{-1} B_k^T (B_k M_k^{-1} B_k^T)^{-1} = -(0, \frac{1}{2}, \frac{1}{2}, 0)^T \qquad \text{for 3D tetrahedral cells.} \tag{3.80}$$

When $\bar{F} \leq 0$,

$$\begin{aligned} \bar{\phi} &= \sum_{i=1}^{m} N_i C_i M_i^{-1} B_i^T (B_i M_i^{-1} B_i^T)^{-1} F_i \\ &= \sum_{i=1}^{m} N_i \Big(-(1-r)F_i, 0, -rF_i \Big)^T \geq 0 \qquad \text{in 2D,} \end{aligned} \tag{3.81}$$

and

$$\bar{\phi} = \sum_{i=1}^{m} N_i \Big(0, -\frac{1}{2F_i}, -\frac{1}{2F_i}, 0 \Big)^T \geq 0 \qquad \text{in 3D.} \tag{3.82}$$

By the monotonicity property of S_λ in (3.17), $\bar{\lambda} \geq 0$ holds. Hence, we reach to the first conclusion:

Theorem 3.22. *If a mesh has all cells satisfying the conditions in Theorem 3.7 or Theorem 3.8, and if $f \geq 0$ in Ω, then $\bar{\lambda}$ obtained from system (3.14) by PWCF method is also non-negative, i.e.,*

$$\bar{F} \leq 0 \Rightarrow \bar{\lambda} \geq 0. \tag{3.83}$$

3.2.7 Monotonicity of original system

Can we get a similar conclusion of (3.83) for $\bar{p}$, i.e., $\bar{F} \leq 0 \Rightarrow \bar{p} \geq 0$? To answer this question, we need to explore the system (3.16). The first equation in (3.16) is:

$$BM^{-1}B^T\bar{p} = -\bar{F} - BM^{-1}C^T\bar{\lambda}. \tag{3.84}$$

By representing B and C in (3.15), we get:

$$\begin{pmatrix} B_1M_1^{-1}B_1^T & & \\ & \ddots & \\ & & B_mM_m^{-1}B_m^T \end{pmatrix} \begin{pmatrix} p_1 \\ \vdots \\ p_m \end{pmatrix} = \begin{pmatrix} -F_1 - B_1M_1^{-1}C_1^TN_1^T\bar{\lambda} \\ \vdots \\ -F_m - B_mM_m^{-1}C_m^TN_m^T\bar{\lambda} \end{pmatrix}, \tag{3.85}$$

or equally,

$$B_kM_k^{-1}B_k^Tp_k = -F_k - B_kM_k^{-1}C_k^TN_k^T\bar{\lambda}, \qquad \forall 1 \leq k \leq m. \tag{3.86}$$

For 2D triangular cell, $B_k M_k^{-1} B_k^T = \frac{1}{r(1-r)} > 0$ and $B_k M_k^{-1} C_k^T = (-\frac{1}{r}, 0, -\frac{1}{1-r})$ for all k. For 3D tetrahedral cell, $B_k M_k^{-1} B_k^T > 0$ by (3.46) and Lemma 3.14, $B_k M_k^{-1} C_k^T = (0, \mu, \mu, 0)$, where

$$\mu = \frac{1}{vol} * \frac{2s_2 s_3 [\mathbf{n}_2 \cdot (\mathbf{n}_1 \times \mathbf{n}_4)][\mathbf{n}_3 \cdot (\mathbf{n}_1 \times \mathbf{n}_4)]}{||\mathbf{n}_1 \times \mathbf{n}_4||^2} < 0, \tag{3.87}$$

therefore, if $\bar{F} \leq 0$, by Theorem 3.22 and above equalities, $\bar{\lambda} \geq 0$ and $B_k M_k^{-1} C_k^T N_k^T \bar{\lambda} \geq 0$. Then (3.86) implies:

$$p_k \geq 0, \qquad \forall 1 \leq k \leq m. \tag{3.88}$$

Theorem 3.23. *By applying PWCF method on 2D triangular mesh or 3D tetrahedral mesh, if mesh cells satisfy conditions in Theorem 3.7 or Theorem 3.8, then the following monotone property holds:*

$$f \geq 0 \ (or\ \bar{F} \leq 0) \Rightarrow \bar{\lambda} \geq 0 \text{ and } \bar{p} \geq 0 \qquad \text{in system } (3.14). \tag{3.89}$$

3.3 Error estimation for triangular mesh

Consider the diffusion equation (2.1) with diffusion tension $K = I$ and $g_D \equiv 0$. If we apply mixed PWCF method, we can get the following linear system:

$$\begin{cases} M\bar{u}_h + B^T \bar{p}_h & = 0 \\ B\bar{u}_h & = \bar{F}_h \end{cases} \tag{3.90}$$

It is shown by Yu. Kuznetsov in [40] that the error estimate on flux $\mathbf{u}_h$ holds:

$$||\mathbf{u}_h - \mathbf{u}^*||_2 \leq 2||\mathbf{u}^*_{h,int} - \mathbf{u}^*||_2, \tag{3.91}$$

where $\mathbf{u}^*$ is the exact solution and

$$\mathbf{u}^*_{h,int} \cdot \mathbf{n}_{kl} = \frac{1}{|\Gamma_{kl}|} \int_{\Gamma_{kl}} \mathbf{u}^* \cdot \mathbf{n} ds, \qquad k < l. \tag{3.92}$$

Next, we start investigating error estimate on p_h for triangular meshes.

3.3.1 Relation between errors on $\mathbf{u}_h$ and on $\bar{p}_h$

In Section 3.1, we showed that the exact solution $(\mathbf{u}^*, p^*)$ of (2.3) satisfies (3.2). Define the bilinear functional

$$b(p, \mathbf{v}) = \sum_{k<l} |\Gamma_{kl}|(p_l - p_k)v_{kl}, \tag{3.93}$$

where $\mathbf{v} = \sum_{k<l} v_{kl}\mathbf{w}_{kl}$. Sum up all the integrations in all ω, we can get the system:

$$\begin{cases} \int_\Omega \mathbf{u}^* \cdot \mathbf{v} dx + b(p^*, \mathbf{v}) & = 0 \\ b(q, \mathbf{u}^*) & = F(q) \end{cases} \tag{3.94}$$

Let $\mathbf{u}^* = \mathbf{u}^*_{h,int} + \overrightarrow{\phi_h}$, then the previous system becomes:

$$\begin{cases} \int_\Omega \mathbf{u}^*_{h,int} \cdot \mathbf{v} dx + b(\bar{p}^*_{h,int}, \mathbf{v}) & = -\int_\Omega \overrightarrow{\phi_h}.\mathbf{v} dx \\ b(q, \mathbf{u}^*_{h,int}) & = F(q) \end{cases} \tag{3.95}$$

where $\bar{p}^*_{h,int}$ has components $p^*_{int,k}$ defined in E_k such that

$$p^*_{int,k} = \frac{1}{|\gamma_k|} \int_{\gamma_k} p^* ds. \tag{3.96}$$

By choosing proper basis of $\mathbf{v}$ (need to meet the same three requirements on $\mathbf{w}$) and q (constant over each mesh cell), we can derive a linear system:

$$\begin{cases} M\bar{u}^*_{h,int} + B^T \bar{p}^*_{h,int} & = \bar{\phi}_h \\ B\bar{u}^*_{h,int} & = \bar{F}_h \end{cases} \tag{3.97}$$

Matrices M and B in this system are exactly same as the ones in (3.90). By assuming

$$\bar{\psi}_h = \bar{u}^*_{h,int} - \bar{u}_h, \tag{3.98}$$

$$\bar{\varphi}_h = \bar{p}^*_{h,int} - \bar{p}_h, \tag{3.99}$$

$$\bar{\phi}_h = \bar{u}^* - \bar{u}^*_{h,int}, \tag{3.100}$$

and subtracting (3.90) from (3.97), we can get:

$$\begin{cases} M\bar{\psi}_h + B^T\bar{\varphi}_h &= \bar{\phi}_h \\ B\bar{\psi}_h &= 0 \end{cases} \tag{3.101}$$

The corresponding condensed system is:

$$BM^{-1}B^T\bar{\varphi}_h = BM^{-1}\bar{\phi}_h. \tag{3.102}$$

Let

$$M_p = \mathrm{diag}\{|E_1|, \cdots, |E_m|\}, \tag{3.103}$$

$$S = M_p^{-\frac{1}{2}}BM^{-1}B^TM_p^{-\frac{1}{2}}, \tag{3.104}$$

then (3.102) can be written as:

$$SM_p^{\frac{1}{2}}\bar{\varphi}_h = M_p^{-\frac{1}{2}}BM^{-1}\bar{\phi}_h. \tag{3.105}$$

Take inner product with $M_p^{\frac{1}{2}}\bar{\varphi}_h$ on both sides:

$$(SM_p^{\frac{1}{2}}\bar{\varphi}_h, M_p^{\frac{1}{2}}\bar{\varphi}_h) = (M_p^{-\frac{1}{2}}BM^{-1}\bar{\phi}_h, M_p^{\frac{1}{2}}\bar{\varphi}_h). \tag{3.106}$$

Let α_h be the smallest eigenvalue of matrix S, then:

$$\begin{aligned}\alpha_h||\bar{\varphi}_h||^2_{M_p} &= \alpha_h(M_p\bar{\varphi}_h, \bar{\varphi}_h)\\ &= \alpha_h(M_p^{\frac{1}{2}}\bar{\varphi}_h, M_p^{\frac{1}{2}}\bar{\varphi}_h)\\ &\leq (SM_p^{\frac{1}{2}}\bar{\varphi}_h, M_p^{\frac{1}{2}}\bar{\varphi}_h)\\ &= (M_p^{-\frac{1}{2}}BM^{-1}\bar{\phi}_h, M_p^{\frac{1}{2}}\bar{\varphi}_h)\\ &= (M^{-\frac{1}{2}}\bar{\phi}_h, M^{-\frac{1}{2}}B^TM_p^{-\frac{1}{2}}M_p^{\frac{1}{2}}\bar{\varphi}_h)\\ &\leq ||M^{-\frac{1}{2}}\bar{\phi}_h||_2||M^{-\frac{1}{2}}B^TM_p^{-\frac{1}{2}}M_p^{\frac{1}{2}}\bar{\varphi}_h||_2.\end{aligned} \tag{3.107}$$

Moreover, because

$$\begin{aligned}||M^{-\frac{1}{2}}B^TM_p^{-\frac{1}{2}}M_p^{\frac{1}{2}}\bar{\varphi}_h||^2_2 &= (M^{-\frac{1}{2}}B^TM_p^{-\frac{1}{2}}M_p^{\frac{1}{2}}\bar{\varphi}_h, M^{-\frac{1}{2}}B^TM_p^{-\frac{1}{2}}M_p^{\frac{1}{2}}\bar{\varphi}_h)\\ &= (M_p^{-\frac{1}{2}}BM^{-1}B^TM_p^{-\frac{1}{2}}M_p^{\frac{1}{2}}\bar{\varphi}_h, M_p^{\frac{1}{2}}\bar{\varphi}_h)\\ &= (SM_p^{\frac{1}{2}}\bar{\varphi}_h, M_p^{\frac{1}{2}}\bar{\varphi}_h)\\ &= (M_p^{-\frac{1}{2}}BM^{-1}\bar{\phi}_h, M_p^{\frac{1}{2}}\bar{\varphi}_h)\\ &= (M^{-\frac{1}{2}}\bar{\phi}_h, M^{-\frac{1}{2}}B^TM_p^{-\frac{1}{2}}M_p^{\frac{1}{2}}\bar{\varphi}_h)\\ &\leq ||M^{-\frac{1}{2}}\bar{\phi}_h||_2||M^{-\frac{1}{2}}B^TM_p^{-\frac{1}{2}}M_p^{\frac{1}{2}}\bar{\varphi}_h||_2,\end{aligned} \tag{3.108}$$

it follows that

$$||M^{-\frac{1}{2}}B^TM_p^{-\frac{1}{2}}M_p^{\frac{1}{2}}\bar{\varphi}_h||_2 \leq ||M^{-\frac{1}{2}}\bar{\phi}_h||_2. \tag{3.109}$$

Hence, (3.107) becomes

$$\alpha_h||\bar{\varphi}_h||^2_{M_p} \leq ||M^{-\frac{1}{2}}\bar{\phi}_h||^2_2, \tag{3.110}$$

or equivalently,

$$||\bar{\varphi}_h||_{M_p} \leq \frac{1}{\sqrt{\alpha_h}}||M^{-\frac{1}{2}}\bar{\phi}_h||_2. \tag{3.111}$$

3.3.2 Equivalence of vector norm and corresponding vector function norm

In (3.111), $\bar{\phi}_h$ is a vector which is composed by elements:

$$\phi_{h,kl} = -\int_{\Omega} \overrightarrow{\phi_h} \cdot \mathbf{w}_{kl} dx = -\int_{\omega_{kl}} \overrightarrow{\phi_h} \cdot \mathbf{w}_{kl} dx, \tag{3.112}$$

where ω_{kl} is the region defined in Figure 3.4 to 3.6, $\mathbf{w}_{kl}$ is the basis function in ω_{kl}, and $\overrightarrow{\phi_h}$ is a vector function defined in Ω.

People are more familiar with the following errors represented by vector function norm

$$||\overrightarrow{\phi_h}||_2 = ||\mathbf{u}^* - \mathbf{u}^*_{h,int}||_2, \tag{3.113}$$

instead of $||M^{-\frac{1}{2}}\bar{\phi}_h||_2$ in (3.111), so we need to find a constant $c > 0$, s.t. $||M^{-\frac{1}{2}}\bar{\phi}_h||_2 \leq c||\overrightarrow{\phi_h}||_2$.

By the definition of $\bar{\phi}_h$ in (3.112), we have:

$$\begin{aligned} ||\bar{\phi}_h||_2^2 &= \sum_{k<l} \Big(\int_{\omega_{kl}} \overrightarrow{\phi_h} \cdot \mathbf{w}_{kl} dx \Big)^2 \\ &\leq \sum_{k<l} \Big(\int_{\omega_{kl}} \overrightarrow{\phi_h} dx \Big)^2 \Big(\int_{\omega_{kl}} \mathbf{w}_{kl} dx \Big)^2 \\ &\leq \sum_{k<l} \Big(\int_{\omega_{kl}} \overrightarrow{\phi_h}^2 dx \Big) \Big(\int_{\omega_{kl}} \mathbf{w}_{kl}^2 dx \Big) \\ &\leq \Big(\sum_{k<l} \int_{\omega_{kl}} \overrightarrow{\phi_h}^2 dx \Big) \Big(\max_{k<l} \int_{\omega_{kl}} \mathbf{w}_{kl}^2 dx \Big) \\ &\leq 2||\overrightarrow{\phi_h}||_2^2 \Big(\max_{k<l} \int_{\omega_{kl}} \mathbf{w}_{kl}^2 dx \Big). \end{aligned} \tag{3.114}$$

We suppose the partition $\{\omega_{kl}\}$ is quasi-uniform, i.e., there exist two positive constants c_1 and c_2, independent of number of cells, such that for all ω_{kl},

$$c_1 h^2 \leq |\omega_{kl}| \leq c_2 h^2, \tag{3.115}$$

where $h := \max_{k<l}\{\text{diam}(\omega_{kl})\}$. Or equivalently there exists a positive number α, such that

$$\frac{\max_{kl} |\omega_{kl}|}{\min_{kl} |\omega_{kl}|} \leq \alpha. \tag{3.116}$$

We also suppose the triangluation is shape regular, i.e., in 2D, there is no triangle whose angle is very small, or say there exists a positive number β, such that

$$\frac{\max_{kl} ||\mathbf{w}_{kl}||}{\min_{kl} ||\mathbf{w}_{kl}||} \leq \beta. \tag{3.117}$$

By above two inequalities from two properties of mesh, we can get

$$\begin{aligned} \max_{k<l} \int_{\omega_{kl}} \mathbf{w}_{kl}^2 dx &\leq \frac{\alpha\beta}{n}\Big(\sum_{k<l} \int_{\omega_{kl}} \mathbf{w}_{kl}^2 dx\Big) \\ &= \frac{\alpha\beta}{n} tr(M) \\ &= \frac{\alpha\beta}{n} \sum_i \lambda_i(M), \end{aligned} \tag{3.118}$$

where n is the size of vector $\bar{\phi}_h$ (or the number of regions ω_{kl}), M is the matrix in (3.90), $tr(M)$ is the trace of M, $\lambda_i(M)$ are eigenvalues of M. Moreover, since M is a normal matrix, it has the property

$$||M||_2 = \max_i \big\{\lambda_i(M)\big\}, \tag{3.119}$$

so (3.115) can be then written as:

$$\begin{aligned} \max_{k<l} \int_{\omega_{kl}} \mathbf{w}_{kl}^2 dx &\leq \frac{\alpha\beta}{n}\Big(n \max_i \big\{\lambda_i(M)\big\}\Big) \\ &= \alpha\beta ||M||_2. \end{aligned} \tag{3.120}$$

By applying (3.114) and (3.120), we can get:

$$\begin{aligned}
||M^{-\frac{1}{2}}\bar{\phi}_h||_2^2 &= (M^{-1}\bar{\phi}_h, \bar{\phi}_h) \\
&\leq ||M^{-1}\bar{\phi}_h||_2||\bar{\phi}_h||_2 \\
&\leq ||M^{-1}||_2||\bar{\phi}_h||_2^2 \\
&\leq ||M^{-1}||_2\Big(2||\overrightarrow{\phi_h}||_2^2\Big)\Big(\max_{kl}\int_{\omega_{kl}} \mathbf{w}_{kl}^2 dx\Big) \\
&\leq 2\alpha\beta||M^{-1}||_2||M||_2||\overrightarrow{\phi_h}||_2^2 \\
&\leq 2\alpha\beta.cond(M)||\overrightarrow{\phi_h}||_2^2,
\end{aligned} \tag{3.121}$$

where $cond(M)$ is the condition number of matrix M. Here, since M is normal,

$$cond(M) = \Big|\frac{\lambda_{max}(M)}{\lambda_{min}(M)}\Big|. \tag{3.122}$$

M is a $n \times n$ sparse matrix, every row of M is composed by at most 5 elements: one diagonal and four off-diagonals from two adjacent cells. Next, we will show

$$cond(M) = \Big|\frac{\lambda_{max}(M)}{\lambda_{min}(M)}\Big| \sim O(1). \tag{3.123}$$

Before we prove this, we need introduce one important theorem:

Theorem 3.24. *If M is a positive definite matrix, and $M = \sum_{k=1}^{n} N_k M_k N_k^T$, where M_k are local matrices which are also positive definite, N_k are assembling matrices, then:*

$$\min_k \frac{(M_k\bar{v}_k, \bar{v}_k)}{(D_k\bar{v}_k, \bar{v}_k)} \leq \frac{(M\bar{v}, \bar{v})}{(D\bar{v}, \bar{v})} \leq \max_k \frac{(M_k\bar{v}_k, \bar{v}_k)}{(D_k\bar{v}_k, \bar{v}_k)} \tag{3.124}$$

where $D = diag(M)$, $D_k = diag(M_k)$ *and* $\bar{v} = \sum_{k=1}^{n} N_k \bar{v}_k$.

Theorem 3.24 indicates that if in each mesh cell, local matrices M_k and D_k are spectrally equivalent, then the universal matrices M and D are also spectrally equivalent. It will be immediately followed that under the assumption Ω_h is both regular and quasi-uniform, $\left|\frac{\lambda_{max}(D)}{\lambda_{min}(D)}\right| \sim O(1)$, therefore, $cond(M) = \left|\frac{\lambda_{max}(M)}{\lambda_{min}(M)}\right| \sim O(1)$. Now we will focus on local matrices M_k for triangular mesh cells. From Subsection 3.2.1, M_k has the form:

$$M_k = Area_k \begin{pmatrix} \frac{r}{\sin^2\theta_1} & \frac{r\cos\theta_1}{\sin^2\theta_1} & 0 \\ \frac{r\cos\theta_1}{\sin^2\theta_1} & \frac{r}{\sin^2\theta_1} + \frac{1-r}{\sin^2\theta_2} & \frac{(1-r)\cos\theta_2}{\sin^2\theta_2} \\ 0 & \frac{(1-r)\cos\theta_2}{\sin^2\theta_2} & \frac{1-r}{\sin^2\theta_2} \end{pmatrix}, \tag{3.125}$$

where $Area_k$ is a constant, θ_1, θ_2 are two base angles, and r is the ratio between the area of subtriangle e_1 and the area of triangular cell $E_k = e_1 \cup e_2$, see Figure 3.14. We consider the ideal case, when $r = \frac{1}{2}$, then M_k becomes:

$$M_k = \frac{Area_k}{2} \begin{pmatrix} \frac{1}{\sin^2\theta_1} & \frac{\cos\theta_1}{\sin^2\theta_1} & 0 \\ \frac{\cos\theta_1}{\sin^2\theta_1} & \frac{1}{\sin^2\theta_1} + \frac{1}{\sin^2\theta_2} & \frac{\cos\theta_2}{\sin^2\theta_2} \\ 0 & \frac{\cos\theta_2}{\sin^2\theta_2} & \frac{1}{\sin^2\theta_2} \end{pmatrix}. \tag{3.126}$$

Because $\frac{(M_k\bar{v}_k,\bar{v}_k)}{(D_k\bar{v}_k,\bar{v}_k)}$ is independent with the constant coefficient $\frac{Area_k}{2}$, it is ignored in the following steps.

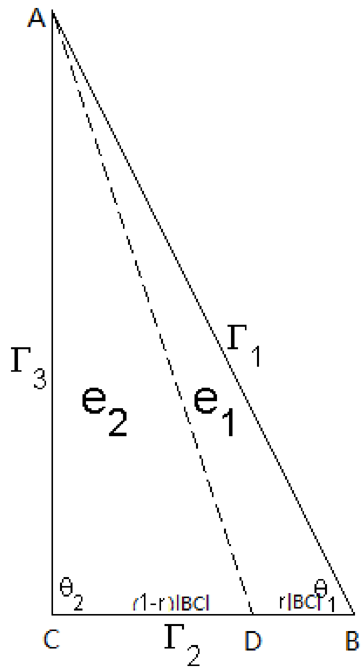

Figure 3.14: Triangular mesh cell with arbitrary shape

$$
\begin{aligned}
&(M_k\bar{v}_k, \bar{v}_k)\\
=&\frac{1}{\sin^2\theta_1}v_1^2 + \frac{2\cos\theta_1}{\sin^2\theta_1}v_1v_2 + \left(\frac{1}{\sin^2\theta_1} + \frac{1}{\sin^2\theta_2}\right)v_2^2 + \frac{1}{\sin^2\theta_2}v_3^2 + \frac{2\cos\theta_2}{\sin^2\theta_2}v_2v_3\\
\leq&2\left(\frac{1}{\sin^2\theta_1}v_1^2 + \left(\frac{1}{\sin^2\theta_1} + \frac{1}{\sin^2\theta_2}\right)v_2^2 + \frac{1}{\sin^2\theta_2}v_3^2\right)\\
=&2(D_k\bar{v}_k, \bar{v}_k),
\end{aligned}
\tag{3.127}
$$

and

$$\begin{aligned}
&101(M_k\bar{v}_k,\bar{v}_k)\\
=&101\left(\frac{1}{\sin^2\theta_1}v_1^2+\frac{2\cos\theta_1}{\sin^2\theta_1}v_1v_2+\Big(\frac{1}{\sin^2\theta_1}+\frac{1}{\sin^2\theta_2}\Big)v_2^2+\frac{1}{\sin^2\theta_2}v_3^2+\frac{2\cos\theta_2}{\sin^2\theta_2}v_2v_3\right)\\
\geq&\frac{1}{\sin^2\theta_1}v_1^2+\Big(\frac{1}{\sin^2\theta_1}+\frac{1}{\sin^2\theta_2}\Big)v_2^2+\frac{1}{\sin^2\theta_2}v_3^2\\
=&(D_k\bar{v}_k,\bar{v}_k).
\end{aligned} \tag{3.128}$$

(3.127) holds because

$$\begin{aligned}
&\frac{1}{\sin^2\theta_1}v_1^2-\frac{2\cos\theta_1}{\sin^2\theta_1}v_1v_2+\Big(\frac{1}{\sin^2\theta_1}+\frac{1}{\sin^2\theta_2}\Big)v_2^2+\frac{1}{\sin^2\theta_2}v_3^2-\frac{2\cos\theta_2}{\sin^2\theta_2}v_2v_3\\
=&\Big(\frac{v_1}{\sin\theta_1}-\frac{\cos\theta_1}{\sin\theta_1}v_2\Big)^2+\Big(\frac{v_3}{\sin\theta_2}-\frac{\cos\theta_2}{\sin\theta_2}v_2\Big)^2+2v_2^2\geq 0.
\end{aligned} \tag{3.129}$$

(3.128) holds because

$$\begin{aligned}
&\frac{100}{\sin^2\theta_1}v_1^2+\frac{202\cos\theta_1}{\sin^2\theta_1}v_1v_2+\Big(\frac{100}{\sin^2\theta_1}+\frac{100}{\sin^2\theta_2}\Big)v_2^2+\frac{100}{\sin^2\theta_2}v_3^2+\frac{202\cos\theta_2}{\sin^2\theta_2}v_2v_3\\
=&\Big(\frac{10v_1}{\sin\theta_1}+\frac{101\cos\theta_1}{10\sin\theta_1}v_2\Big)^2+\Big(\frac{10v_3}{\sin\theta_2}+\frac{101\cos\theta_2}{10\sin\theta_2}v_2\Big)^2\\
&+\frac{v_2^2}{\sin^2\theta_1}\Big(100\sin^2\theta_1-\frac{201}{100}\cos^2\theta_1\Big)+\frac{v_2^2}{\sin^2\theta_2}\Big(100\sin^2\theta_2-\frac{201}{100}\cos^2\theta_2\Big)\geq 0,
\end{aligned} \tag{3.130}$$

under the regularity condition for triangulation.

Therefore, we are able to find two positive constants c_1 and c_2 which are independent of step size h, such that for any k

$$c_1\leq\frac{(M_k\bar{v}_k,\bar{v}_k)}{(D_k\bar{v}_k,\bar{v}_k)}\leq c_2. \tag{3.131}$$

Hence, by Theorem 3.24, it holds that:

$$c_1 \le \frac{(M\bar{v}, \bar{v})}{(D\bar{v}, \bar{v})} \le c_2. \tag{3.132}$$

Consequently, under the assumption triangulation is both regular and quasi-uniform, we have the conclusion:

$$cond(M) = \left|\frac{\lambda_{max}(M)}{\lambda_{min}(M)}\right| \sim O(1). \tag{3.133}$$

3.3.3 Lower bound on spectrum of condensed matrix S

(3.133) can be equivalently expressed into the following propostion:

Proposition 3.25. *Under the regularity assumption made the inequalities*

$$c_1 h^2 I \le M_{pwcf} \le c_2 h^2 I \tag{3.134}$$

hold with the constants c_1 and c_2 independent of Ω_h, i.e., the matrices M_{pwcf} defined in (3.126) is spectrally equivalent to $h^2 I$.

Remark 3.26. *Here, we can loose the regularity condition on triangulation Ω_h. There are two types of irregular triangular cells in general:*

1. *At least one base angle is very small, see Figure 3.15.*

2. *The top angle is very small, see Figure 3.16.*

To make all inequalities above hold for PWCF method, we only need to guarantee that all mesh cells are not of type 1, but type 2 is acceptable. However, for RT_0 method, neither type 1 or 2 is acceptable.

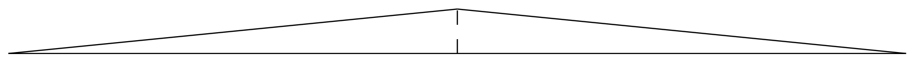

Figure 3.15: Irregular triangular mesh cell of type 1

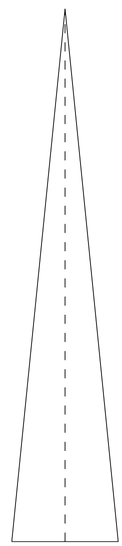

Figure 3.16: Irregular triangular mesh cell of type 2

Now, error estimate (3.111) can be written as:

$$||\bar{\varphi}_h||_{M_p} \leq \frac{c}{\sqrt{\alpha_h}}||\overrightarrow{\phi_h}||_2, \tag{3.135}$$

where c is a constant independent of Ω_h. Our final task is to find an lower bound for α_h.

Recall that α_h is the minimal eigenvalue for the eigenvalue problem

$$M_p^{-\frac{1}{2}} B M^{-1} B^T M_p^{-\frac{1}{2}} \bar{p} = \alpha \bar{p}, \tag{3.136}$$

which is equivalent to the problem:

$$B M^{-1} B^T \bar{p} = \alpha M_p \bar{p}, \tag{3.137}$$

which can also be written into the form:

$$\begin{cases} M\bar{w} - B^T\bar{p} & = 0 \\ B\bar{w} & = \alpha M_p \bar{p} \end{cases} \tag{3.138}$$

It is shown by Yu. Kuznetsov in [37] that the minimal eigenvalue for problem (3.138) has a lower bound independent of Ω_h if M is the mass matrix for classical mixed finite element methods, including RT_0 method, for regular shaped triangular meshes. However, there is no such conclusion for general PWCF method. From Proposition 3.25, M_{pwcf} and $h^2 I$ are spectrally equivalent, hence, if we can show M_{RT_0} is also spectrally equivalent to $h^2 I$, then α_h in (3.135) will have a lower bound independent of mesh Ω_h.

Consider a general triangular mesh cell in Figure 3.17. Suppose the height of the triangle is always 1, and two base angles are θ_1 and θ_2. Then RT_0 basis for this triangle is composed by:

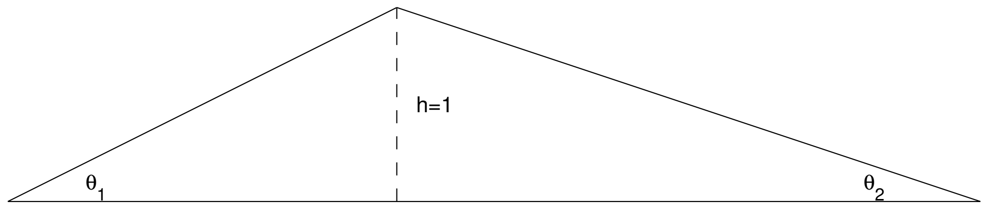

Figure 3.17: General triangular mesh cell for RT_0 method

$$\begin{aligned} \mathbf{w}_1 &= \frac{1}{h_1}\begin{pmatrix} x_1 \\ x_2 - 1 \end{pmatrix}, \\ \mathbf{w}_2 &= \frac{1}{h_2}\begin{pmatrix} x_1 + \cot\theta_1 \\ x_2 \end{pmatrix}, \\ \mathbf{w}_3 &= \frac{1}{h_3}\begin{pmatrix} x_1 - \cot\theta_2 \\ x_2 \end{pmatrix}, \end{aligned} \tag{3.139}$$

where three heights are:

$$\begin{aligned} h_1 &= 1, \\ h_2 &= \sin\theta_2(\cot\theta_1 + \cot\theta_2), \\ h_3 &= \sin\theta_1(\cot\theta_1 + \cot\theta_2). \end{aligned} \tag{3.140}$$

By Newton-Cotes quadrature rule, the symmetric positive definite mass matrix $M_k =$

$\frac{Area_k}{6}\widetilde{M_k}$ can be explicitly represented as:

$$\begin{aligned}
\widetilde{M_k}(1,1) &= \frac{\cot^2\theta_1 + \cot^2\theta_2 - \cot\theta_1\cot\theta_2 + 3}{h_1^2}, \\
\widetilde{M_k}(2,2) &= \frac{3\cot^2\theta_1 + \cot^2\theta_2 + 3\cot\theta_1\cot\theta_2 + 1}{h_2^2}, \\
\widetilde{M_k}(3,3) &= \frac{\cot^2\theta_1 + 3\cot^2\theta_2 + 3\cot\theta_1\cot\theta_2 + 1}{h_3^2}, \\
\widetilde{M_k}(1,2) &= \frac{-\cot^2\theta_1 + \cot^2\theta_2 + \cot\theta_1\cot\theta_2 - 1}{h_1h_2}, \\
\widetilde{M_k}(1,3) &= \frac{\cot^2\theta_1 - \cot^2\theta_2 + \cot\theta_1\cot\theta_2 - 1}{h_1h_3}, \\
\widetilde{M_k}(2,3) &= \frac{-\cot^2\theta_1 - \cot^2\theta_2 - 3\cot\theta_1\cot\theta_2 + 1}{h_2h_3},
\end{aligned} \tag{3.141}$$

where $Area_k$ is the area of triangular cell E_k.

The minimal eigenvalue for matrix $\widetilde{M_k}$ is 2, therefore,

$$c_1 h^2 I \le M_k, \tag{3.142}$$

where c_1 is a constant. On the other hand, let $D_k = \mathrm{diag}(M_k)$, it is not difficult to show that

$$M_k \le 3D_k. \tag{3.143}$$

The reason is, for any $\bar{u} \in \mathbb{R}^3$, we have:

$$
\begin{aligned}
&(M_k\bar{u}, \bar{u}) \\
&= \int_{E_k} (u_1\mathbf{w}_1 + u_2\mathbf{w}_2 + u_3\mathbf{w}_3)^2 dx \\
&= \int_{E_k} u_1^2\mathbf{w}_1^2 + u_2^2\mathbf{w}_2^2 + u_3^2\mathbf{w}_3^2 + 2u_1u_2(\mathbf{w}_1 \cdot \mathbf{w}_2) + 2u_1u_3(\mathbf{w}_1 \cdot \mathbf{w}_3) + 2u_2u_3(\mathbf{w}_2 \cdot \mathbf{w}_3) dx,
\end{aligned} \tag{3.144}
$$

so

$$
\begin{aligned}
&((3D_k - M_k)\bar{u}, \bar{u}) \\
&= \int_{E_k} 2u_1^2\mathbf{w}_1^2 + 2u_2^2\mathbf{w}_2^2 + 2u_3^2\mathbf{w}_3^2 \\
&\quad - 2u_1u_2(\mathbf{w}_1 \cdot \mathbf{w}_2) - 2u_1u_3(\mathbf{w}_1 \cdot \mathbf{w}_3) - 2u_2u_3(\mathbf{w}_2 \cdot \mathbf{w}_3) dx \\
&= \int_{E_k} (u_1\mathbf{w}_1 - u_2\mathbf{w}_2)^2 + (u_1\mathbf{w}_1 - u_3\mathbf{w}_3)^2 + (u_2\mathbf{w}_2 - u_3\mathbf{w}_3)^2 dx \geq 0.
\end{aligned} \tag{3.145}
$$

Therefore, if the maximum element of D_k has a upper bound c_2, then M_k is spectrally equivalent to $h^2 I$.

Observe the diagonal entries in (3.141), under the assumption of regular triangulation, i.e., there exists an angle $\vartheta > 0$, such that $\theta_1, \theta_2, \theta_3 \geq \vartheta$, then

$$
\begin{aligned}
\widetilde{M}_k(1,1) &\leq 3\cot^2\vartheta + 3, \\
\widetilde{M}_k(2,2) &\leq \frac{7\cot^2\vartheta + 1}{\sin^2\vartheta \tan^2\frac{\vartheta}{2}}, \\
\widetilde{M}_k(3,3) &\leq \frac{7\cot^2\vartheta + 1}{\sin^2\vartheta \tan^2\frac{\vartheta}{2}}.
\end{aligned} \tag{3.146}
$$

Choose $c_2' = \max\{3\cot^2\vartheta + 3, \frac{7\cot^2\vartheta+1}{\sin^2\vartheta\tan^2\frac{\vartheta}{2}}\}$, then

$$M_k \leq 3D_k \leq \frac{1}{2}c_2' Area_k I \leq c_2 h^2 I. \tag{3.147}$$

Proposition 3.27. *Under the regularity assumption made the inequalities*

$$c_1 h^2 I \leq M_{RT_0} \leq c_2 h^2 I \tag{3.148}$$

hold with the constants c_1 and c_2 independent of Ω_h, i.e., the matrices M_{RT_0} defined in (3.141) is spectrally equivalent to $h^2 I$.

Consequently, minimal eigenvalue α_h in (3.135) has a lower bound independent of Ω_h. The final result for error estimate on $\bar{p}_h$ is:

Theorem 3.28. *If a triangulation Ω_h is quasi-uniform and regular, then*

$$||\bar{p}_h - \bar{p}^*_{h,int}||_{M_p} \leq c_0||\mathbf{u}^*_{h,int} - \mathbf{u}^*||_2, \tag{3.149}$$

where c is a positive constant independent of Ω_h. Or equivalently,

$$||p_h - p^*||_2 \leq c(||\mathbf{u}^*_{h,int} - \mathbf{u}^*||_2 + ||p^*_{h,int} - p^*||_2), \tag{3.150}$$

where p^* is the exact solution, p_h and $p^*_{h,int}$ are piecewise constant functions in $\mathbf{P}_h$.

3.4 Algebraic equivalance to finite volume method

Consider the algebraic system (3.14) with homogenous Dirichlet boundary, i.e., $\bar{G}_D \equiv 0$. Eliminating the variables $\bar{u}$ and $\bar{\lambda}$, we can obtain the system in terms of the variable $\bar{p}$ only:

$$S_p \bar{p} = -\bar{F}, \tag{3.151}$$

with the reduced matrix

$$S_p = BM^{-1}(M - C^T(CM^{-1}C^T)^{-1}C)M^{-1}B^T. \tag{3.152}$$

In this section, we will explore the matrix S_p for different types of meshes, and find their relationships to finite volume methods.

3.4.1 Rectangular mesh

Consider two adjacent mesh cells E_k and E_l with a common interface $\Gamma_{kl} \equiv \Gamma_{k,2} \equiv \Gamma_{l,4}$, as shown in Figure 3.18. Assembling two local systems for the cells E_k and E_l, we can get the following equations:

$$\left\{ \begin{array}{ccccccc} & & |\Gamma_{k,2}|u_{k,2} & + & |\Gamma_{l,4}|u_{l,4} & = & 0, \\ \frac{1}{2}|E_k|u_{k,2} & - & |\Gamma_{k,2}|p_k & + & |\Gamma_{k,2}|\lambda_{kl} & = & 0, \\ \frac{1}{2}|E_l|u_{l,4} & - & |\Gamma_{l,4}|p_l & + & |\Gamma_{l,4}|\lambda_{kl} & = & 0. \end{array} \right. \tag{3.153}$$

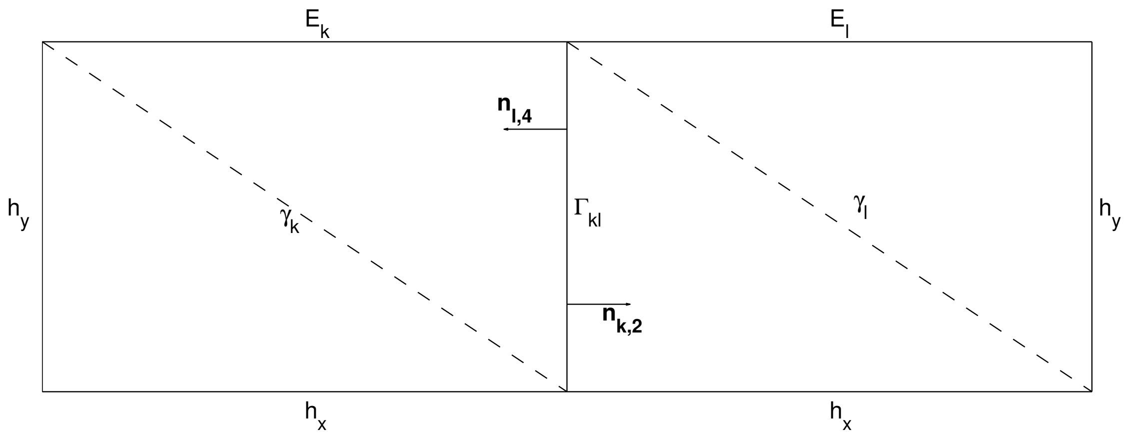

Figure 3.18: Two adjacent rectangular cells E_k and E_l with common interface Γ_{kl}

The mesh is uniform, therefore $|E_k| = |E_l| = h_x h_y$, and $\Gamma_{kl} = h_y$. This implies

$$u_{k,2} = -u_{l,4} = -\frac{p_l - p_k}{h_x}, \tag{3.154}$$

which is same as the formula used in finite volume method. Note that for PWCF method, variables are defined as

$$p_k = \frac{1}{\gamma_k} \int_{\gamma_k} p_h ds, \tag{3.155}$$

$$u_{k,j} = \frac{1}{\Gamma_{k,j}} \int_{\Gamma_{k,j}} (\mathbf{u}_h \cdot \mathbf{n}_{k,j}) ds, \tag{3.156}$$

with $p_h \in \mathbf{P}_h$, $\mathbf{u}_h \in \mathbf{V}_h$.

It is proved in [40] that for any quadrilateral mesh and diffusion problem (2.1) with piecewise constant symmetric positive tensor K, the classical solution $\mathbf{u}^*$ and its interpolant in $\mathbf{V}_h$, $\mathbf{u}^*_{h,int}$, the following error estimate holds:

$$||\mathbf{u}_h - \mathbf{u}^*||_{K^{-1}} \le 2||\mathbf{u}^*_{h,int} - \mathbf{u}^*||_{K^{-1}}, \tag{3.157}$$

where $\mathbf{u}_h \in \mathbf{V}_h$ is the solution obtained by PWCF method. Therefore, this error estimate also holds for corresponding finite volume method.

3.4.2 Triangular mesh

Can we get a similar result for triangular mesh? Consider a mesh composed by congruent equilateral triangles. Let us investigate two adjacent mesh cells E_k and E_l with a common interface $\Gamma_{kl} \equiv \Gamma_{k,2} \equiv \Gamma_{l,2}$, as shown in Figure 3.19. Assembling two local systems for the cells E_k and E_l, we can get the following equations:

$$\left\{\begin{array}{ccccccccccccc} & & & & & & & & |\Gamma_{k,2}|u_{k,2} & + & |\Gamma_{l,2}|u_{l,2} & = & 0, \\ \frac{1}{3}|E_k|u_{k,1} & + & \frac{4}{3}|E_k|u_{k,2} & + & \frac{1}{3}|E_k|u_{k,3} & - & |\Gamma_{k,2}|p_k & + & |\Gamma_{k,2}|\lambda_{kl} & = & 0, \\ \frac{1}{3}|E_l|u_{l,1} & + & \frac{4}{3}|E_l|u_{l,2} & + & \frac{1}{3}|E_l|u_{l,3} & - & |\Gamma_{l,2}|p_l & + & |\Gamma_{l,2}|\lambda_{kl} & = & 0. \end{array}\right. \tag{3.158}$$

After simplification, we will get

$$u_{k,2} = -u_{l,2} = \frac{1}{8}(u_{l,1} + u_{l,3} - u_{k,1} - u_{k,3}) + \frac{\sqrt{3}}{4}(p_k - p_l). \tag{3.159}$$

If we further consider two adjacent mesh cells E_k and E_m with common interface $\Gamma_{k,1}$, then $u_{k,1}$ can be represented as linear combination of p_k, p_m and more $u_{k,\cdot}$ and

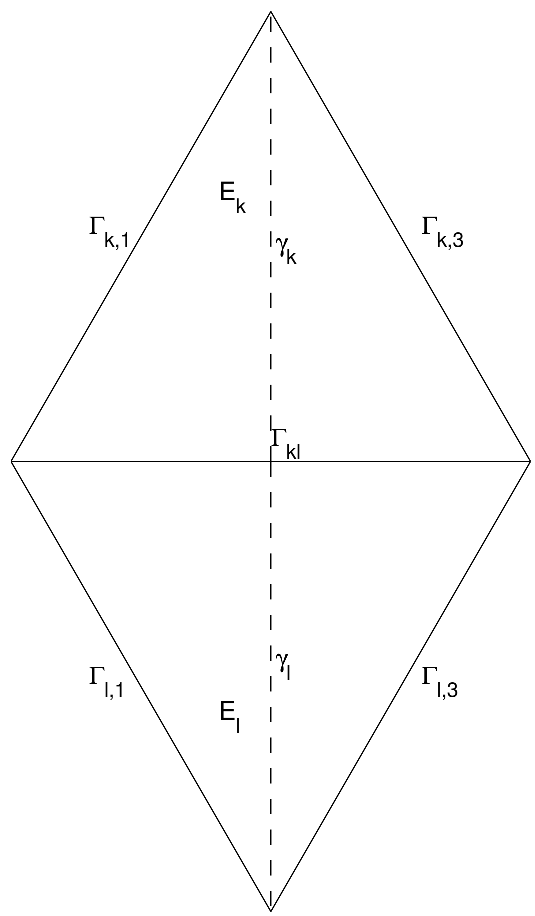

Figure 3.19: Two adjacent triangular cells E_k and El with common interface Γ_{kl}

$u_{m,\cdot}$. Do this again and again, we will find out that $u_{k,2}$ is represented as linear combination of all p_i over the mesh. Therefore, for triangular meshes, algebraic systems for PWCF method and finite volume method are not equivalent.

CHAPTER 4

PWCF Method on Locally Refined Meshes

In this chapter, we will investigate PWCF method on locally refined meshes. Rectangular and triangular meshes are discussed. We will focus on the following topics: approaches to implement local refinement and their monotonicities, stencils.

4.1 Rectangular mesh

For the sake of simplicity, let us consider a square mesh with size h on its coarse part and size $\frac{h}{2}$ on the fine part. Let E_k be a coarse cell which has a common interface Γ_1 with two fine cells. We denote the other coarse cells that share the interface Γ_j with E_k by $E_{k,j}$, $j = 2, 3, 4$, and two fine cells by $E_{k,11}$ and $E_{k,12}$. An illustration is given in Figure 4.1.

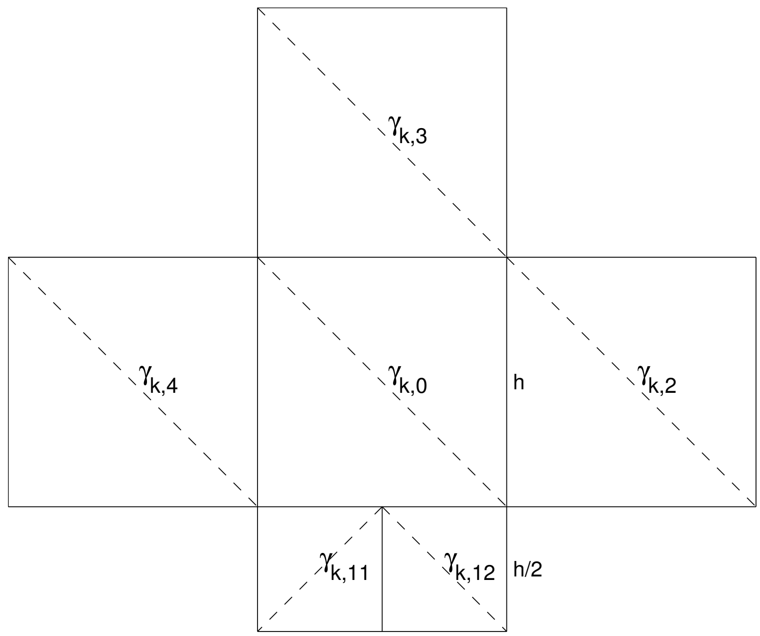

Figure 4.1: Rectangular mesh with local refinement

The discretization of the conservation law for the cell E_k can be written as:

$$\sum_{j=1}^{4} |\Gamma_j| u_{k,j} = F_k, \tag{4.1}$$

with

$$u_{k,j} = -\frac{p_{k,j} - p_k}{h}, \qquad j = 2, 3, 4. \tag{4.2}$$

Here, p_k and $p_{k,j}$ are discrete solutions approximating p_k^* and $p_{k,j}^*$, respectively, where

$$p_k^* = \frac{1}{|\gamma_{k,0}|} \int_{\gamma_{k,0}} p^* ds, \tag{4.3}$$

$$p_{k,j}^* = \frac{1}{|\gamma_{k,j}|} \int_{\gamma_{k,j}} p^* ds, \qquad j = 2, 3, 4. \tag{4.4}$$

Similar to the computation in Section 3.4.1, on Γ_1, we have:

$$
\begin{array}{rcrcrcrcl}
 & & \frac{1}{2}|E_k|u_{k,1} & - & |\Gamma_{k,1}|p_k & + & |\Gamma_{k,1}|\lambda_{k,1} & = & 0, \\
-\frac{1}{2}(|E_{k,11}|+|E_{k,12}|)u_{k,1} & - & \frac{1}{2}|\Gamma_{k,1}|p_{k,11} & - & \frac{1}{2}|\Gamma_{k,1}|p_{k,12} & + & |\Gamma_{k,1}|\lambda_{k,1} & = & 0,
\end{array}
\tag{4.5}
$$

therefore,

$$
u_{k,1} = -\frac{2p_{k,11} + 2p_{k,12} - 4p_k}{3h}. \tag{4.6}
$$

Substituting (4.2), (4.6) into (4.1), the following 6-point stencil is obtained:

$$
\frac{13}{3}p_k - \frac{2}{3}p_{k,11} - \frac{2}{3}p_{k,12} - p_{k,2} - p_{k,3} - p_{k,4} = F_k. \tag{4.7}
$$

One immediate consequence from this scheme is that the global condensed matrix S_p is monotone.

4.2 Triangular mesh

Let us consider a triangular mesh with local refinement, see Figure 4.2. In this section, we first review the usual refinement procedure and find out that the monotonicity disappears under both conformal and non-conformal schemes. Then, we introduce a new approach to implement refinement, and investigate its monotone condition.

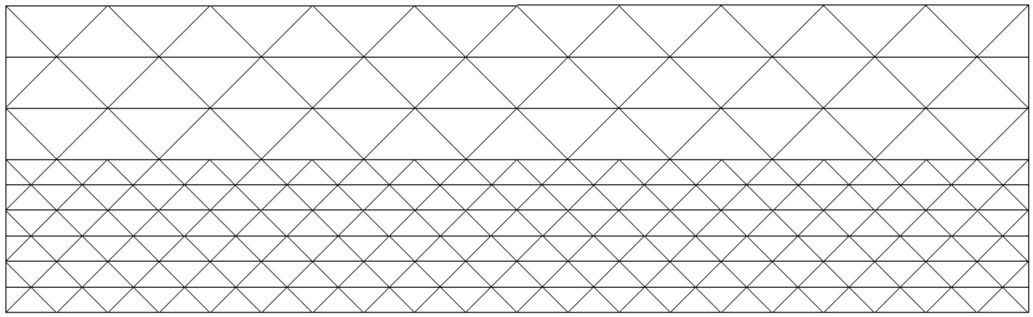

Figure 4.2: Triangular mesh with local refinement

4.2.1 Usual approach to implement refinement

4.2.1.1 Description of the usual refinement procedure and respective monotone condition

Suppose there are two triangular mesh cells with no refinement, i.e., cell E_1 and E_2 have same step size h, and $E_1 \cap E_2 = \Gamma_1$. The usual refinement procedure is:

1. Choose arbitrary point F on Γ_1, and connect AF. E_1 is then partitioned into two triangular cells with size h. (We often choose the mid-point of Γ_1)

2. Choose two points G and H on Γ_4 and Γ_5, correspondingly, connect FG, FH, and GH. E_2 is then partitioned into four triangular cells with size $\frac{h}{2}$. (We also pick mid-points of Γ_4 and Γ_5)

By these two steps, we can obtain local refinement: cells with sizes h and $\frac{h}{2}$ are adjacent. However, by doing such refinement procedure, is the condensed matrix S_λ defined in (3.20) monotone?

The answer is "no". As discussed in Subsection 3.2.1, the universal system is assembled by local systems, so S_λ is monotone if and only if every local condensed

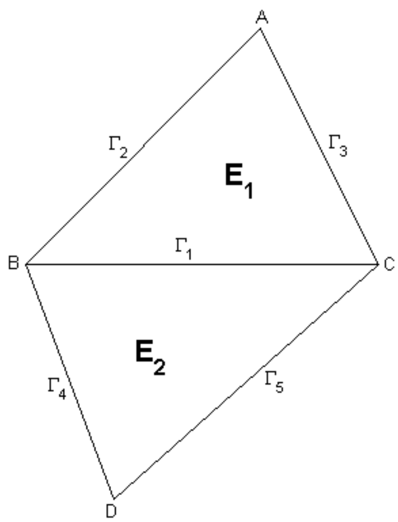

Figure 4.3: Mesh cell before refinement procedure

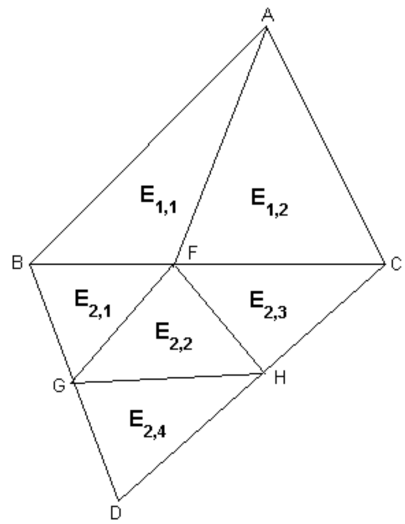

Figure 4.4: Mesh cell after refinement procedure

matrices $S_{\lambda,k}$ on mesh cell E_k are (singular) M-matrices. Moreover, for triangular mesh cell E_k, local condensed matrix $S_{\lambda,k}$ (for both RT_0 and PWCF methods) is a singular M-matrix if and only if E_k is not an obtuse triangle. However, by usual refinement procedure, when E_1 is partitioned into two subtriangles by connecting one vertex and one point on opposite side, we cannot guarantee neither of the two new subtriangles are obtuse triangles, for instance, $E_{1,1}$ in Figure 4.4 is an obtuse triangles. Therefore, although original discretization scheme is monotone, after usual refinement procedure, its monotonicity disappears.

4.2.1.2 Non-conforming scheme and resulting special pentagonal element

Instead of a conforming scheme for the usual refinement procedure, let us now consider a new non-conforming scheme. Suppose one triangular cell E_1 with height h is adjacent with two triangular cells E_2 and E_3 with height $\frac{h}{2}$, see Figure 4.5. On the interface $\Gamma_1 = E_1 \cap (E_2 \cup E_3)$, we introduce degree of freedom u_1 and λ_1, and suppose $p(E_2) = p(E_3)$. As a result, two "macro" cells are formed (Figure 4.6), namely, triangular element E_1 and pentagonal element $E_{2,3} = E_2 \cup E_3$. The universal system (3.14) is then assembling of local systems on triangular elements and pentagonal elements. We have already discussed the monotone condition for triangular elements in Subsection 3.2.1, next we will take an exploration on the pentagonal elements.

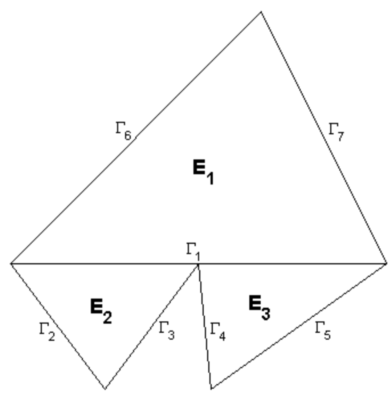

Figure 4.5: Local refinment appears

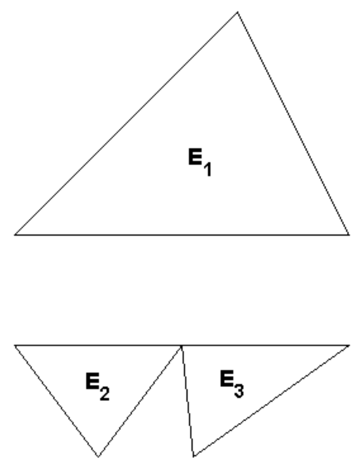

Figure 4.6: One triangular and one pentagonal element

4.2.1.3 PWCF basis vector functions on pentagonal elements

PWCF basis for the pentagonal element in Figure 4.7 are:

$$\mathbf{w}_1 = \begin{cases} (-\frac{\cos\theta_1}{\sin\theta_1}, 1) & \text{in } E_{1,1}, \\ (\frac{\cos\theta_2}{\sin\theta_2}, 1) & \text{in } E_{1,2}, \\ (-\frac{\cos\theta_3}{\sin\theta_3}, 1) & \text{in } E_{2,1}, \\ (\frac{\cos\theta_4}{\sin\theta_4}, 1) & \text{in } E_{2,2}. \end{cases} \tag{4.8}$$

$$\mathbf{w}_2 = \begin{cases} (-\frac{1}{\sin\theta_1}, 0) & \text{in } E_{1,1}, \\ (0,0) & \text{in others.} \end{cases} \tag{4.9}$$

$$\mathbf{w}_3 = \begin{cases} (\frac{1}{\sin\theta_2}, 0) & \text{in } E_{1,2}, \\ (0,0) & \text{in others.} \end{cases} \tag{4.10}$$

$$\mathbf{w}_4 = \begin{cases} (-\frac{1}{\sin\theta_3}, 0) & \text{in } E_{2,1}, \\ (0,0) & \text{in others.} \end{cases} \tag{4.11}$$

$$\mathbf{w}_5 = \begin{cases} (\frac{1}{\sin\theta_4}, 0) & \text{in } E_{2,2}, \\ (0,0) & \text{in others.} \end{cases} \tag{4.12}$$

4.2.1.4 PWCF matrices on pentagonal elements

From this subsection, we assume pentagonal element E_k is composed by two congruent triangles e_1 and e_2 with height h, and each triangle is partitioned into two by connecting bottom vertex and mid-point of its opposite side. By selecting the basis

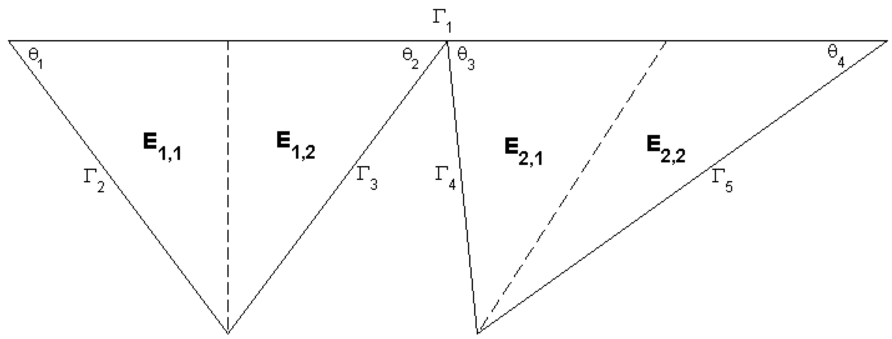

Figure 4.7: General case of pentagonal element

derived from previous subsection, we can get the local PWCF matrices:

$$M_k = Area_k \begin{pmatrix} \frac{1}{2\sin^2\theta_1} + \frac{1}{2\sin^2\theta_2} & \frac{\cos\theta_1}{4\sin^2\theta_1} & \frac{\cos\theta_2}{4\sin^2\theta_2} & \frac{\cos\theta_1}{4\sin^2\theta_1} & \frac{\cos\theta_2}{4\sin^2\theta_2} \\ \frac{\cos\theta_1}{4\sin^2\theta_1} & \frac{1}{4\sin^2\theta_1} & 0 & 0 & 0 \\ \frac{\cos\theta_2}{4\sin^2\theta_2} & 0 & \frac{1}{4\sin^2\theta_2} & 0 & 0 \\ \frac{\cos\theta_1}{4\sin^2\theta_1} & 0 & 0 & \frac{1}{4\sin^2\theta_1} & 0 \\ \frac{\cos\theta_2}{4\sin^2\theta_2} & 0 & 0 & 0 & \frac{1}{4\sin^2\theta_2} \end{pmatrix}, \tag{4.13}$$

$$B_k = h^2 \begin{pmatrix} -\frac{\cos\theta_1}{\sin\theta_1} - \frac{\cos\theta_2}{\sin\theta_2} & -\frac{1}{\sin\theta_1} & -\frac{1}{\sin\theta_2} & 0 & 0 \\ -\frac{\cos\theta_1}{\sin\theta_1} - \frac{\cos\theta_2}{\sin\theta_2} & 0 & 0 & -\frac{1}{\sin\theta_1} & -\frac{1}{\sin\theta_2} \end{pmatrix}, \tag{4.14}$$

$$C_k = h^2 \begin{pmatrix} \frac{2\cos\theta_1}{\sin\theta_1} + \frac{2\cos\theta_2}{\sin\theta_2} & & & & \\ & \frac{1}{\sin\theta_1} & & & \\ & & \frac{1}{\sin\theta_2} & & \\ & & & \frac{1}{\sin\theta_1} & \\ & & & & \frac{1}{\sin\theta_2} \end{pmatrix}. \tag{4.15}$$

Therefore, the local condensed matrix is:

$$S_{\lambda,k} = \frac{h^2}{Area_k}\begin{pmatrix} 4(\cot\theta_1+\cot\theta_2)^2 & & & & \\ -2\cot\theta_1(\cot\theta_1+\cot\theta_2) & \csc^2\theta_1+1 & & Symmentry & \\ -2\cot\theta_2(\cot\theta_1+\cot\theta_2) & \cot\theta_1\cot\theta_2-2 & \csc^2\theta_2+1 & & \\ -2\cot\theta_1(\cot\theta_1+\cot\theta_2) & \cot^2\theta_1 & \cot\theta_1\cot\theta_2 & \csc^2\theta_1+1 & \\ -2\cot\theta_2(\cot\theta_1+\cot\theta_2) & \cot\theta_1\cot\theta_2 & \cot^2\theta_2 & \cot\theta_1\cot\theta_2-2 & \csc^2\theta_2+1 \end{pmatrix}, \quad (4.16)$$

where $Area_k$ is the area of pentagonal element E_k.

From (4.16), we can easily derive 4 types stencil for variable $\bar{\lambda}$, see Figure 4.8 to Figure 4.11. (Here, we suppose the coarse and fine triangular cells are equilateral triangles, and $h_c/h_f = 2$.)

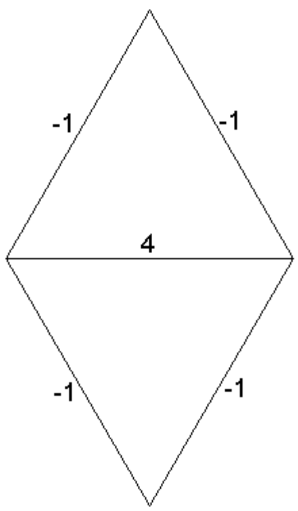

Figure 4.8: Stencil type 1

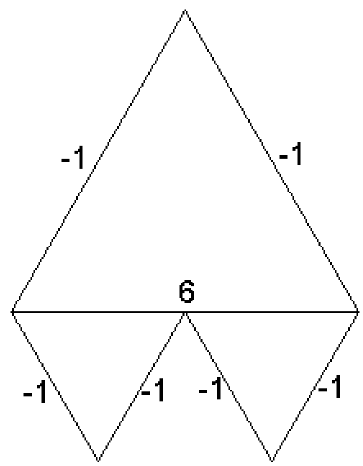

Figure 4.9: Stencil type 2

4.2.1.5 Monotone condition for $S_{\lambda,k}$ on pentagonal elements

By checking the components of condensed matrix $S_{\lambda,k}$ in (4.16), we find that the off-diagonal entries $\cot^2\theta_1$, $\cot^2\theta_2$ are always positive, therefore, under the non-conformal scheme for usual refinement procedure, we still have:

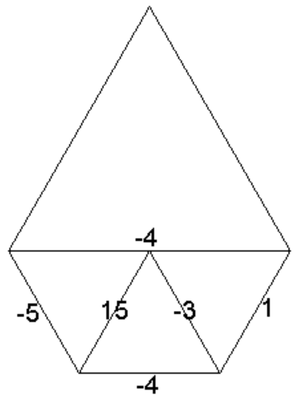

Figure 4.10: Stencil type 3

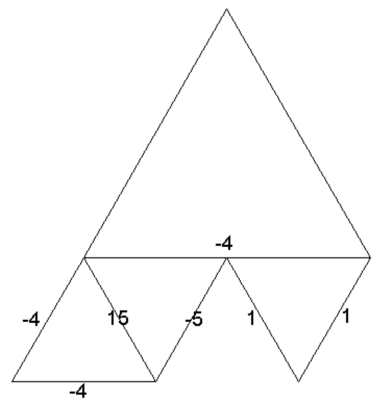

Figure 4.11: Stencil type 4

Theorem 4.1. *$S_{\lambda,k}$ is not (singular) M-matrix on any pentagonal element.*

4.2.2 New approach to do refinement

Since by usual refinement method, the algebraic system cannot be monotone for either conformal or non-conformal schemes, people may consider one alternative refinement method:

Connect vertex D and mid-point F on Γ_1, and a special triangular element composed by two subtriangles is obtained, see Figure 4.13.

The local condensed matrix $S_{\lambda,k}$ on the special triangular element is (equilateral triangular cell, $h=1$):

$$S_{\lambda,k} = \begin{pmatrix} 1.0104 & -0.2887 & -0.8660 & 0.1443 \\ -0.2887 & 0.5774 & 0 & -0.2887 \\ -0.8660 & 0 & 1.7321 & -0.8660 \\ 0.1443 & -0.2887 & -0.8660 & 1.0104 \end{pmatrix}. \tag{4.17}$$

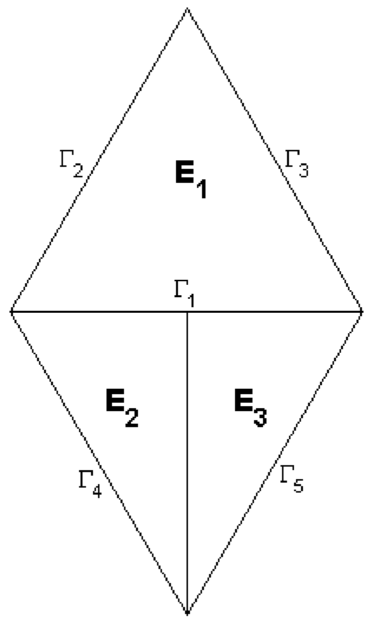

Figure 4.12: Local refinment by an alternative way

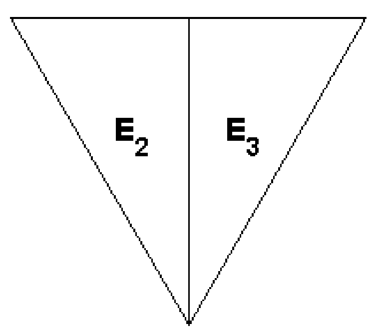

Figure 4.13: Special triangular element

It indicates that S_λ is not monotone even for equilateral triangular mesh. Therefore, in order to keep the monotonicity of condensed matrix S_λ, we cannot partition mesh cell by choosing any point on Γ_1, instead, we need to find a way of partition to make every subtriangles to be non-obtuse.

4.2.2.1 Right-triangular meshes

For the triangular meshes with cells having one base angle being right angle, we can do the refinement procedure as in Figure 4.14 to keep montonicity.

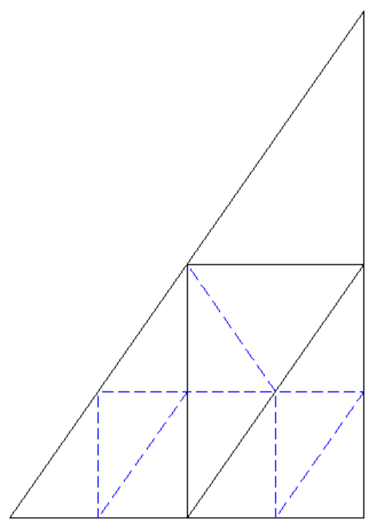

Figure 4.14: Refinement on right triangular mesh

4.2.2.2 Isoceles meshes

In Figure 4.15, we show one feasible procedure to implement refinement. For equilateral mesh, all the small triangles are non-obtuse, so the monotonicity is kept. The critical condition on base angle θ to successfully apply this refinement method is

$$\tan(\theta) \geq \frac{1+\sqrt{5}}{2}, \tag{4.18}$$

or approximately, $\theta \geq 58°$. Figure 4.16 shows the case when θ reaches this critical value.

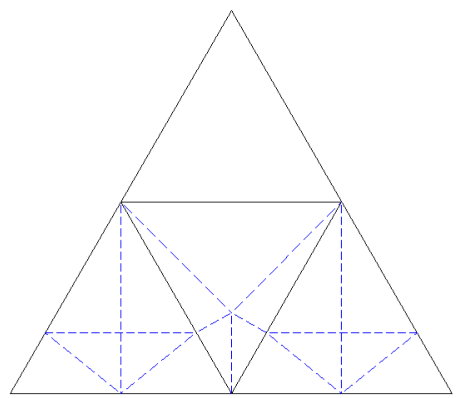

Figure 4.15: Refinement on equilateral triangular mesh

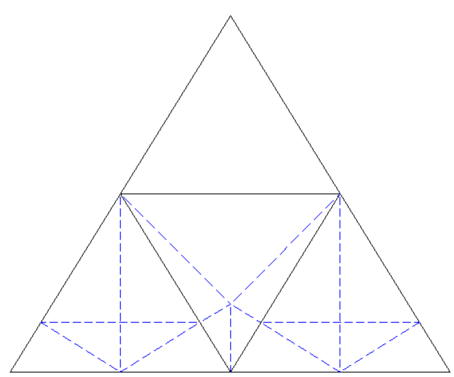

Figure 4.16: Refinement on critical triangular mesh

When $\theta < 58°$, by doing such refinement, the monotonicity disappears, because obtuse triangles appear. When this happens, we can make $h_{large}/h_{small} = 1/4$ or less to overcome this problem. See Figure 4.17 and Figure 4.18.

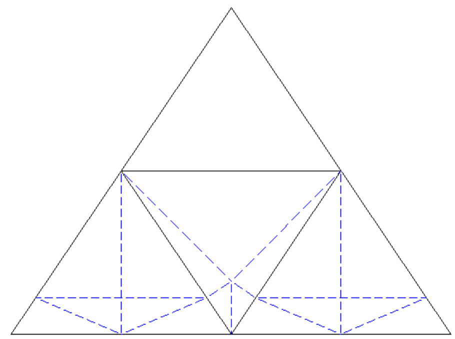

Figure 4.17: Bad refinement on isoceles triangular mesh, $\theta = 56°$

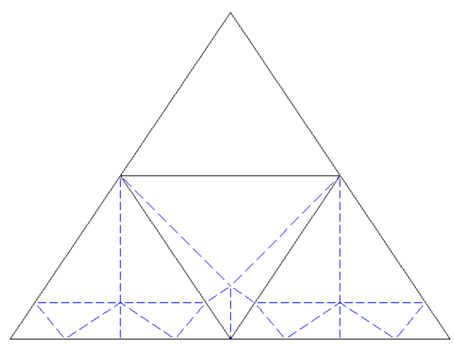

Figure 4.18: Good refinement on isoceles triangular mesh, $\theta = 56°$

4.2.2.3 General triangular meshes

For general triangular meshes, we can do refinement similarly as in Subsection 4.2.2.2, see Figure 4.19. However, under some circumstances, obtuse triangles may appear:

1. Two base angles are two small, see Figure 4.20. (By experiment, it happens when $\theta_1 + \theta_2 \geq 123°$ approximately.)

2. The upper angle is two small, see Figure 4.21. (By experiment, it happens when $\theta_3 \geq 30°$ approximately.)

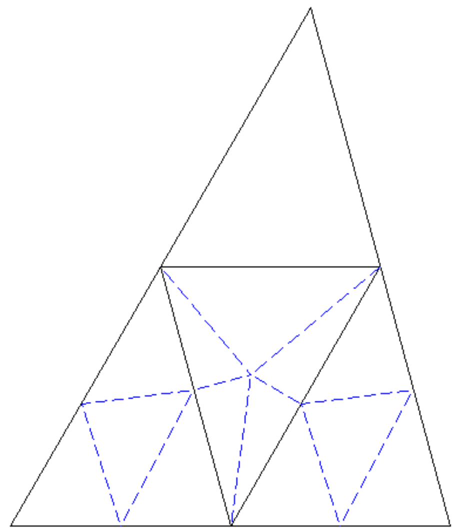

Figure 4.19: Good refinement on one general mesh cell

3. Two base angles have huge difference, see Figure 4.22. (By experiment, it happens when $|\theta_1 - \theta_2| \leq 30^\circ$ approximately.)

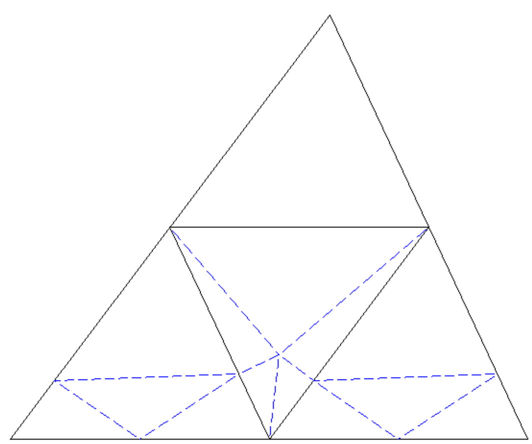

Figure 4.20: Bad refinement on one general mesh cell, reason 1

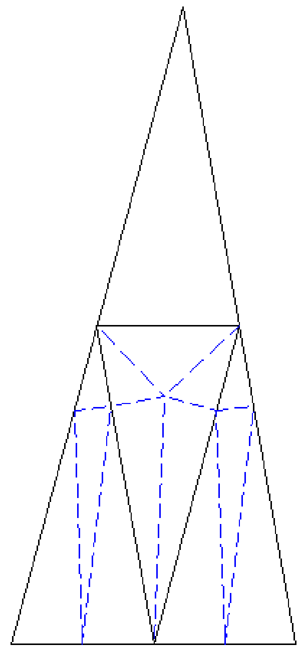

Figure 4.21: Bad refinement on one general mesh cell, reason 2

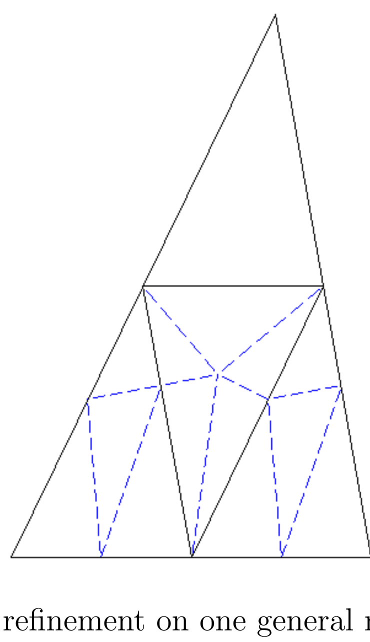

Figure 4.22: Bad refinement on one general mesh cell, reason 3

CHAPTER 5

Numerical Experiments

Consider the diffusion equation (2.1) with Direchelet boundary (2.2) in 3D, with diffusion tension $K = I$ and domain Ω being a cuboid in $\mathbb{R}^3$. In this chapter, a special prismatic grid generated based on Voronoi mesh is first build, whose cells are prisms with lateral faces orthogonal to (x, y)-plane, top and bottom faces being polygons with same number of vertices and parallel to (x, y)-plane. Then, after constructing dual grid to this prismatic grid, we implement PWCF method, and verify error estimations from numerical results.

5.1 Prismatic grid

Let Ω be a cube, i.e., $\Omega = [-1,1] \times [-1,1] \times [-1,1]$. To generate prismatic grid, we do the following procedures:

1. Generate $n+1$ parallel layers inside cube Ω (including top and bottom faces of Ω). Denote them by layer 0 to layer n (top to bottom). See Figure 5.1.

2. On the top square face, randomly generate a polygonal mesh. For our implementation, quadrilateral Voronoi mesh is generated. See Figure 5.2.

3. The mesh for layer k is derived from the mesh for layer $k-1$, where $1 \leq k \leq n$. In particular, to generate the quadrilateral mesh for layer k, we do some very small and random perturbations on every vertices of the mesh cells on layer $k-1$, and denote the new perturbed mesh to be mesh for layer k. See Figure 5.3.

4. Connect corresponding vertices of meshes on layer $k-1$ and layer k to generate prismatic cells between these two layers. See Figure 5.4.

5. Repeat 3 and 4 for all k, so that all the desired cells for 3D prismatic grid are generated.

On this prismatic grid, we will apply PWCF method. However, the discretization scheme on this prismatic grid is different from the classical one. For the classical one, people introduce unknowns p_i in cells and u_i on interfaces between cells. While for the new approach, p_i are defined on interfaces between cells, and u_i are defined on some certain faces inside cells.

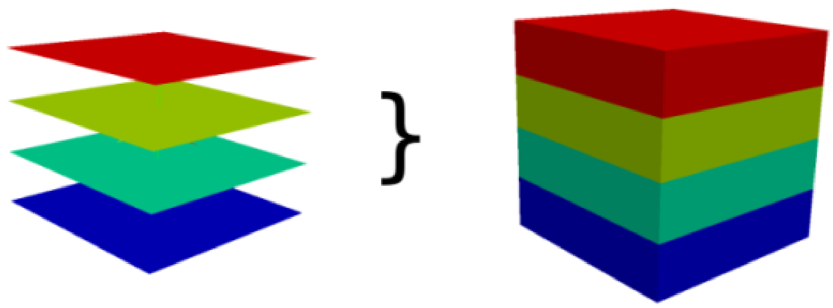

Figure 5.1: Layers in Ω

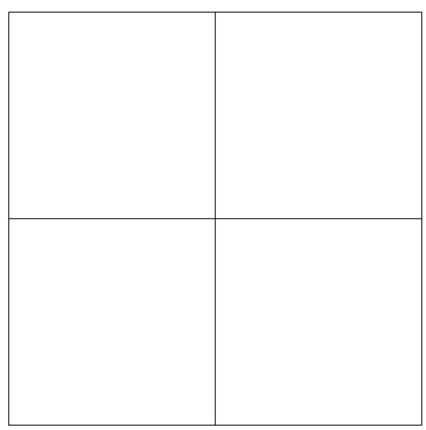

Figure 5.2: Polygonal mesh on top layer

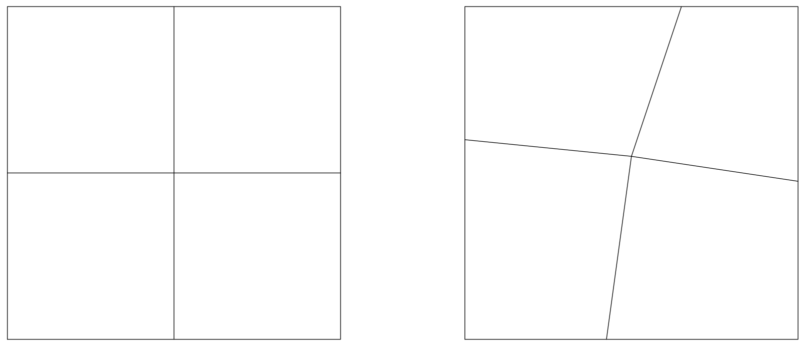

Figure 5.3: How to derive mesh on layer k from layer $k-1$

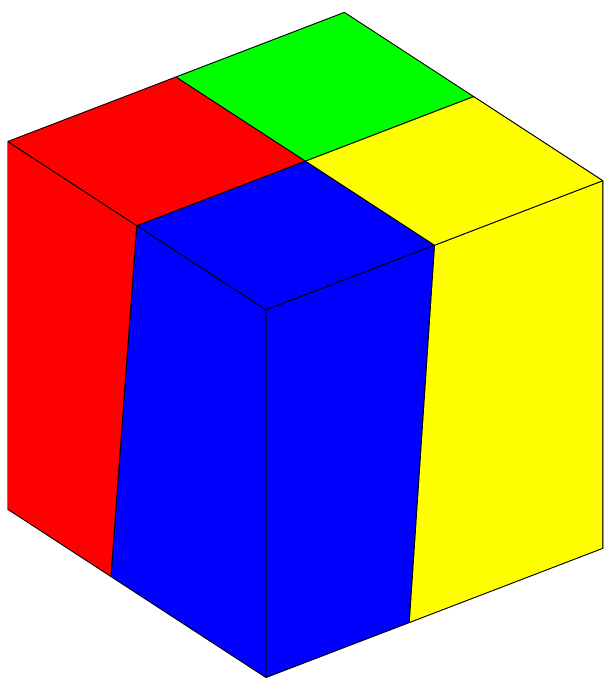

Figure 5.4: Prismatic grid generated from two layers in Figure 5.3

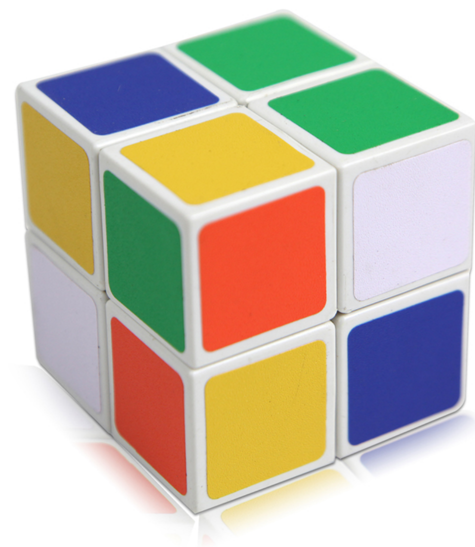

Figure 5.5: Magic cube is a grid generated from 3 uniform square mesh layers

To implement the new discretization scheme, the prismatic grid need to be proceeded further. First, divide all polygonal interfaces into triangles. (Since for our experiment, all interfaces are quadrilaterals, so we simply connect one pair of vertices on either diagonal.) Then connect center (geometric mean) of each grid cell to all vertices of this cell. As a result, every prismatic cell is divided into several tetrahedrons, see Figure 5.6. Other consequences are:

- Triangular faces on the interface of two grid cells are the interfaces of two tetrahedrons belonging to two different grid cells, see Figure 5.7.
- Triangular faces inside a grid cell are the interfaces of two tetrahedrons belonging to the same cell.

Unknowns for the new discretization method are then defined on these two types of triangular faces, i.e., p_i are defined on triangular faces (a), and u_i are defined on triangular face (b). For instance, for the cell in Figure 5.6, locally speaking, DOF on p_i is 12, and DOF on u_i is 18.

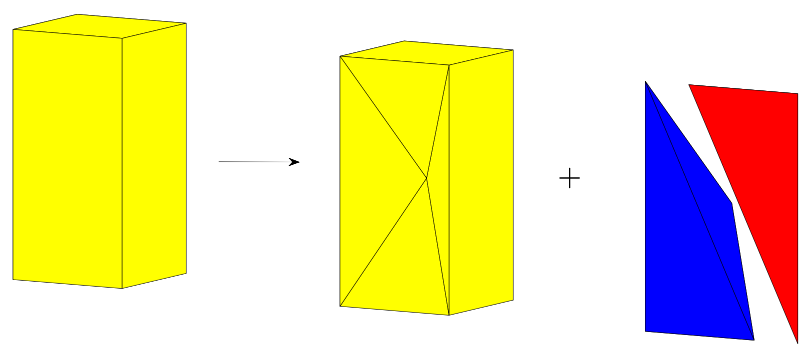

Figure 5.6: Divide one prismatic cell into six pyramids and then divide each pyramid with quadrilateral base into two tetrahedrons

5.2 Mixed fomulation

Consider the mixed form of the diffusion problem:

$$\begin{cases} \mathbf{u} + \nabla p & = 0 \qquad \text{in } \Omega, \\ \nabla \cdot \mathbf{u} & = f \qquad \text{in } \Omega, \\ p & = g \qquad \text{on } \partial\Omega. \end{cases} \tag{5.1}$$

In order to get the mixed finite element discretization by PWCF method, in each prismatic cell V, we need to introduce piecewise constant vector field basis $\mathbf{w}$ on each

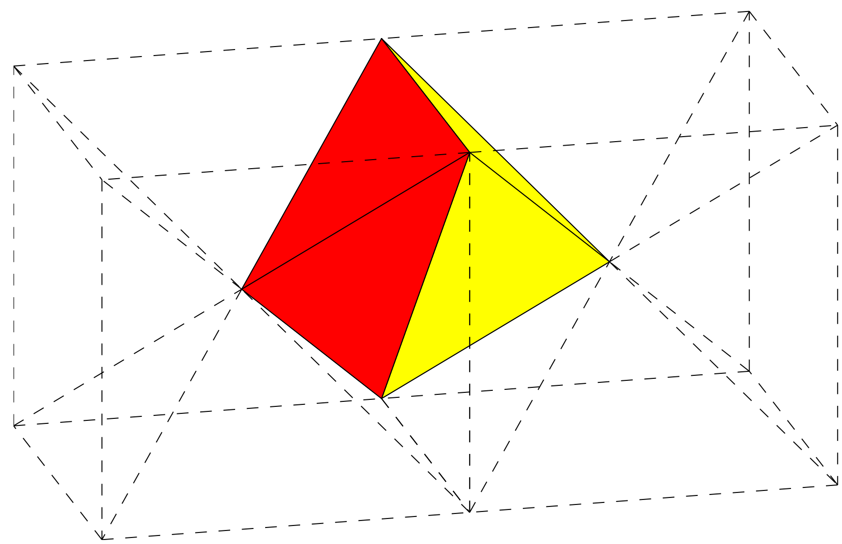

Figure 5.7: Union of two tetrahedrons which belong to different prismatic cells is a PWCF "macro" cell

union of two tetrahedrons which have a triangular interface inside V. We denote these two tetrahedrons by E_k and E_l. (In Figure 5.6, blue and red tetrahedrons are one pair of such tetrahedrons in yellow prismatic cell.) $\mathbf{w}$ satisfies:

1. $\mathbf{w}$ are two constants in two tetrahedrons of E_k and E_l correspondingly.

2. $\mathbf{w} \cdot \mathbf{n}_{\Gamma_{kl}} = 1$ on Γ_{kl}, where $\Gamma_{kl} = E_k \cap E_l$ is a triangular interface.

3. $\mathbf{w} \cdot \mathbf{n} = 0$ on other four triangular faces of E_k and E_l inside prismatic cell V. (There are two more triangular faces γ_l and γ_k for E_k and E_l, which are on the boundary of V.)

Let $\omega = E_k \cup E_l$, then we have:

$$
\begin{aligned}
&\int_\omega \mathbf{u} \cdot \mathbf{w} dx + \int_\omega (\nabla p) \cdot \mathbf{w} dx \\
&= \int_\omega \mathbf{u} \cdot \mathbf{w} dx + \int_{\partial\omega} p(\mathbf{n}_\omega \cdot \mathbf{w}) ds = 0,
\end{aligned}
\tag{5.2}
$$

or equivalently,

$$\int_{\omega} \mathbf{u} \cdot \mathbf{w} dx + |\Gamma_{kl}|(p_l - p_k) = 0, \tag{5.3}$$

where $p_l = \frac{1}{|\gamma_l|} \int_{\gamma_l} pds$, $p_k = \frac{1}{|\gamma_k|} \int_{\gamma_k} pds$, and $\gamma_l = E_l \cap \partial V$, $\gamma_k = E_k \cap \partial V$.

If we find all such basis vectors $\mathbf{w}$ for all cells, write $\mathbf{u}$ as linear combination of $\mathbf{w}$, and introduce boundary condition (if necessay), we can get the linear system:

$$\begin{cases} M\bar{u}_h + B^T\bar{p}_h & = \bar{G}_h \\ B\bar{u}_h & = \bar{F}_h \end{cases} \tag{5.4}$$

A good property for this system is, M is a block diagonal matrix and can be easily inverted, i.e., $M = \text{diag}\{M_1, \cdots, M_m\}$, where m is the number of prismatic cells, and M_i is exactly right defined on prismatic grid cells V_i, with entries $M_i(l,k) = \int_{V_i} \mathbf{w_l} \cdot \mathbf{w_k} dx$. Therefore, we can take advantage of this property by using Schur complement to solve this system, i.e.,

$$\begin{cases} BM^{-1}B^T\bar{p}_h & = BM^{-1}\bar{G}_h - \bar{F}_h \\ \bar{u}_h & = M^{-1}(\bar{G}_h - B^T\bar{p}_h) \end{cases}, \tag{5.5}$$

where $M^{-1} = \text{diag}\{M_1^{-1}, \cdots, M_m^{-1}\}$ is very cheap to obtain.

5.3 Numerical results

In this section, we use the method described above to test some functions on grids with different step sizes. On the very top layer, the mesh is uniform square mesh, with number of squares $n = 4^k, k = 1, 2, 3\cdots$. The following information and results are provided:

1. Number of layers.
2. Total number of prismatic grid cells.
3. Grid cell size h, which is the diagonal length of prismatic cells.
4. Degree of freedoms on $\bar{p}_h$.
5. Degree of freedoms on $\bar{u}_h$.
6. Error on $\mathbf{u}_h$, i.e., $||\mathbf{u}_h - \mathbf{u}^*||_2$, where $\mathbf{u}^*$ is the real solution.
7. Error on $\mathbf{u}^*_{h,int}$, i.e., $||\mathbf{u}^*_{h,int} - \mathbf{u}^*||_2$, where

$$\mathbf{u}^*_{h,int} \cdot \mathbf{n}_{kl} = \frac{1}{|\Gamma_{kl}|} \int_{\Gamma_{kl}} \mathbf{u}^* \cdot \mathbf{n} ds, \qquad k < l. \tag{5.6}$$

8. Ratio $c = \frac{||\mathbf{u}_h - \mathbf{u}^*||_2}{||\mathbf{u}^*_{h,int} - \mathbf{u}^*||_2}$. The reason to check this ratio is: it is already proved that

$$||\mathbf{u}_h - \mathbf{u}^*||_2 \leq 2||\mathbf{u}^*_{h,int} - \mathbf{u}^*||_2, \tag{5.7}$$

so we want to verify it from numerical results and investigate how large the real ratio between these two errors goes to.

In addition, in the C++ program, we use Simpson's method to evaluate line and triangular integrals, use Newton-Cotes quadrature rule that is accurate up to order

2 to evaluate integrals in tetrahedrons, and use conjugate gradient method to solve the first linear equation in (5.5).

Table 5.1 to Table 5.6 show the results without and with small perturbations (meshes on lower layer is derived from the meshes on higher layer with small random perturbations). For the perturbation, we tested on several values, for instance, 1%, 2%, here, the percentage indicates how significant the perturbation is. For example, in our test case, the region is a sqaure $[-1,1] \times [-1,1]$, if the perturbations have percentage 1%, then they are random numbers from interval $[-0.01, 0.01]$ in the directions of both x-axis and y-axis.

Table 5.1: $f(x,y,z) = 0$, $g(x,y,z) = 1$, real solution is $p(x,y,z) = 1$

# of layers	total # of cells	h	DOF on p_h	DOF on $\mathbf{u}_h$	$\|\|\mathbf{u}_h - \mathbf{u}^*\|\|_2$	$\|\|\mathbf{u}^*_{h,int} - \mathbf{u}^*\|\|_2$	c
No Perturbation							
3	8	1.73205	24	144	1.66447e-15	0	inf
5	64	0.866025	288	1152	6.89779e-15	0	inf
9	512	0.433013	2688	9216	2.21199e-14	0	inf
Perturbation Percentage: 0.5%							
3	8	1.73205	24	144	1.62973e-15	0	inf
5	64	0.866025	288	1152	6.21557e-15	0	inf
9	512	0.433013	2688	9216	1.67631e-14	0	inf
Perturbation Percentage: 1%							
3	8	1.73205	24	144	1.33398e-15	0	inf
5	64	0.866025	288	1152	5.98046e-15	0	inf
9	512	0.433013	2688	9216	1.70497e-14	0	inf
Perturbation Percentage: 2%							
3	8	1.73205	24	144	1.73771e-15	0	inf
5	64	0.866025	288	1152	6.14535e-15	0	inf
9	512	0.433013	2688	9216	1.73529e-14	0	inf

Table 5.2: $f(x, y, z) = 0$, $g(x, y, z) = x + y + z$, real solution is $p(x, y, z) = x + y + z$

# of layers	total # of cells	h	DOF on p_h	DOF on $\mathbf{u}_h$	$\|\|\mathbf{u}_h - \mathbf{u}^*\|\|_2$	$\|\|\mathbf{u}^*_{h,int} - \mathbf{u}^*\|\|_2$	c
No Perturbation							
3	8	1.73205	24	144	2.12471e-15	0	inf
5	64	0.866025	288	1152	5.59639e-15	0	inf
9	512	0.433013	2688	9216	1.82666e-14	0	inf
Perturbation Percentage: 0.5%							
3	8	1.73205	24	144	2.57654e-15	8.37545e-16	3.0763
5	64	0.866025	288	1152	6.13208e-15	9.72204e-16	6.3074
9	512	0.433013	2688	9216	1.59932e-14	9.72002e-16	16.4539
Perturbation Percentage: 1%							
3	8	1.73205	24	144	2.26871e-15	9.81696e-16	2.31101
5	64	0.866025	288	1152	6.23175e-15	9.88107e-16	6.30676
9	512	0.433013	2688	9216	1.67775e-14	1.02385e-15	16.3867
Perturbation Percentage: 2%							
3	8	1.73205	24	144	2.2555e-15	9.45372e-16	2.38583
5	64	0.866025	288	1152	5.73213e-15	1.00068e-15	5.72824
9	512	0.433013	2688	9216	1.64681e-14	1.03479e-15	15.9145

Table 5.3: $f(x, y, z) = -6$, $g(x, y, z) = x^2 + y^2 + z^2$, real solution is $p(x, y, z) = x^2 + y^2 + z^2$

# of layers	total # of cells	h	DOF on p_h	DOF on $\mathbf{u}_h$	$\|\|\mathbf{u}_h - \mathbf{u}^*\|\|_2$	$\|\|\mathbf{u}^*_{h,int} - \mathbf{u}^*\|\|_2$	c
No Perturbation							
3	8	1.73205	24	144	2.82843	2.82843	1
5	64	0.866025	288	1152 1.41421	1.41421	1	
9	512	0.433013	2688	9216	0.707107	0.707107	1
Perturbation Percentage: 0.5%							
3	8	1.73205	24	144	2.82844	2.82845	0.999996
5	64	0.866025	288	1152	1.41431	1.41437	0.999957
9	512	0.433013	2688	9216	0.707422	0.707627	0.999711
Perturbation Percentage: 1%							
3	8	1.73205	24	144	2.82847	2.82851	0.999985
5	64	0.866025	288	1152	1.41462	1.41486	0.999828
9	512	0.433013	2688	9216	0.708376	0.70919	0.998852
Perturbation Percentage: 2%							
3	8	1.73205	24	144	2.8286	2.82877	0.999942
5	64	0.866025	288	1152	1.41583	1.4168	0.999315
9	512	0.433013	2688	9216	0.712248	0.715431	0.995551

Table 5.4: $f(x, y, z) = 0$, $g(x, y, z) = xyz$, real solution is $p(x, y, z) = xyz$

# of layers	total # of cells	h	DOF on p_h	DOF on $\mathbf{u}_h$	$\|\|\mathbf{u}_h - \mathbf{u}^*\|\|_2$	$\|\|\mathbf{u}^*_{h,int} - \mathbf{u}^*\|\|_2$	c
No Perturbation							
3	8	1.73205	24	144	0.924493	0.959872	0.963142
5	64	0.866025	288	1152	0.451019	0.473552	0.952417
9	512	0.433013	2688	9216	0.224084	0.235971	0.949625
Perturbation Percentage: 0.5%							
3	8	1.73205	24	144	0.924498	0.959869	0.963151
5	64	0.866025	288	1152	0.451381	0.474124	0.952033
9	512	0.433013	2688	9216	0.224515	0.236577	0.949016
Perturbation Percentage: 1%							
3	8	1.73205	24	144	0.924517	0.959884	0.963155
5	64	0.866025	288	1152	0.451873	0.474878	0.951557
9	512	0.433013	2688	9216	0.225448	0.23792	0.94758
Perturbation Percentage: 2%							
3	8	1.73205	24	144	0.924595	0.959968	0.963152
5	64	0.866025	288	1152	0.453246	0.476932	0.950337
9	512	0.433013	2688	9216	0.228799	0.242828	0.942226

Table 5.5: $f(x, y, z) = -6(x + y + z)$, $g(x, y, z) = x^3 + y^3 + z^3$, real solution is $p(x, y, z) = x^3 + y^3 + z^3$

# of layers	total # of cells	h	DOF on p_h	DOF on $\mathbf{u}_h$	$\|\|\mathbf{u}_h - \mathbf{u}^*\|\|_2$	$\|\|\mathbf{u}^*_{h,int} - \mathbf{u}^*\|\|_2$	c
No Perturbation							
3	8	1.73205	24	144	3.6702	3.98336	0.921382
5	64	0.866025	288	1152	2.04946	2.11936	0.967015
9	512	0.433013	2688	9216	1.06231	1.07505	0.988152
Perturbation Percentage: 0.5%							
3	8	1.73205	24	144	3.66968	3.98348	0.921226
5	64	0.866025	288	1152	2.05124	2.12164	0.966818
9	512	0.433013	2688	9216	1.06261	1.07567	0.987854
Perturbation Percentage: 1%							
3	8	1.73205	24	144	3.66916	3.98361	0.921064
5	64	0.866025	288	1152	2.05331	2.12447	0.966506
9	512	0.433013	2688	9216	1.06392	1.07806	0.986887
Perturbation Percentage: 2%							
3	8	1.73205	24	144	3.66811	3.98396	0.920721
5	64	0.866025	288	1152	2.05831	2.13176	0.965547
9	512	0.433013	2688	9216	1.06966	1.08818	0.982974

Table 5.6: $f(x, y, z) = 3\pi^2 \sin(\pi x) \sin(\pi y) \sin(\pi z)$, $g(x, y, z) = 0$, real solution is $p(x, y, z) = \sin(\pi x) \sin(\pi y) \sin(\pi z)$

# of layers	total # of cells	h	DOF on p_h	DOF on $\mathbf{u}_h$	$\|\|\mathbf{u}_h - \mathbf{u}^*\|\|_2$	$\|\|\mathbf{u}^*_{h,int} - \mathbf{u}^*\|\|_2$	c
No Perturbation							
3	8	1.73205	24	144	6.44923	6.44923	1
5	64	0.866025	288	1152	3.29991	3.40107	0.970256
9	512	0.433013	2688	9216	1.77977	1.83436	0.97024
Perturbation Percentage: 0.5%							
3	8	1.73205	24	144	6.44931	6.44931	0.999999
5	64	0.866025	288	1152	3.29901	3.40073	0.970091
9	512	0.433013	2688	9216	1.78113	1.83595	0.970141
Perturbation Percentage: 1%							
3	8	1.73205	24	144	6.44924	6.44926	0.999997
5	64	0.866025	288	1152	3.29846	3.4013	0.969766
9	512	0.433013	2688	9216	1.78496	1.84152	0.969284
Perturbation Percentage: 2%							
3	8	1.73205	24	144	6.44871	6.44879	0.999988
5	64	0.866025	288	1152	3.29841	3.40517	0.968648
9	512	0.433013	2688	9216	1.80005	1.86459	0.965388

5.4 Conclusion

From the numerical results, we can get the following conclusions:

1. $||\mathbf{u}_h - \mathbf{u}^*||_2 \sim O(h)$.

2. $c < 2$, actually c is close to 1.

3. For constant and linear functions, the numerical solutions are accurate.

Appendices

APPENDIX A

Proofs of Lemmas

A.1 Proof of Lemma 3.9

Lemma 3.9. *Let* $\mathbf{a}$, $\mathbf{b}$, $\mathbf{c}$ *be vectors in* $\mathbb{R}^3$, *then*

$$\mathbf{a} \times (\mathbf{b} \times \mathbf{c}) = (\mathbf{a} \cdot \mathbf{c})\mathbf{b} - (\mathbf{a} \cdot \mathbf{b})\mathbf{c}. \tag{3.39}$$

Proof. This equality is known as triple product expansion, or Lagrange's formula ([31], p.1679). □

A.2 Proof of Lemma 3.10

Lemma 3.10. *Let* $\mathbf{a}$, $\mathbf{b}$, $\mathbf{c}$ *be vectors in* $\mathbb{R}^3$, *then*

$$(\mathbf{a}\times\mathbf{b})\cdot(\mathbf{c}\times\mathbf{d}) = (\mathbf{a}\cdot\mathbf{c})(\mathbf{b}\cdot\mathbf{d}) - (\mathbf{a}\cdot\mathbf{d})(\mathbf{b}\cdot\mathbf{c}). \tag{3.40}$$

Proof. This equality is known as Binet-Cauchy identity ([23], p.114) or Lagrange's identity ([10], p.185). □

A.3 Proof of Lemma 3.11

Lemma 3.11. *Let* $\mathbf{a}$, $\mathbf{b}$, $\mathbf{c}$ *be vectors in* $\mathbb{R}^3$, *then*

$$\Big[\mathbf{a}\cdot(\mathbf{b}\times\mathbf{c})\Big]^2 = ||\mathbf{a}||^2||\mathbf{b}\times\mathbf{c}||^2 - (\mathbf{a}\cdot\mathbf{b})\Big[(\mathbf{b}\times\mathbf{c})\cdot(\mathbf{a}\times\mathbf{c})\Big] + (\mathbf{a}\cdot\mathbf{c})\Big[(\mathbf{b}\times\mathbf{c})\cdot(\mathbf{a}\times\mathbf{b})\Big]. \tag{3.41}$$

Proof. By triple product expansion formula, the left-hand side is:

$$\begin{aligned}
&(\mathbf{a}\cdot(\mathbf{b}\times\mathbf{c}))^2\\
=&||\mathbf{a}||^2||\mathbf{b}\times\mathbf{c}||^2 - \Big[\mathbf{a}\times(\mathbf{b}\times\mathbf{c})\Big]^2\\
=&||\mathbf{a}||^2||\mathbf{b}\times\mathbf{c}||^2 - \Big[(\mathbf{a}\cdot\mathbf{c})\mathbf{b} - (\mathbf{a}\cdot\mathbf{b})\mathbf{c}\Big]^2\\
=&||\mathbf{a}||^2||\mathbf{b}\times\mathbf{c}||^2 - (\mathbf{a}\cdot\mathbf{c})^2||\mathbf{b}||^2 - (\mathbf{a}\cdot\mathbf{b})^2||\mathbf{c}||^2 + 2(\mathbf{a}\cdot\mathbf{c})(\mathbf{a}\cdot\mathbf{b})(\mathbf{b}\cdot\mathbf{c}).
\end{aligned} \tag{A.1}$$

On the other hand, by Binet-Cauchy identity, the right-hand side is:

$$\begin{aligned}&||\mathbf{a}||^2||\mathbf{b}\times\mathbf{c}||^2-(\mathbf{a}\cdot\mathbf{b})\Big[(\mathbf{b}\times\mathbf{c})\cdot(\mathbf{a}\times\mathbf{c})\Big]+(\mathbf{a}\cdot\mathbf{c})\Big[(\mathbf{b}\times\mathbf{c})\cdot(\mathbf{a}\times\mathbf{b})\Big]\\=&||\mathbf{a}||^2||\mathbf{b}\times\mathbf{c}||^2-(\mathbf{a}\cdot\mathbf{c})^2||\mathbf{b}||^2-(\mathbf{a}\cdot\mathbf{b})^2||\mathbf{c}||^2+2(\mathbf{a}\cdot\mathbf{c})(\mathbf{a}\cdot\mathbf{b})(\mathbf{b}\cdot\mathbf{c}).\end{aligned}\tag{A.2}$$

□

A.4 Proof of Lemma 3.12

Lemma 3.12. *Let* $\mathbf{a}$, $\mathbf{b}$, $\mathbf{c}$, $\mathbf{d}$ *be vectors in* $\mathbb{R}^3$, *then*

$$\begin{aligned}&\Big[\mathbf{a}\cdot(\mathbf{c}\times\mathbf{d})\Big]*\Big[\mathbf{b}\cdot(\mathbf{c}\times\mathbf{d})\Big]\\=&(\mathbf{a}\cdot\mathbf{b})||\mathbf{c}\times\mathbf{d}||^2-(\mathbf{a}\cdot\mathbf{c})\Big[(\mathbf{c}\times\mathbf{d})\cdot(\mathbf{b}\times\mathbf{d})\Big]+(\mathbf{a}\cdot\mathbf{d})\Big[(\mathbf{c}\times\mathbf{d})\cdot(\mathbf{b}\times\mathbf{c})\Big]\\=&(\mathbf{a}\cdot\mathbf{b})||\mathbf{c}\times\mathbf{d}||^2-(\mathbf{b}\cdot\mathbf{c})\Big[(\mathbf{c}\times\mathbf{d})\cdot(\mathbf{a}\times\mathbf{d})\Big]+(\mathbf{b}\cdot\mathbf{d})\Big[(\mathbf{c}\times\mathbf{d})\cdot(\mathbf{a}\times\mathbf{c})\Big].\end{aligned}\tag{3.42}$$

Proof. By using Lemma 3.11 and Binet-Cauchy identity, we have:

$$
\begin{aligned}
&\Big[\mathbf{a}\cdot(\mathbf{c}\times\mathbf{d})\Big] * \Big[\mathbf{b}\cdot(\mathbf{c}\times\mathbf{d})\Big] \\
=&\frac{1}{2}\Bigg\{\Big[(\mathbf{a}+\mathbf{b})\cdot(\mathbf{c}\times\mathbf{d})\Big]^2 - \Big[\mathbf{a}\cdot(\mathbf{c}\times\mathbf{d})\Big]^2 - \Big[\mathbf{b}\cdot(\mathbf{c}\times\mathbf{d})\Big]^2\Bigg\} \\
=&\frac{1}{2}\Bigg\{\Big[(\mathbf{a}+\mathbf{b})^2 - ||\mathbf{a}||^2 - ||\mathbf{b}||^2\Big] * ||\mathbf{c}\times\mathbf{d}||^2 - \Big[(\mathbf{a}+\mathbf{b})\cdot\mathbf{c}\Big]\Big[(\mathbf{c}\times\mathbf{d})\cdot\big[(\mathbf{a}+\mathbf{b})\times\mathbf{d}\big]\Big] \\
&\quad + \Big[(\mathbf{a}+\mathbf{b})\cdot\mathbf{d}\Big]\Big[(\mathbf{c}\times\mathbf{d})\cdot\big[(\mathbf{a}+\mathbf{b})\times\mathbf{c}\big]\Big] + (\mathbf{a}\cdot\mathbf{c})\Big[(\mathbf{c}\times\mathbf{d})\cdot(\mathbf{a}\times\mathbf{d})\Big] - (\mathbf{a}\cdot\mathbf{d})\Big[(\mathbf{c}\times\mathbf{d})\cdot(\mathbf{a}\times\mathbf{c})\Big] \\
&\quad + (\mathbf{b}\cdot\mathbf{c})\Big[(\mathbf{c}\times\mathbf{d})\cdot(\mathbf{b}\times\mathbf{d})\Big] - (\mathbf{b}\cdot\mathbf{d})\Big[(\mathbf{c}\times\mathbf{d})\cdot(\mathbf{b}\times\mathbf{c})\Big]\Bigg\} \\
=&(\mathbf{a}\cdot\mathbf{b})||\mathbf{c}\times\mathbf{d}||^2 + \frac{1}{2}\Bigg\{ - (\mathbf{a}\cdot\mathbf{c})\Big[(\mathbf{c}\times\mathbf{d})\cdot(\mathbf{b}\times\mathbf{d})\Big] + (\mathbf{a}\cdot\mathbf{d})\Big[(\mathbf{c}\times\mathbf{d})\cdot(\mathbf{b}\times\mathbf{c})\Big] \\
&\qquad - (\mathbf{b}\cdot\mathbf{c})\Big[(\mathbf{a}\times\mathbf{d})\cdot(\mathbf{a}\times\mathbf{d})\Big] + (\mathbf{b}\cdot\mathbf{d})\Big[(\mathbf{c}\times\mathbf{d})\cdot(\mathbf{a}\times\mathbf{c})\Big]\Bigg\} \\
=&(\mathbf{a}\cdot\mathbf{b})||\mathbf{c}\times\mathbf{d}||^2 - (\mathbf{a}\cdot\mathbf{c})\Big[(\mathbf{c}\times\mathbf{d})\cdot(\mathbf{b}\times\mathbf{d})\Big] + (\mathbf{a}\cdot\mathbf{d})\Big[(\mathbf{c}\times\mathbf{d})\cdot(\mathbf{b}\times\mathbf{c})\Big] \\
=&(\mathbf{a}\cdot\mathbf{b})||\mathbf{c}\times\mathbf{d}||^2 - (\mathbf{b}\cdot\mathbf{c})\Big[(\mathbf{c}\times\mathbf{d})\cdot(\mathbf{a}\times\mathbf{d})\Big] + (\mathbf{b}\cdot\mathbf{d})\Big[(\mathbf{c}\times\mathbf{d})\cdot(\mathbf{a}\times\mathbf{c})\Big].
\end{aligned}
\tag{A.3}
$$

□

A.5 Proof of Lemma 3.13

Lemma 3.13. *The inverse of matrix M_k defined in (3.35) is:*

$$
M_k^{-1} = \frac{1}{vol}\begin{pmatrix}
||\mathbf{n}_1||^2 & \mathbf{n}_1\cdot\mathbf{n}_2 & \mathbf{n}_1\cdot\mathbf{n}_3 & \mathbf{n}_1\cdot\mathbf{n}_4 \\
\mathbf{n}_2\cdot\mathbf{n}_1 & ||\mathbf{n}_2||^2 + \frac{(\mathbf{n}_2\cdot(\mathbf{n}_1\times\mathbf{n}_4))^2}{||\mathbf{n}_1\times\mathbf{n}_4||^2} & \mathbf{n}_2\cdot\mathbf{n}_3 - \frac{(\mathbf{n}_2\cdot(\mathbf{n}_1\times\mathbf{n}_4))(\mathbf{n}_3\cdot(\mathbf{n}_1\times\mathbf{n}_4))}{||\mathbf{n}_1\times\mathbf{n}_4||^2} & \mathbf{n}_2\cdot\mathbf{n}_4 \\
\mathbf{n}_3\cdot\mathbf{n}_1 & \mathbf{n}_3\cdot\mathbf{n}_2 - \frac{(\mathbf{n}_3\cdot(\mathbf{n}_1\times\mathbf{n}_4))(\mathbf{n}_2\cdot(\mathbf{n}_1\times\mathbf{n}_4))}{||\mathbf{n}_1\times\mathbf{n}_4||^2} & ||\mathbf{n}_3||^2 + \frac{(\mathbf{n}_3\cdot(\mathbf{n}_1\times\mathbf{n}_4))^2}{||\mathbf{n}_1\times\mathbf{n}_4||^2} & \mathbf{n}_3\cdot\mathbf{n}_4 \\
\mathbf{n}_4\cdot\mathbf{n}_1 & \mathbf{n}_4\cdot\mathbf{n}_2 & \mathbf{n}_4\cdot\mathbf{n}_3 & ||\mathbf{n}_4||^2
\end{pmatrix}. \tag{3.43}
$$

Proof. We prove this lemma by matrix multiplication.

$$
\begin{aligned}
&M(1,:) * M^{-1}(:,1)\\
=&\frac{1}{2}\Bigg\{\frac{||\mathbf{n}_1||^2||\mathbf{n}_3\times\mathbf{n}_4||^2-(\mathbf{n}_3\cdot\mathbf{n}_1)\Big[(\mathbf{n}_3\times\mathbf{n}_4)\cdot(\mathbf{n}_1\times\mathbf{n}_4)\Big]+(\mathbf{n}_4\cdot\mathbf{n}_1)\Big[(\mathbf{n}_3\times\mathbf{n}_4)\cdot(\mathbf{n}_1\times\mathbf{n}_3)\Big]}{(\mathbf{n}_1\cdot(\mathbf{n}_3\times\mathbf{n}_4))^2}\\
&\quad+\frac{||\mathbf{n}_1||^2||\mathbf{n}_2\times\mathbf{n}_4||^2-(\mathbf{n}_2\cdot\mathbf{n}_1)\Big[(\mathbf{n}_2\times\mathbf{n}_4)\cdot(\mathbf{n}_1\times\mathbf{n}_4)\Big]+(\mathbf{n}_4\cdot\mathbf{n}_1)\Big[(\mathbf{n}_2\times\mathbf{n}_4)\cdot(\mathbf{n}_1\times\mathbf{n}_2)\Big]}{(\mathbf{n}_1\cdot(\mathbf{n}_2\times\mathbf{n}_4))^2}\Bigg\}\\
=&1.
\end{aligned}
\tag{A.4}
$$

$$
\begin{aligned}
&M(1,:) * M^{-1}(:,4)\\
=&\frac{1}{2}\Bigg\{\frac{(\mathbf{n}_1\cdot\mathbf{n}_4)||\mathbf{n}_3\times\mathbf{n}_4||^2-(\mathbf{n}_3\cdot\mathbf{n}_4)\Big[(\mathbf{n}_3\times\mathbf{n}_4)\cdot(\mathbf{n}_1\times\mathbf{n}_4)\Big]+||\mathbf{n}_4||^2\left[(\mathbf{n}_3\times\mathbf{n}_4)\cdot(\mathbf{n}_1\times\mathbf{n}_3)\right]}{(\mathbf{n}_1\cdot(\mathbf{n}_3\times\mathbf{n}_4))^2}\\
&\quad+\frac{(\mathbf{n}_1\cdot\mathbf{n}_4)||\mathbf{n}_2\times\mathbf{n}_4||^2-(\mathbf{n}_2\cdot\mathbf{n}_4)\Big[(\mathbf{n}_2\times\mathbf{n}_4)\cdot(\mathbf{n}_1\times\mathbf{n}_4)\Big]+||\mathbf{n}_4||^2\left[(\mathbf{n}_2\times\mathbf{n}_4)\cdot(\mathbf{n}_1\times\mathbf{n}_2)\right]}{(\mathbf{n}_1\cdot(\mathbf{n}_2\times\mathbf{n}_4))^2}\Bigg\}\\
=&\frac{(\mathbf{n}_1\cdot\mathbf{n}_4)\Big[1-(\mathbf{n}_3\cdot\mathbf{n}_4)^2\Big]-(\mathbf{n}_3\cdot\mathbf{n}_4)\Big[\mathbf{n}_1\cdot\mathbf{n}_3-(\mathbf{n}_1\cdot\mathbf{n}_4)(\mathbf{n}_3\cdot\mathbf{n}_4)\Big]+(\mathbf{n}_1\cdot\mathbf{n}_3)(\mathbf{n}_3\cdot\mathbf{n}_4)-\mathbf{n}_1\cdot\mathbf{n}_4}{2(\mathbf{n}_1\cdot(\mathbf{n}_3\times\mathbf{n}_4))^2}\\
&\quad+\frac{(\mathbf{n}_1\cdot\mathbf{n}_4)\Big[1-(\mathbf{n}_2\cdot\mathbf{n}_4)^2\Big]-(\mathbf{n}_2\cdot\mathbf{n}_4)\Big[\mathbf{n}_1\cdot\mathbf{n}_2-(\mathbf{n}_1\cdot\mathbf{n}_4)(\mathbf{n}_2\cdot\mathbf{n}_4)\Big]+(\mathbf{n}_1\cdot\mathbf{n}_2)(\mathbf{n}_2\cdot\mathbf{n}_4)-\mathbf{n}_1\cdot\mathbf{n}_4}{2(\mathbf{n}_1\cdot(\mathbf{n}_2\times\mathbf{n}_4))^2}\\
=&0.
\end{aligned}
\tag{A.5}
$$

$$
\begin{aligned}
&M(1,:)*M^{-1}(:,2)\\
=&\frac{1}{2}\Bigg\{\frac{(\mathbf{n}_1\cdot\mathbf{n}_2)||\mathbf{n}_3\times\mathbf{n}_4||^2+(\mathbf{n}_4\cdot\mathbf{n}_2)\Big[(\mathbf{n}_3\times\mathbf{n}_4)\cdot(\mathbf{n}_1\times\mathbf{n}_3)\Big]}{(\mathbf{n}_1\cdot(\mathbf{n}_3\times\mathbf{n}_4))^2}\\
&-\frac{\Big[\mathbf{n}_3\cdot\mathbf{n}_2-\frac{(\mathbf{n}_3\cdot(\mathbf{n}_1\times\mathbf{n}_4))(\mathbf{n}_2\cdot(\mathbf{n}_1\times\mathbf{n}_4))}{||\mathbf{n}_1\times\mathbf{n}_4||^2}\Big](\mathbf{n}_3\times\mathbf{n}_4)\cdot(\mathbf{n}_1\times\mathbf{n}_4)}{(\mathbf{n}_1\cdot(\mathbf{n}_3\times\mathbf{n}_4))^2}\\
&+\frac{(\mathbf{n}_1\cdot\mathbf{n}_2)||\mathbf{n}_2\times\mathbf{n}_4||^2+(\mathbf{n}_4\cdot\mathbf{n}_2)\Big[(\mathbf{n}_2\times\mathbf{n}_4)\cdot(\mathbf{n}_1\times\mathbf{n}_2)\Big]}{(\mathbf{n}_1\cdot(\mathbf{n}_2\times\mathbf{n}_4))^2}\\
&-\frac{\Big[||\mathbf{n}_2||^2+\frac{(\mathbf{n}_2\cdot(\mathbf{n}_1\times\mathbf{n}_4))^2}{||\mathbf{n}_1\times\mathbf{n}_4||^2}\Big](\mathbf{n}_2\times\mathbf{n}_4)\cdot(\mathbf{n}_1\times\mathbf{n}_4)}{(\mathbf{n}_1\cdot(\mathbf{n}_2\times\mathbf{n}_4))^2}\Bigg\}\\
=&\frac{1}{2}\Bigg\{\frac{(\mathbf{n}_1\cdot\mathbf{n}_2)||\mathbf{n}_3\times\mathbf{n}_4||^2||\mathbf{n}_1\times\mathbf{n}_4||^2-(\mathbf{n}_1\cdot\mathbf{n}_2)\Big[(\mathbf{n}_1\times\mathbf{n}_4)\cdot(\mathbf{n}_3\times\mathbf{n}_4)\Big]^2}{(\mathbf{n}_1\cdot(\mathbf{n}_3\times\mathbf{n}_4))^2||\mathbf{n}_1\times\mathbf{n}_4||^2}\\
&-\frac{(\mathbf{n}_2\cdot\mathbf{n}_4)\Big[(\mathbf{n}_1\times\mathbf{n}_4)\cdot(\mathbf{n}_3\times\mathbf{n}_4)\Big]\Big[(\mathbf{n}_1\times\mathbf{n}_3)\cdot(\mathbf{n}_1\times\mathbf{n}_4)\Big]}{(\mathbf{n}_1\cdot(\mathbf{n}_3\times\mathbf{n}_4))^2||\mathbf{n}_1\times\mathbf{n}_4||^2}\\
&+\frac{(\mathbf{n}_2\cdot\mathbf{n}_4)\Big[(\mathbf{n}_3\times\mathbf{n}_4)\cdot(\mathbf{n}_1\times\mathbf{n}_3)\Big]||\mathbf{n}_1\times\mathbf{n}_4||^2}{(\mathbf{n}_1\cdot(\mathbf{n}_3\times\mathbf{n}_4))^2||\mathbf{n}_1\times\mathbf{n}_4||^2}\\
&+\frac{(\mathbf{n}_1\cdot\mathbf{n}_2)\Big[1-(\mathbf{n}_2\cdot\mathbf{n}_4)^2\Big]+(\mathbf{n}_4\cdot\mathbf{n}_2)\Big[(\mathbf{n}_1\cdot\mathbf{n}_2)\cdot(\mathbf{n}_2\cdot\mathbf{n}_4)-\mathbf{n}_1\cdot\mathbf{n}_4\Big]}{(\mathbf{n}_1\cdot(\mathbf{n}_2\times\mathbf{n}_4))^2}\\
&-\frac{\Big[||\mathbf{n}_2||^2+\frac{(\mathbf{n}_2\cdot(\mathbf{n}_1\times\mathbf{n}_4))^2}{||\mathbf{n}_1\times\mathbf{n}_4||^2}\Big]\Big[(\mathbf{n}_2\times\mathbf{n}_4)\cdot(\mathbf{n}_1\times\mathbf{n}_4)\Big]}{(\mathbf{n}_1\cdot(\mathbf{n}_2\times\mathbf{n}_4))^2}\Bigg\}\\
=&\frac{1}{2}\Bigg\{\frac{(\mathbf{n}_1\cdot\mathbf{n}_2)||(\mathbf{n}_1\times\mathbf{n}_4)\times(\mathbf{n}_3\times\mathbf{n}_4)||^2}{(\mathbf{n}_1\cdot(\mathbf{n}_3\times\mathbf{n}_4))^2||\mathbf{n}_1\times\mathbf{n}_4||^2}\\
&+\frac{(\mathbf{n}_2\cdot\mathbf{n}_4)(\mathbf{n}_1\cdot\mathbf{n}_4)*\Big[(\mathbf{n}_1\cdot\mathbf{n}_4)^2+(\mathbf{n}_3\cdot\mathbf{n}_4)^2+(\mathbf{n}_1\cdot\mathbf{n}_3)^2-(\mathbf{n}_3\cdot\mathbf{n}_4)\Big]}{(\mathbf{n}_1\cdot(\mathbf{n}_3\times\mathbf{n}_4))^2||\mathbf{n}_1\times\mathbf{n}_4||^2}\\
&-\frac{2(\mathbf{n}_1\cdot\mathbf{n}_3)(\mathbf{n}_1\cdot\mathbf{n}_4)}{(\mathbf{n}_1\cdot(\mathbf{n}_3\times\mathbf{n}_4))^2||\mathbf{n}_1\times\mathbf{n}_4||^2}+\frac{(\mathbf{n}_1\times\mathbf{n}_4)\cdot(\mathbf{n}_2\times\mathbf{n}_4)}{(\mathbf{n}_1\cdot(\mathbf{n}_2\times\mathbf{n}_4))^2}\\
&-\frac{\Big[||\mathbf{n}_2||^2+\frac{(\mathbf{n}_2\cdot(\mathbf{n}_1\times\mathbf{n}_4))^2}{||\mathbf{n}_1\times\mathbf{n}_4||^2}\Big]\Big[(\mathbf{n}_2\times\mathbf{n}_4)\cdot(\mathbf{n}_1\times\mathbf{n}_4)\Big]}{(\mathbf{n}_1\cdot(\mathbf{n}_2\times\mathbf{n}_4))^2}\Bigg\}\\
=&\frac{1}{2}\Bigg\{\frac{||(\mathbf{n}_1\times\mathbf{n}_4)\times(\mathbf{n}_3\times\mathbf{n}_4)||^2\Big[(\mathbf{n}_1\times\mathbf{n}_4)\cdot(\mathbf{n}_2\times\mathbf{n}_4)\Big]}{(\mathbf{n}_1\cdot(\mathbf{n}_3\times\mathbf{n}_4))^2||\mathbf{n}_1\times\mathbf{n}_4||^2}-\frac{(\mathbf{n}_1\times\mathbf{n}_4)\cdot(\mathbf{n}_2\times\mathbf{n}_4)}{||\mathbf{n}_1\times\mathbf{n}_4||^2}\Bigg\}\\
=&0.
\end{aligned}
\tag{A.6}
$$

$$
\begin{aligned}
&M(2,:)*M^{-1}(:,1)\\
=&\frac{1}{2}\left\{\frac{-||\mathbf{n}_1||^2\Big[(\mathbf{n}_1\times\mathbf{n}_4)\cdot(\mathbf{n}_2\times\mathbf{n}_4)\Big]+(\mathbf{n}_2\cdot\mathbf{n}_1)||\mathbf{n}_1\times\mathbf{n}_4||^2-(\mathbf{n}_4\cdot\mathbf{n}_1)\Big[(\mathbf{n}_1\times\mathbf{n}_4)\cdot(\mathbf{n}_1\times\mathbf{n}_2)\Big]}{(\mathbf{n}_2\cdot(\mathbf{n}_1\times\mathbf{n}_4))^2}\right\}\\
=&\frac{1}{2}\left\{\frac{-\Big[\mathbf{n}_1\cdot\mathbf{n}_2-(\mathbf{n}_1\cdot\mathbf{n}_4)(\mathbf{n}_2\cdot\mathbf{n}_4)\Big]+(\mathbf{n}_2\cdot\mathbf{n}_1)\Big[1-(\mathbf{n}_1\cdot\mathbf{n}_4)^2\Big]}{(\mathbf{n}_2\cdot(\mathbf{n}_1\times\mathbf{n}_4))^2}\right.\\
&\quad\left.-\frac{(\mathbf{n}_4\cdot\mathbf{n}_1)\Big[\mathbf{n}_2\cdot\mathbf{n}_4-(\mathbf{n}_1\cdot\mathbf{n}_2)(\mathbf{n}_1\cdot\mathbf{n}_4)\Big]}{(\mathbf{n}_2\cdot(\mathbf{n}_1\times\mathbf{n}_4))^2}\right\}\\
=&0.
\end{aligned}
\tag{A.7}
$$

$$
\begin{aligned}
&M(2,:)*M^{-1}(:,2)\\
=&\frac{1}{2}\left\{\frac{-(\mathbf{n}_1\cdot\mathbf{n}_2)\Big[(\mathbf{n}_1\times\mathbf{n}_4)\cdot(\mathbf{n}_2\times\mathbf{n}_4)\Big]-(\mathbf{n}_4\cdot\mathbf{n}_2)\Big[(\mathbf{n}_1\times\mathbf{n}_4)\cdot(\mathbf{n}_1\times\mathbf{n}_2)\Big]}{(\mathbf{n}_2\cdot(\mathbf{n}_1\times\mathbf{n}_4))^2}\right.\\
&\quad\left.+\frac{\Big[||\mathbf{n}_2||^2+\frac{(\mathbf{n}_2\cdot(\mathbf{n}_1\times\mathbf{n}_4))^2}{||\mathbf{n}_1\times\mathbf{n}_4||^2}\Big]||\mathbf{n}_1\times\mathbf{n}_4||^2}{(\mathbf{n}_2\cdot(\mathbf{n}_1\times\mathbf{n}_4))^2}\right\}\\
=&\frac{1}{2}\left\{\frac{-(\mathbf{n}_1\cdot\mathbf{n}_2)\Big[(\mathbf{n}_1\times\mathbf{n}_4)\cdot(\mathbf{n}_2\times\mathbf{n}_4)\Big]-(\mathbf{n}_4\cdot\mathbf{n}_2)\Big[(\mathbf{n}_1\times\mathbf{n}_4)\cdot(\mathbf{n}_1\times\mathbf{n}_2)\Big]}{(\mathbf{n}_2\cdot(\mathbf{n}_1\times\mathbf{n}_4))^2}\right.\\
&\quad\left.+\frac{||\mathbf{n}_2||^2||\mathbf{n}_1\times\mathbf{n}_4||^2+(\mathbf{n}_2\cdot(\mathbf{n}_1\times\mathbf{n}_4))^2}{(\mathbf{n}_2\cdot(\mathbf{n}_1\times\mathbf{n}_4))^2}\right\}\\
=&\frac{1}{2}*\frac{2(\mathbf{n}_2\cdot(\mathbf{n}_1\times\mathbf{n}_4))^2}{(\mathbf{n}_2\cdot(\mathbf{n}_1\times\mathbf{n}_4))^2}\\
=&1.
\end{aligned}
\tag{A.8}
$$

$$
\begin{aligned}
&M(2,:) * M^{-1}(:,3)\\
=&\frac{1}{2}\left\{\frac{-(\mathbf{n}_1\cdot\mathbf{n}_3)\Big[(\mathbf{n}_1\times\mathbf{n}_4)\cdot(\mathbf{n}_2\times\mathbf{n}_4)\Big]-(\mathbf{n}_4\cdot\mathbf{n}_3)\Big[(\mathbf{n}_1\times\mathbf{n}_4)\cdot(\mathbf{n}_1\times\mathbf{n}_2)\Big]}{(\mathbf{n}_2\cdot(\mathbf{n}_1\times\mathbf{n}_4))^2}\right.\\
&\left.+\frac{\Big[\mathbf{n}_2\cdot\mathbf{n}_3-\frac{(\mathbf{n}_3\cdot(\mathbf{n}_1\times\mathbf{n}_4))(\mathbf{n}_2\cdot(\mathbf{n}_1\times\mathbf{n}_4))}{||\mathbf{n}_1\times\mathbf{n}_4||^2}\Big]||\mathbf{n}_1\times\mathbf{n}_4||^2}{(\mathbf{n}_2\cdot(\mathbf{n}_1\times\mathbf{n}_4))^2}\right\}\\
=&\frac{1}{2}\left\{\frac{-(\mathbf{n}_1\cdot\mathbf{n}_3)\Big[(\mathbf{n}_1\times\mathbf{n}_4)\cdot(\mathbf{n}_2\times\mathbf{n}_4)\Big]+(\mathbf{n}_1\cdot\mathbf{n}_3)\Big[(\mathbf{n}_1\times\mathbf{n}_4)\cdot(\mathbf{n}_2\times\mathbf{n}_4)\Big]}{(\mathbf{n}_2\cdot(\mathbf{n}_1\times\mathbf{n}_4))^2}\right.\\
&\left.+\frac{(\mathbf{n}_4\cdot\mathbf{n}_3)\Big[(\mathbf{n}_1\times\mathbf{n}_4)\cdot(\mathbf{n}_1\times\mathbf{n}_2)\Big]-(\mathbf{n}_4\cdot\mathbf{n}_3)\Big[(\mathbf{n}_1\times\mathbf{n}_4)\cdot(\mathbf{n}_1\times\mathbf{n}_2)\Big]}{(\mathbf{n}_2\cdot(\mathbf{n}_1\times\mathbf{n}_4))^2}\right\}\\
=&0.
\end{aligned}
\tag{A.9}
$$

$$
\begin{aligned}
&M(2,:) * M^{-1}(:,4)\\
=&\frac{1}{2}\left\{\frac{-(\mathbf{n}_1\cdot\mathbf{n}_4)\Big[(\mathbf{n}_1\times\mathbf{n}_4)\cdot(\mathbf{n}_2\times\mathbf{n}_4)\Big]+(\mathbf{n}_2\cdot\mathbf{n}_4)||\mathbf{n}_1\times\mathbf{n}_4||^2-||\mathbf{n}_4||^2\Big[(\mathbf{n}_1\times\mathbf{n}_4)\cdot(\mathbf{n}_1\times\mathbf{n}_2)\Big]}{(\mathbf{n}_2\cdot(\mathbf{n}_1\times\mathbf{n}_4))^2}\right\}\\
=&\frac{1}{2}\left\{\frac{-(\mathbf{n}_1\cdot\mathbf{n}_4)\Big[\mathbf{n}_1\cdot\mathbf{n}_2-(\mathbf{n}_1\cdot\mathbf{n}_4)(\mathbf{n}_2\cdot\mathbf{n}_4)\Big]+(\mathbf{n}_2\cdot\mathbf{n}_4)\Big[1-(\mathbf{n}_1\cdot\mathbf{n}_4)^2\Big]}{(\mathbf{n}_2\cdot(\mathbf{n}_1\times\mathbf{n}_4))^2}\right.\\
&\left.+\frac{-\mathbf{n}_2\cdot\mathbf{n}_4+(\mathbf{n}_1\cdot\mathbf{n}_4)(\mathbf{n}_1\cdot\mathbf{n}_2)\Big]}{(\mathbf{n}_2\cdot(\mathbf{n}_1\times\mathbf{n}_4))^2}\right\}\\
=&0.
\end{aligned}
\tag{A.10}
$$

Similarly, we can get other elements of MM^{-1}, and the result is $MM^{-1}=I$. □

A.6 Proof of Lemma 3.14

Lemma 3.14.

$$s_2\Big[\mathbf{n}_2\cdot(\mathbf{n}_1\times\mathbf{n}_4)\Big]=-s_3\Big[\mathbf{n}_3\cdot(\mathbf{n}_1\times\mathbf{n}_4)\Big]. \tag{3.44}$$

Proof. Let $\mathbf{u}_1 = \overrightarrow{V_1V_2}$, $\mathbf{u}_2 = \overrightarrow{V_1V_3}$, $\mathbf{u}_3 = \overrightarrow{V_1V_4}$, then we have

$$\mathbf{n}_1 = \frac{(\mathbf{u}_3 - \mathbf{u}_2) \times (\mathbf{u}_2 - \mathbf{u}_1)}{s_1}, \tag{A.11}$$

$$\mathbf{n}_2 = \frac{\mathbf{u}_2 \times \mathbf{u}_3}{s_2}, \tag{A.12}$$

$$\mathbf{n}_3 = \frac{\mathbf{u}_3 \times \mathbf{u}_1}{s_3}, \tag{A.13}$$

$$\mathbf{n}_4 = \frac{\mathbf{u}_1 \times \mathbf{u}_2}{s_4}. \tag{A.14}$$

As a result,

$$\begin{aligned} \mathbf{n}_2 \cdot (\mathbf{n}_1 \times \mathbf{n}_4) = \mathbf{n}_1 \cdot (\mathbf{n}_4 \times \mathbf{n}_2) = \mathbf{n}_1 \cdot \left\{ \frac{(\mathbf{u}_1 \times \mathbf{u}_2) \times (\mathbf{u}_2 \times \mathbf{u}_3)}{s_2 s_4} \right\} \\ = \frac{\Big[(\mathbf{u}_3 \times \mathbf{u}_1) \cdot \mathbf{u}_2\Big]\Big[\mathbf{u}_2 \cdot (\mathbf{u}_1 \times \mathbf{u}_3)\Big]}{s_1 s_2 s_4}, \end{aligned} \tag{A.15}$$

and

$$\begin{aligned} \mathbf{n}_3 \cdot (\mathbf{n}_1 \times \mathbf{n}_4) = \mathbf{n}_1 \cdot (\mathbf{n}_4 \times \mathbf{n}_3) = \mathbf{n}_1 \cdot \left\{ \frac{(\mathbf{u}_1 \times \mathbf{u}_2) \times (\mathbf{u}_3 \times \mathbf{u}_1)}{s_3 s_4} \right\} \\ = -\frac{\Big[(\mathbf{u}_3 \times \mathbf{u}_2) \cdot \mathbf{u}_1\Big]\Big[\mathbf{u}_1 \cdot (\mathbf{u}_2 \times \mathbf{u}_3)\Big]}{s_1 s_3 s_4}. \end{aligned} \tag{A.16}$$

Therefore, $s_2\Big[\mathbf{n}_2 \cdot (\mathbf{n}_1 \times \mathbf{n}_4)\Big] = -s_3\Big[\mathbf{n}_3 \cdot (\mathbf{n}_1 \times \mathbf{n}_4)\Big]$. □

Bibliography

[1] T. Arbogast, C. Dawson, and P. Keenan. Mixed finite element methods as finite difference methods for solving elliptic equations on triangular elements. Technical report, Tech. Report 93-53, Dept. of Comput. and Applied Math., Rice University, 1993.

[2] T. Arbogast, M. F. Wheeler, and I. Yotov. Mixed finite elements for elliptic problems with tensor coefficients as cell-centered finite differences. *SIAM Journal on Numerical Analysis*, 34(2):828–852, 1997.

[3] C. Bernardi. Optimal finite-element interpolation on curved domains. *SIAM Journal on Numerical Analysis*, 26(5):1212–1240, 1989.

[4] E. Bertolazzi. Discrete conservation and discrete maximum principle for elliptic pdes. *Mathematical Models and Methods in Applied Sciences*, 8(04):685–711, 1998.

[5] J. Bramble and B. Hubbard. On finite difference analogue of elliptic boundary problem which is neither diagonally dominant nor of non-negative type. *Journal of Mathematics and Physics*, 43(2):117, 1964.

[6] J. H. Bramble and B. E. Hubbard. New monotone type approximations for elliptic problems. *Math. Comp*, 18:349–367, 1964.

[7] J. H. Bramble and M. Zlámal. Triangular elements in the finite element method. *Mathematics of Computation*, 24(112):809–820, 1970.

[8] F. Brezzi, J. Douglas, M. Fortin, and L. D. Marini. Efficient rectangular mixed finite elements in two and three space variables. *Modélisation mathématique et analyse numérique*, 21(4):581–604, 1987.

[9] F. Brezzi, J. Douglas Jr, and L. D. Marini. Two families of mixed finite elements for second order elliptic problems. *Numerische Mathematik*, 47(2):217–235, 1985.

[10] I. N. Bronshtein, K. A. Semendyayev, G. Musiol, and H. Muehlig. *Handbook of mathematics*. Springer Science & Business Media, 2007.

[11] E. Burman and A. Ern. Nonlinear diffusion and discrete maximum principle for stabilized galerkin approximations of the convection–diffusion-reaction equation. *Computer Methods in Applied Mechanics and Engineering*, 191(35):3833–3855, 2002.

[12] G. Chavent and J. Roberts. A unified physical presentation of mixed, mixed-hybrid finite elements and standard finite difference approximations for the determination of velocities in waterflow problems. *Advances in Water Resources*, 14(6):329–348, 1991.

[13] Z. Chen and J. Douglas Jr. Prismatic mixed finite elements for second order elliptic problems. *Calcolo*, 26(2-4):135–148, 1989.

[14] I. Christie and C. Hall. The maximum principle for bilinear elements. *International Journal for Numerical Methods in Engineering*, 20(3):549–553, 1984.

[15] P. G. Ciarlet. Discrete maximum principle for finite-difference operators. *Aequationes mathematicae*, 4(3):338–352, 1970.

[16] P. G. Ciarlet and P.-A. Raviart. Maximum principle and uniform convergence for the finite element method. *Computer Methods in Applied Mechanics and Engineering*, 2(1):17–31, 1973.

[17] R. W. Clough. The finite element method in plane stress analysis. 1960.

[18] R. Courant et al. Variational methods for the solution of problems of equilibrium and vibrations. *Bull. Amer. Math. Soc*, 49(1):1–23, 1943.

[19] L. C. Cowsar, A. Weiser, and M. F. Wheeler. Parallel multigrid and domain decomposition algorithms for elliptic equations. In *Fifth International Symposium on Domain Decomposition Methods for Partial Differential Equations*, number 55, page 376. SIAM, 1992.

[20] J. Douglas and J. E. Roberts. Global estimates for mixed methods for second order elliptic equations. *Mathematics of computation*, 44(169):39–52, 1985.

[21] R. Eymard, T. Gallouët, and R. Herbin. Finite volume methods. *Handbook of numerical analysis*, 7:713–1018, 2000.

[22] K. Feng. Finite differences schemes based on variational principle. *Chinese Journal of Applied Mathematics and Numerical Mathematics*, 2:23862, 1965.

[23] H. Feshbach and P. Morse. *Methods of Theoretical Physics, Part I.* McGraw-Hill Book Co., Inc., London, 1953.

[24] G. E. Forsythe and W. R. Wasow. Finite-difference methods for partial differential equations. 1960.

[25] M. Fortin and F. Brezzi. *Mixed and hybrid finite element methods.* Springer, 1991.

[26] L. Gastaldi and R. Nochetto. Optimal l-error estimates for nonconforming and mixed finite element methods of lowest order. *Numerische Mathematik*, 50(5):587–611, 1987.

[27] R. Glowinski, W. Kinton, and M. Wheeler. Acceleration of domain decomposition algorithms for mixed finite elements by multi-level methods. In *Proceedings of the Third International Symposium on Domain Decomposition Methods for Partial Differential Equations, R. Glowinski et al., eds., SIAM*, pages 263–290, 1990.

[28] R. Glowinski and M. F. Wheeler. Domain decomposition and mixed finite element methods for elliptic problems. In *First international symposium on domain decomposition methods for partial differential equations*, pages 144–172. SIAM: Philadelphia, 1988.

[29] A. Hrennikoff. Solution of problems of elasticity by the framework method. *Journal of applied mechanics*, 8(4):169–175, 1941.

[30] K. Ishihara. Strong and weak discrete maximum principles for matrices associated with elliptic problems. *Linear Algebra and its Applications*, 88:431–448, 1987.

[31] K. Itō. *Encyclopedic dictionary of mathematics*, volume 1. MIT press, 1993.

[32] E. Kikinzon, Y. A. Kuznetsov, and Z. Liu. Monotonicity in rt_0 and pwcf methods on triangular and tetrahedral meshes. *Numerical Analysis and Scientific Computing Preprint Series, Department of Mathematics, University of Houston*, (35), 2015.

[33] S. Korotov and M. Krízek. Acute type refinements of tetrahedral partitions of polyhedral domains. *SIAM Journal on Numerical Analysis*, 39(2):724–733, 2001.

[34] S. Korotov, M. Křížek, and P. Neittaanmäki. Weakened acute type condition for tetrahedral triangulations and the discrete maximum principle. *Mathematics of Computation*, 70(233):107–119, 2001.

[35] H.-J. Kuo and N. S. Trudinger. A note on the discrete aleksandrov-bakelman maximum principle. *Taiwanese Journal of Mathematics*, 4(1):pp–55, 2000.

[36] Y. Kuznetsov, K. Lipnikov, and M. Shashkov. Mimetic finite difference methods on polygonal meshes for diffusion-type problems. *Comp. Geosciences*, 8:301–324, 2004.

[37] Y. A. Kuznetsov. Matrix analysis of mixed finite element methods for the diffusion equation. one. *J. Numer. Math.*, 0:1–19, 2005.

[38] Y. A. Kuznetsov. Mixed finite element method for diffusion equations on polygonal meshes with mixed cells. *J. Numer. Math.*, 14(4):305–315, 2006.

[39] Y. A. Kuznetsov. *Mixed Finite Element Methods on Polyhedral Meshes for Diffusion Equations*. Springer, Heidelberg, 2007.

[40] Y. A. Kuznetsov. Approximation with piece-wise constant fluxes for diffusion equations. *J. Numer. Math.*, 14(4):309–328, 2011.

[41] Y. A. Kuznetsov and S. Repin. New mixed finite element method on polygonal and polyhedral meshes. *Russian J. Numer. Anal. Math. Modelling*, 18:261–278, 2003.

[42] M. Lenoir. Optimal isoparametric finite elements and error estimates for domains involving curved boundaries. *SIAM journal on numerical analysis*, 23(3):562–580, 1986.

[43] A. Mazzia. An analysis of monotonicity conditions in the mixed hybrid finite element method on unstructured triangulations. *International Journal for Numerical Methods in Engineering*, 76(3):351–375, 2008.

[44] I. D. Mishev. Finite volume methods on voronoi meshes. *Numerical methods for Partial Differential equations*, 14(2):193–212, 1998.

[45] M. Nakata, A. Weiser, and M. F. Wheeler. Some superconvergence results for mixed finite element methods for elliptic problems on rectangular domains. *The Mathematics of Finite Elements and Applications V, JR Whiteman, ed., Academic Press, London*, pages 367–389, 1985.

[46] J.-C. Nédélec. Mixed finite elements in $\mathbb{R}^3$. *Numerische Mathematik*, 35(3):315–341, 1980.

[47] R. Pless. Lecture 16: Fortune's algorithm and voronoi diagrams, 2015.

[48] P.-A. Raviart and J.-M. Thomas. A mixed finite element method for 2-nd order elliptic problems. In *Mathematical aspects of finite element methods*, pages 292–315. Springer, 1977.

[49] T. F. Russell and M. F. Wheeler. Finite element and finite difference methods for continuous flows in porous media. *The mathematics of reservoir simulation*, 1:35–106, 1983.

[50] A. H. Schatz. A weak discrete maximum principle and stability of the finite element method in l∞ on plane polygonal domains. i. *Mathematics of Computation*, 34(149):77–91, 1980.

[51] J. Shen. Mixed finite element methods on distorted rectangular grids. *Techincal Report ISC*, pages 94–13, 1994.

[52] R. S. Varga. On a discrete maximum principle. *SIAM Journal on Numerical Analysis*, 3(2):355–359, 1966.

[53] R. S. Varga. *Matrix iterative analysis*, volume 27. Springer Science & Business, 2009.

[54] A. Weiser and M. F. Wheeler. On convergence of block-centered finite differences for elliptic problems. *SIAM Journal on Numerical Analysis*, 25(2):351–375, 1988.

[55] M. Zlámal. Curved elements in the finite element method. i. *SIAM Journal on Numerical Analysis*, 10(1):229–240, 1973.